Università degli Studi di Ferrara

DOTTORATO DI RICERCA IN

"SCIENZE BIOMEDICHE E BIOTECNOLOGICHE"

CICLO XXXII

COORDINATORE Prof. Pinton Paolo

The role of c subunit of F_1F_O-ATP synthase in mitochondrial permeability transition pore activity for the treatment of reperfusion injury after myocardial infarction

Settore Scientifico Disciplinare MED/04

Dottoranda
Dott. Pedriali Gaia

Tutore
Prof. Pinton Paolo

Anni 2016/2019

Abbreviations

$\Delta\psi_{m:}$ Mitochondrial Transmembrane Potential
ACE: Angiotensin II Converting Enzyme.
ADP: Adenosine Diphosphate
a.f.u.: Arbitrary Fluorescence Units
ALS: Amyotrophic Lateral Sclerosis
ANP: Atrial Natriuretic Peptide
ANT: Adenine Nucleotide Translocator
ATP: Adenosine Triphosphate
BAD: BCL-2-Associated Agonist Of Cell Death
CETSA: Cellular Thermal Shift Assay
CKMT1: Creatine Kinase, Mitochondrial 1
cMRI: Cardiac Magnetic Resonance Imaging
CPP: Coronary Perfusion Pressure
CsA: Cyclosporin A
CytC: Cytochrome C
CYPD: Cyclophilin-D
DMF-DMA: Dimethylformamide Dimethyl Acetal
EDP: End-Diastolic Pressure
ER: Endoplasmic Reticulum
FMC: First Medical Contact.
GIK: Glucose/Insulin/Potassium
GSK3β: Glycogen Synthase Kinase 3β
HF: Heart Failure
HK1: Hexokinase 1
HK2: Hexokinase 2
HR: Heart Rate.
IF-1: Inhibitor Protein
IHD: Ischemic Heart Diseases
IMM: Inner Mitochondrial Membrane
IPC: Ischemic Pre-Conditioning
I/R Injury: Ischemia-Reperfusion Injury
IS: Infarct Size
KHB: Krebs-Henseleit Buffer
LAD: Left Anterior Descending.
LV: Left Ventricular
LVDP: Left Ventricular Developed Pressure
LVEF: Left Ventricle Ejection Fraction.
MBzR: Mitochondrial Benzodiazepine Receptor
MCU: Mitochondrial Calcium Uniporter
MI: Myocardial Infarction
MLD: Minimal Lumen Diameter.
MMC: Mitochondrial Megachannel
MOMP: Mitochondrial Outer Membrane Permeabilization
MPT: Mitochondrial Permeability Transition
mPTP: Mitochondrial Permeability Transition Pore
MSI: Myocardial Salvage Index
MTT: 3-(4,5-Dimethylthiazol-2-Yl)-2,5-Diphenyltetrazolium Bromide
MVD: Multivessel Disease.

NADH: Nicotinamide Adenine Dinucleotide
OMM: Outer Mitochondrial Membrane
OS: Onset Of Symptoms.
OSCP: Oligomycin Sensitivity-Conferring Protein
PCD: Programmed Cell Death
PCI: Primary Percutaneous Interventions
PI: Propidium Iodide
Pkcε: Protein Kinase Cε
PKG: Protein Kinase Cgmp-Dependent
PLA: Proximity Ligation Assay
PTPC: Mitochondrial Permeability Transition Pore Complex
RCD: Regulated Cell Death
RI: Reperfusion Injury
RIC: Remote Ischemic Conditioning
ROS: Reactive Oxygen Species
RR: Ruthenium Red
RVD: Reference Vessel Diameter.
SAR: Structure−Activity Relationship
SBP: Systolic Blood Pressure.
SPG7: Paraplegin Matrix AAA Peptidase Subunit
STEMI: ST-Segment Elevation Myocardial Infarction
TMSCN : Trimethyl Silyl Cyanide
TOMM20: Translocase Of Outer Mitochondrial Membrane 20
tPTP: Transient mPTP opening
TSPO: Translocator Protein (18 Kda)
TUNEL: Terminal Deoxynucleotidyl Transferase Dutp Nick-End Labeling
VDAC: Voltage-Dependent Anion Channel
WMSI: Wall Motion Score Index.

Introduction

1. Mitochondrial Permeability Transition

• Mitochondrial Permeability Transition

The mitochondrial permeability transition (MPT) has been described for the first time in 1979, with terms of Ca^{2+}-induced membrane transition, this phenomenon involved endogenous NADH (nicotinamide adenine dinucleotide), ADP (adenosine diphosphate), and energization and acts as a protective mechanism activated by mitochondria (1).
Only about 10 years later researchers focused on this process associating this with programmed cell death (PCD) and so to pathophysiological implications. They found out that alteration of mitochondrial function such as reduction of mitochondrial transmembrane potential ($\Delta\psi_m$) or ROS (reactive oxygen species) generation were key events during early PCD (2), in particular reduction of $\Delta\psi_m$ was an obligate irreversible step of ongoing lymphocyte death, preceding other alterations of cellular physiology (3).
Nowadays the state of the art describes the MPT as a sudden increase in permeability of the inner mitochondrial membrane (IMM) to solutes with molecular mass up to 1.5 kDa; there is also the opening of the mitochondrial permeability transition pore (mPTP), a voltage-dependent, high-conductance channel located in the Inner Mitochondrial Membrane (IMM) that leads to the dissipation of $\Delta\psi_m$ and the consequent arrest in all $\Delta\psi_m$-dependent mitochondrial activities, including ATP (adenosine triphosphate) synthesis (4) (5). The loss of $\Delta\psi_m$ coincides with the massive entry of positively charged ions into the mitochondrial matrix driven by their electronegative nature and, in addition, also water flows into the mitochondrial matrix, causing an osmotic imbalance and leading to the swelling of the organelle and the rupture of the outer mitochondrial membrane (OMM).
In turn, this provokes the release into the cytosol of several factors that are normally confined within the intermembrane space, these proteins are involved in the effector phase of apoptosis (such as cytochrome C, AIF, SMAC/DIABLO and EndoG) into the cytosol (6) (7).
Since 1996 it has been discovered an evident physiological difference in cells undergoing apoptosis versus necrosis for what it concerns intracellular levels of ATP: when they are high, apoptosis can initiate and proceed, but when the energy level decrease the necrotic pathway is chosen for regulated cell death (RCD) (8).
Recently, it has been found, in adult cardiac myocytes, a different kind of MPT event with transient feature and with low conductance, named transient mPTP openings (tPTP) or MitoWinks. Its function has been associated to mitochondrial and cell survival as a physiological process that permits to reset mitochondria (9).

• Mitochondrial Permeability Transition Pore Complex

The last two decades have been invested in defining the precise molecular composition of the mitochondrial permeability transition pore complex (PTPC) but despite the intense experimental efforts the real composition is still unclear.
Since 1990s, single-channel electrophysiological recordings from rat liver mitoplast (mitochondria stripped of the outer membrane) defined a mitochondrial megachannel (MMC) activated by Ca^{2+} and inhibited by Mg^{2+}, Cyclosporin A, and ADP, probably

acting at matrix-side sites, such as mPTP. These results identified the existence of this pore that increase the conductance of the IMM during MPT (10) (11).
Shortly thereafter, the same group, has defined a voltage dependence of MMC very similar to that of VDAC (voltage-dependent anion channel), in fact, purified VDAC molecules reconstituted in planar bilayers or proteoliposomes formed a dimeric channel (12) so, they defined a model with two cooperating VDAC channels involved in mPTP formation and function plus presumably an adenine nucleotide translocator (ANT) dimer and a third component known to be part of the mitochondrial benzodiazepine receptor (mBzR) (13). For the first time it has been associated an OMM protein, VDAC, with a phenomenon that occurred in IMM, MPT, suggesting that this megachannel would be formed by different proteins in a big complex.
In a different work, in fact, researchers isolated the mBzR and defined the interaction with VDAC and ANT, OMM and IMM channel proteins enhancing the hypothesis that mBzR may act as transport site at the junction of the two mitochondrial membranes (14).
More evidences of these interactions in forming PTPC were emerged in 1996, when, in rat brain, it was documented the presence of an high molecular weight complex comprising VDAC, ANT, hexokinase 1 (HK1) and creatine kinase, mitochondrial 1 (CKMT1); complexes were incorporated into artificial bilayer membranes and showed a high conductance, asymmetrically voltage dependent and an ATP retaining ability (15). Furthermore, this PTP-like structure opening was Ca^{2+}-dependent and inhibited by ADP, ATP and glucose (16).

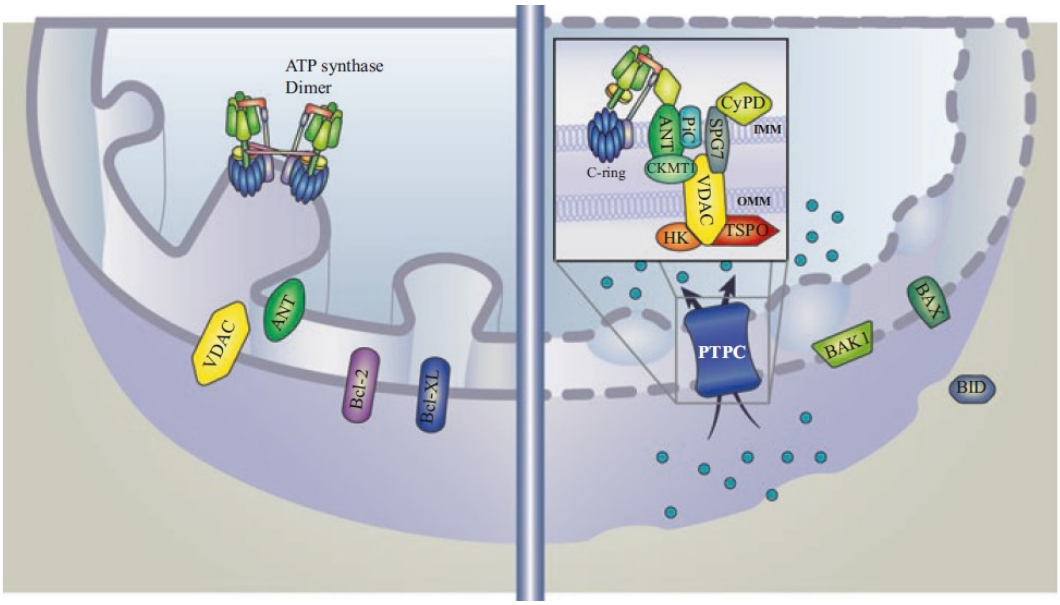

Figure 1. Hypothetical PTPC molecular structure. MPT is mediated by the opening of a supramolecular entity, called PTPC, assembled at the juxtaposition between mitochondrial membranes. Structural and functional studies show that multiple mitochondrial and cytosolic proteins intervene in the formation or regulation of the PTPC, yet the actual pore-forming unit of the complex remains elusive. These proteins include VDAC, ANT, HK, CYPD, PiC, TSPO, CKMT1. (Morganti C, Bonora M, Sbano L, Morciano G, Aquila G, Campo G, Wieckowski MR, Giorgi C, Pinton P (2018) The Mitochondrial Permeability Transition Pore. Mitochondrial Biology and Experimental Therapeutics).

Lately, another participant of the complex mPTP has found: cyclophilin-D (CYPD), it interacts with VDAC and ANT forming a complex at contact sites between the two membranes (17).
In 1998, purified ANT molecules reconstituted in proteoliposomes were found to form an oligomeric channel capable to induce the MPT (18).

At this point of knowledge, the first PTP complex model is composed by a supramolecular entity assembled at the interface between the IMM and the OMM by the physical and functional interaction of VDAC, ANT, HK1 and CKMT1, and CYPD is not part of the pore but only a regulator.
Actually, consequent evidences had changed the components of this first model.
In fact, through genetic modulation of ANT in mouse liver it has been discovered that mitochondria lacking ANT could still be induced to undergo MPT, resulting in release of cytochrome c and, in particular, hepatocytes without ANT remained competent to respond to various initiators of cell death, suggesting that ANTs are non-essential structural components of the PTPC, although they participate in regulation (19).
Analogously, it has been performed the deletion of the three VDAC genes and these knock-out mitochondria shown unaltered Ca^{2+}- and oxidative-stress-induced MPT and cell death, demonstrating that VDACs too are not essential for both MPT and Bcl-2 family member-driven cell death (20).
Another genetic study has been done on Ppif-/- mice, where mitochondrial CYPD had been inactivated: mitochondria derived were desensitized to Ca^{2+}, insensitive to Cyclosporin A (CsA), a well-known and potent inhibitor of the PTP, so, the PTP can form and open in the absence of CYPD, this protein is the target of CsA, and is able to modulates the sensitivity of the PTP to Ca^{2+} but not its regulation by the proton electrochemical gradient, adenine nucleotides, and oxidative stress (21).
CYPD has a crucial role in the process of MPT, regulating the opening of the complex, but it is mainly localized within the mitochondrial matrix so it is improbable its direct involvement in forming the pore; it is probably an auxiliary, modulatory component of the complex, which forms and has essentially the same properties even in Ppif-/- mitochondria (22).
Since 1965, inorganic phosphate is known to produce swelling of isolated mitochondria, it is an MPT-promoting metabolite, and the complex may possess a specific binding site (23).
In physiological conditions, inorganic phosphate is transported across the IMM by mitochondrial carrier including SLC25A3 (best known as PHC or PiC) and SLC25A24 (also known as APC1) (24): PiC imports inorganic phosphate into mitochondrial matrix coupled to either the co-import of H^+ ions or the export of OH^- ions, whereas APC1 exports ATP and Mg^{2+} ions.
For example, APC1 can regulate the matrix adenine nucleotide content, modulating the sensitivity of mitochondria to undergo MPT (25), in particular, it has been demonstrated its negative feedback control between cellular Ca^{2+} overload and mPTP-dependent cell death (26). Also PiC has been correlated to mPTP, in particular it binds CYPD and ANT controlling pore opening (27). This evidence has been enhanced also by a high-throughput genetic screen that demonstrated that PiC was able to interact with members of the permeability transition pore complex ANT and VDAC, and its binding to ANT was stabilized in the presence of apoptotic activators (28).
Purified PiC molecules reconstituted in liposomes has shown an action as coupled antiport and uncoupled uniport (29), suggesting a potential pore-forming role for PTP complex.
Actually, in 2012 it has been shown that PiC silencing doesn't affect neither mitochondrial Ca^{2+} accumulation nor mPTP opening (30), suggesting that PiC was not so essential for PTPC and MPT process.
In vivo models of mouse strains overexpressing or with decreased levels of mitochondrial PiC has demonstrated that mitochondria isolated from the hearts of these transgenic models compared to their controls presented no differences in Ca^{2+}-induced MPT,

indicating that PiC localized in mitochondria is not an essential component of the MPT pore (31); furthermore, PiC loss desensitize mPTP opening confirming its regulating activity (32).
SPG7, paraplegin matrix AAA peptidase subunit, was another genetic candidate to be a PTPC component: silencing experiments has led to the conclusion that this protein is necessary in Ca^{2+} and ROS-induced mPTP opening, in fact disruption of SPG7-CYPD binding impaired mPTP complex activity and revealed a role of SPG7 as a core component of the PTP at the OMM and IMM contact site (33).
In the last few years, through the fluorescence-imaging-based techniques developed in order to study MPT (34), another protein was investigated to the role of PTPC component: the mitochondrial F_1F_O ATP synthase, particularly the c subunit of the F_O domain (which in humans is encoded by three genes, ATP5G1, ATP5G2 and ATP5G3) (35), (36), (37).

- **Regulatory Components**

Different proteins have been shown to regulate the activity of the core PTPC (VDAC, ANT and CYPD composed), including cytosolic and mitochondrial proteins.
The translocator protein (18 kDa) (TSPO) is localized at the OMM and together with VDAC and ANT, OMM and IMM channel proteins, respectively, formed the mitochondrial benzodiazepine receptor (mBzR), an important transport sites at the junction of two mitochondrial membranes (14). Several different studies reported the effect of endogenous (38) and exogenous (39), (40) TSPO agonists to provoke MPT in isolated mitochondria. The effects of the different TSPO ligands on cell death exhibited a great degree of variability: these compounds might have a cytoprotective or cytotoxic role (41), (42), (43), (44).
Different kinases, such as CKMT1, HK1, HK2, glycogen synthase kinase 3β (GSK3β) and protein kinase Cε (PKCε) have physical interaction with core PTPC units suggesting a functional role as regulatory proteins. For example, CKMT1 is localized to the mitochondrial intermembrane space and it has been demonstrated its interaction with VDAC and ANT (15), (16) but also its function in phosphorylation of creatine, a reaction that is tightly coupled to oxidative phosphorylation and of consequence to the availability of ATP and ADP (45), (46): it has to be clarified if MPT-modulatory activity of CKMT1 originates from its physical interaction with the PTPC components or its catalytic activity.
Hexokinase isoforms I and II bind to OMM in large part by interacting with VDAC isoforms (47) and can control glycolytic metabolism and suppresses the release of intermembrane space proteins inhibiting apoptosis (48).
In fact, by inhibiting the association between HK2 and VDAC, through cell-permeant peptides or chemicals, cell undergoes the inhibition of glycolysis and the induction of MOMP (mitochondrial outer membrane permeabilization) (49), (50). However, it has been demonstrated that apoptosis induced by the HK2 peptide is not affected by genetic ablation of VDAC, suggesting that HK2 detachment from mitochondria transduces a mPTP opening signal that results in cell death independently from VDAC (51).
In vitro studies demonstrated that PKCε can directly bind and phosphorylate VDAC promoting HK2 binding and consequent mPTP opening inhibition (52).
At the same way, it has been demonstrated that GSK3β when activated can phosphorylate VDAC, inhibiting the binding of HK2 (53).
Furthermore, phosphorylation on Ser9, known to inhibiting activity of GSK3β, has been associated to suppression of mPTP opening due to reduction in physical interaction of ANT to CYPD (54).

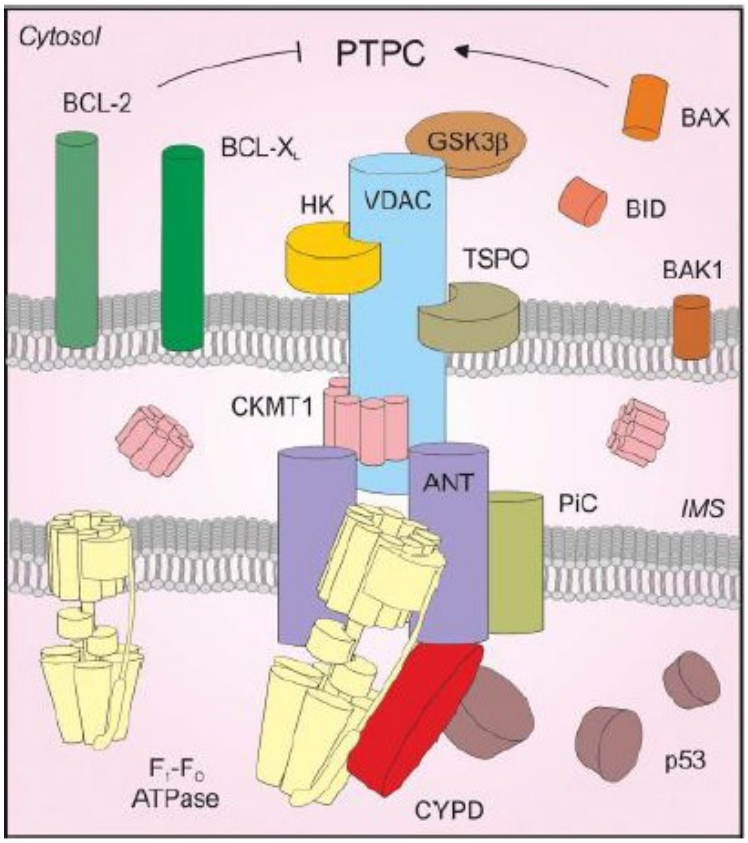

Figure 2. Possible configuration of the PTPC. MPT is mediated by the opening of a supramolecular entity assembled at the juxtaposition between mitochondrial membranes. Such a large multiprotein complex is commonly known as PTPC. Structural and functional studies performed throughout the past two decades suggest that multiple mitochondrial and cytosolic proteins intervene in the formation or regulation of the PTPC, yet the actual pore-forming unit of the complex remains elusive. These proteins include (but are not limited to): various isoforms of VDAC, ANT and HK, CYPD, PiC, TSPO, CKMT1, GSK3β, p53, as well as several members of the Bcl-2 protein family. The precise composition of the PTPC, however, remains elusive. Recent data indicate that the mitochondrial ATP synthase, in particular, the c subunit of the F_O domain, has a critical role in MPT. Whether the c subunit truly constitutes the pore-forming unit of the PTPC, however, has not yet been formally demonstrated (5).

It has consequently found that activation of the mitochondrial fraction of GSK-3α/β is connected to phosphorylation of CYPD, which in turn facilitates PTP opening (55).
Inhibition of GSK3β has been linked also with several upstream signal transducers, for example, via protein kinase B/Akt and mTOR/p70(s6k) pathways, PKC pathways, protein kinase cGMP-dependent (PKG), or protein kinase A pathways mediated MPT-inhibitory effects (56), (57), (58).
Several core components of the PTPC physically and functionally interact with components of the machinery that controls MOMP, including both pro- and anti-apoptotic members of the Bcl-2 protein family as well as p53, enhancing the importance of a tight relationship between this two regulated cell death processes for an extremely regulated crosstalk.
For example, some explanations derived from the identification of the interaction of Bcl-2 family of proteins, in particular Bax, Bak or BCL-xL, to VDAC in order to regulate the $\Delta\psi_m$ and the release of cytochrome c during apoptosis (59), (60), even if the MPT-modulatory activity of these proteins remains to be confirmed.
Other evidences derives from the demonstration that the proapoptotic molecule Bax and the constitutive mitochondrial protein ANT cooperate within the PTPC to increase mitochondrial membrane permeability and to trigger cell death (61), (62). Similarly it has been demonstrated for Bid: it acts on PTPC to induce apoptosis through its functional interaction with ANT (63).
In addition, BCL-2-associated agonist of cell death (BAD) has been associated to a sensitization of mPTP to Ca^{2+} through a Bcl-xL-sensitive and VDAC-mediated process due to a missed interaction between these two proteins (64).

Recent data indicate that in response to oxidative stress, a pool of p53 accumulates in the mitochondrial matrix and triggers mPTP opening and necrosis by physical interaction with CypD (65).
In conclusion, in spite of a significant experimental effort, the precise molecular composition of the PTPC remains elusive and further studies are required to obtain precise insights into this issue. Accumulating evidences indicate that the mitochondrial ATP synthase, the multiprotein complex that catalyzes the synthesis of ATP while dissipating the chemiosmotic gradient generated by the respiratory chain across the inner mitochondrial membrane, constitutes a central PTPC component.

- **Molecular composition of mitochondrial F_1F_O ATP synthase**

The mitochondrial F_1F_O ATP synthase is a large multiprotein complex consisting of a globular domain that protrudes into the mitochondrial matrix (F_1 domain, also known as soluble component) and an inner mitochondrial membrane-embedded domain (F_O domain); the domains are interconnected by a central and a lateral stalk (66). Mammalian ATP synthases contain 15 different subunits: α, β, γ, δ, ε, a, b, c, d, e, f, g, A6L, F6 and O (also known as oligomycin sensitivity-conferring protein, OSCP) forming a fully functional holoenzyme with a total molecular weight of ~ 600 kDa.

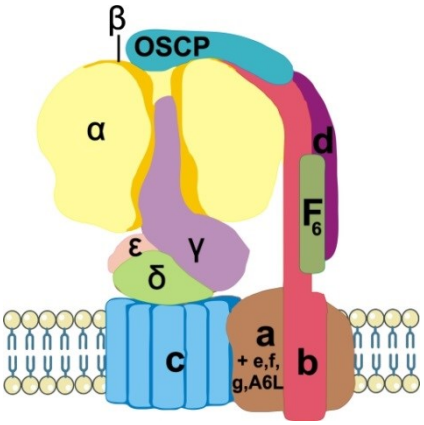

Figure 3. F_1F_O ATP synthase structural composition.

Through cryomicroscopy it has been determined the structure of intact ATP synthase from bovine heart mitochondria: the mammalian F_1 domain is composed of three α/β dimers and interacts with one copy of the γ, δ and ε subunits (central stalk) as well as with the b, d, F6 and O subunits (peripheral stalk), providing a physical bridge between the soluble and proton-translocating (F_O) components of the holoenzyme (67). The F_O domain, instead, is composed by a ring-shaped oligomer of c subunits stabilized by binding of cardiolipin, a lipid that is highly enriched in (if not confined to) the IMM (68).
C subunits in the so-called c-ring change in number across species (10 in humans) (69). Site-directed mutagenesis studies in *E. coli* have defined the components of the F_O domain as highly hydrophobic and with a critical carboxyl group (most often as part of a Glu or Asp residue) directly involved in the translocation of protons across the IMM (70). The other constituents of ATP synthase, that is, the a, e, f, g and A6L subunits interact with the c-ring: it is known that the a subunit physically interacts with the b subunit, while A6L appears to bridge F_O to other components of the peripheral stalk (69).
Two main sites of possible pore-formation in mitochondrial F_1F_O ATP synthase have been proposed: the monomer–monomer interface of the dimer and the c-ring by itself and in the context of mitochondrial F_1F_O ATP synthase.

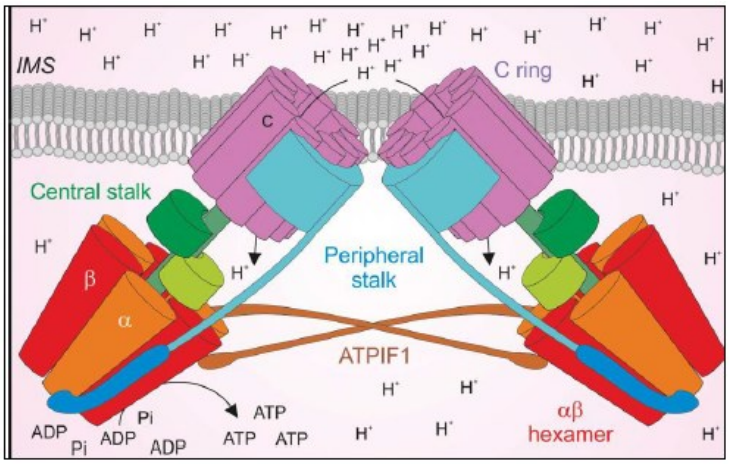

Figure 4. Molecular and supramolecular organization of the mammalian ATP synthase (5).

- **Mitochondrial F_1F_O ATP synthase as the possible molecular identity of the PTP complex**

The specific attentions in the mitochondrial F_1F_O ATP synthase as the possible molecular identity of the PTP complex has been started after the screening for potential CYPD binding partners. In particular, studies of native gel electrophoresis purification and immunoprecipitation of F_1F_O synthase revealed that CYPD associates to the lateral stalk of ATP synthase and modulates the activity of the complex (71). Furthermore, a consequent study has shown that CYPD binds the OSCP of the enzyme (35).
Most important, in this study, Giorgio et al. proposed that the PTPC forms from dimers of the F_1F_O ATP synthase: in fact, dimers excised and extracted from blue native gels and reconstituted into lipid bilayers have been reported to provoke currents that are consistent with the known electrophysiological properties of the PTPC. These data have not been reproduced by other groups and appear to contradict several studies demonstrating, for instance, the cytoprotective effects of inhibitor protein (IF-1) that promote F_1F_O ATP synthase dimerization (72). In 2016, Gerle suggested an uncomplicated proof of Giorgio's affirmations: the loss of PTPC-specific subunits during extraction from the excised gel bands or reconstitution into the black membrane, in fact, bovine F_1F_O ATP synthase comprises 17 different subunits of which the two F_O subunits DAPIT and 6.8 kDa are easily lost during extraction from the IMM (73).
The dimerization interface was visualized for the first time in 2015, at the α-helical level for the F_1F_O ATP synthase from the algae *Polytomella* (74) and no pore-forming site has been found, however, dimerization structures of bovine, *Drosophila* or yeast enzyme have not been reported yet. In conclusion, a more accurate examination of the monomer–monomer interface as a potential pore-forming site remains to prove. All the results described can't provide a robust evidence excluding a key role for F_1F_O ATP synthase dimers in the MPT. Only recently, our group reported a link to MPT induction and F_1F_O ATP synthase dimers dissociation and that stabilization of F_1F_O ATP synthase dimers by genetic approaches inhibits PTPC opening (75).

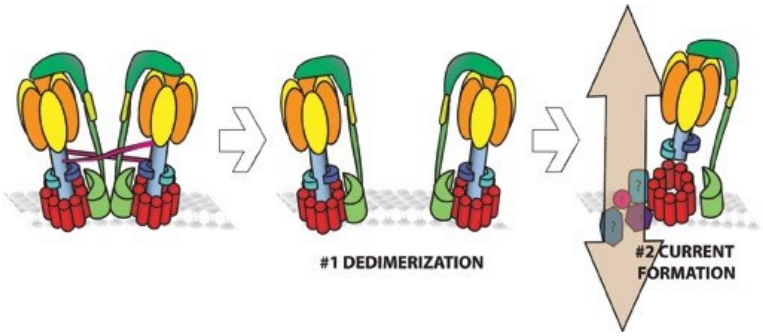

Figure 5. F_1F_O ATP synthase dimer dissociation plays a crucial role in MPT and allows PTPC opening. (75)

- **C subunit role**

The other possible option for the pore-forming entity within the components that make up the mitochondrial F_1F_O ATP synthase involves its proton-transporting c-ring: it possess a pore like shape with a diameter similar to the predicted pore diameter of the PTP. ATP synthase membrane rotors consist of a ring of c subunits whose stoichiometry is variable across different species (76). C-ring is structurally the best characterized sub-complex of the F_1F_O ATP synthase membrane domain, including numerous high resolution X-ray crystal structures from *Spirulina platensis* or *Saccharomyces cerevisiae* (77), (78).
C subunit protein contains an highly conserved glycine zipper domain fundamental for the tight disposition of c subunits within c-rings (79), in fact, variations of this motif of glycine repeats (GxGxGxGxG) in the first (N-terminal) α-helix can influence the stoichiometry and consequent structure of c-rings modulating ATP synthases functionality (76). C subunits of F_1F_O ATP synthase are encoded by three genes, ATP5G1, ATP5G2 and ATP5G3, and it has been shown that cells depleted of ATP5G1 or ATP5G3 exhibit reduced sensitivity to MPT-driven regulated cell death (36), (37).
In recent years different essential studies on c subunit of F_1F_O ATP synthase has been made by our group and in particular we provided experimental evidence that the c subunit plays a pivotal role in mPTP activity and mPTP formation, demonstrating a strong correlation between the mPTP functional state and c subunit expression.
In fact, in 2013, Bonora et al. through a study of genetic inhibition of F_1F_O ATP synthase different subunits demonstrated that c subunit constitutes an important component of the PTPC: in particular, it plays a critical role in the CsA-dependent opening of the PTPC induced by cytosolic Ca^{2+} increase, c subunit expression modifications act on mitochondrial fragmentation and this protein is able to control MOMP and cell death consequent to mPTP opening induced by oxidative stress in different cell lines (36).
In a subsequent work, our group confirmed that F_1F_O ATP synthase dimers dissociation is required for PTPC opening and c-ring conformation is essential for this process (75). These findings were confirmed by silencing studies on ATPIF1, a subunit of the F_1F_O ATP synthase known to promote dimerization (72) and on ATP5I, which has a motif of the transmembrane domain fundamental to the dimerization/oligomerization of ATP synthase complex in the mitochondrial membrane (80). These data obtained by two genetically distinct approaches indicate that stabilizing F_1F_O ATP synthase dimers limits PTPC opening and MPT and that the dissociation of dimers is a cause, not a consequence, of MPT. Furthermore, the dissociation of dimers is required for a correct conformation of c-rings to open PTPC and it has been demonstrated that c-ring-targeting agents are able to inhibit PTPC opening *ex vivo* in a model of cardiac reperfusion injury.
Taken together, these findings suggest that PTPC opening is a multistep process that involves disassembly of F_1F_O ATP synthase dimers and rearrangement of c-rings and that the c subunit of the F_1F_O ATP synthase may constitute a promising target for the development of novel cardio-, neuro-, or nephro-protective agents.
It is not to omit that some groups affirmed the opposite, through experiments with purified dimers of the ATP synthase reconstituted into lipid bilayers found out the opening of a channel with currents that were mPTP electrophysiological equivalent, so these results indicate that mPTP forms from dimers of the ATP synthase (35).
On the other hand, other independent groups have confirmed and extended our observations, for example Alavian et al. in 2014, demonstrated that the purified reconstituted c-rings created a voltage-sensitive channel, which persistent opening caused a strong depolarization of the IMM in cells. Furthermore c subunit overexpression

made cells more sensible to death whereas its depletion protected cells from Ca^{2+}-induced IMM depolarization and ROS-induced apoptosis (37). Indeed, major evidence for the so-called “c-ring hypothesis” is derived from other experiments on purified phosphorylated and non-phosphorylated forms of c subunit: this work has shown a role of c subunit as structural and/or regulatory component of PTPC and its activity might be modulated by Ca^{2+}-dependent phosphorylation (81).
In support of our hypothesis other evidences has shown that c subunit from purified mitochondria in presence of Ca^{2+}, inorganic polyphosphate (polyP) and polyhydroxybutyrate (PHB) can create ion channels with properties near to the native mPTP, moreover this channel complex increases during mPTP opening and can be decreased by CsA and RR (Ruthenium Red, a mitochondrial calcium uptake blocker), connecting Ca^{2+} and mPTP opening to this complex formed also by c subunit (82).
The c subunit is a hydrophobic protein with properties that are similar to those of lipids, and it is not expected to be able to form water-filled pores in its c-ring. Therefore, these data suggest that the c subunit is responsible for forming the Ca^{2+}-dependent channel with the help of polyP possibly serving as the hydrophilic coating of the pore (83). Therefore, several increasing evidence for the pivotal roles of c subunits in the MPT has been found (84).

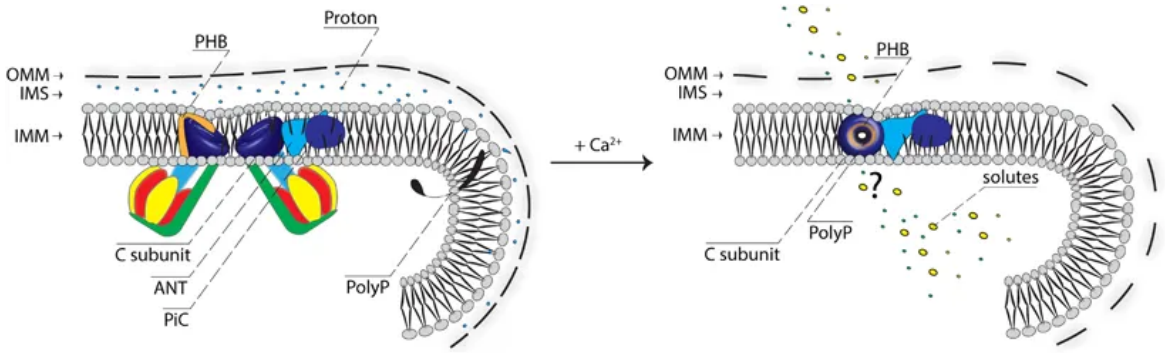

Figure 6. Hypothetical structure of the central conducting pore part. A portion of the mitochondrial structure is represented. In healthy cells (on the left), C subunit is part of the dimeric F_1F_O ATP synthase and contributes to ATP production (in blue – the C-ring). The model proposed (on the right) is that during Ca^{2+}-induced MPT, the C subunit associates with polyP (in black) and PHB (in orange) allowing the generation of a water-permeable channel. A question mark has been inserted in the figure because other rearrangements could be required (83).

Despite that, in 2017 Walker group discovered the MPT in the absence of c subunit, generating a clonal cell, HAP1-A12, in which ATP5G1, ATP5G2, and ATP5G3 were disrupted. These cells preserved the characteristic properties of the PTP even if lacking c subunit protein. These data are the results of a single cell clone, so clonal adjustment cannot be excluded. Indeed, they reported that HAP1-A12 cells assembled a vestigial ATP synthase, with intact F_1-catalytic and peripheral stalk domains and supernumerary subunits e, f, and g but without membrane subunits ATP6 and ATP8. The authors did not exclude the possibility that the PTPC could be associated with the ATP synthase complex, but they speculated that the most likely components available to form the pore were the b, e, f, and g subunits (85).
In 2013 Bonora et al. examined PTPC formation after c subunit silencing, demonstrating, for the first time, that the c subunit of F_O is required for MPT, mitochondrial fragmentation and cell death induced by mitochondrial Ca^{2+} overload and oxidative stress (37).
In addition it has been shown that both *in vivo* for the *E. coli* enzyme (86) both *in vitro* for reconstituted rotor rings (87) phospholipids occupy the internal lumen of the c ring in a lipid plug.

“C-ring hypothesis” has to prove the several interactions of the modulating molecular players of PTP and importantly how this lipid plug is removed or the diameter of the c-ring substantially widened, in particular, this opening occurs in a reversible manner and while exhibiting several sub-states of conductance.
CYPD was not shown to interact with the c-ring, but rather it binds to the OSCP, so the c-ring by itself appears too simple to allow for regulation and modulation. Therefore, the c-ring in the context of either monomeric or dimeric F_1F_o ATP synthase is a more likely candidate for a physiological relevant site of pore formation. In the intact mitochondrial F_1F_o ATP synthase the central stalk (CS) makes tight contact with the c-ring at multiple sites, but it does not seal it off from bulk solution and keeps the c-ring's lumen connected to the matrix (88). That leaves the lipid plug as the only barrier to pore formation. Prolonged high matrix Ca^{2+} enlarges the c-ring leading to conformational rearrangement of c subunits accompanied by diameter widening of the c-ring suggesting a way to pore-formation (37). This capability of c-ring to deform might be supported by different evidences (89), (90), but direct structural evidence for this kind of flexibility, however, has not been reported yet.
Another potential site for pore formation has been found at the interface between the c-ring and the a subunit: electron cryomicroscopy (cryoEM) studies of the *Polytomella* F_1F_o ATPases dimer have revealed a hairpin of long, horizontal, membrane-intrinsic α-helices in the a subunit next to the c-ring rotor that are capable to create channels in the membrane that provide access to the proton-binding sites in the rotor ring (91). Despite this, another group has investigated mPTP in cells devoid of mitochondrial DNA (ρ(0) cells), which encodes the a and A6L subunits, and found out a functional mPTP, suggesting that these two subunits are not part of the complex.
More recently it has been proposed a different model: the death finger model, here, movement of a p-side density that connects the lipid-plug of the c-ring with the distal membrane bending F_O domain allows reversible opening of the c-ring and structural cross-talk with OSCP and the catalytic (αβ)(3) hexamer (73). However our group has produced grounded data indicating that MPT involves the dissociation (not the association) of F_1F_o ATP synthase dimers in combination with the formation of poorly selective pores across the IMM by c-rings.

- ## mPTP opening inhibitors and c subunit

Extensive effort has been invested in the synthesis and testing of new mPTP opening inhibitors, such as substituted cinnamic anilides, with an activity additive with that of CsA, suggesting for a molecular target different from CYPD (92). These compounds has been tested in order to attenuate opening of the mPTP and limit reperfusion injury in a rabbit model of acute myocardial infarction. Another compound, GNX-4728, has been tested in an amyotrophic lateral sclerosis (ALS) animal model and this mPTP-acting drug has increased the survival of ALS mice protecting against motor neuron degeneration and mitochondrial degeneration (93). These are only two studies to cite in order to enhance the importance of a clear knowledge of mPTP functioning and composition, in particular because this complex must be a molecular target in several pathologies or metabolic impairments and finding small molecule drug candidates might be decisive.
To the best of our knowledge, none of these inhibitors were designed to target the c subunit expressed in eukaryotic cells or for cardioprotective purposes in the treatment of myocardial infarction (MI). However, Danshensu (DSS), the effective component of *Salvia miltiorrhiza* (Danshen) a traditional Chinese herb, has been widely used in clinic for

treatment of cardiovascular diseases in China. In a 2013 study, they reported that Danshensu modulated c subunit protein expression and provided significant cardioprotection against myocardial I/R injury, and the potential mechanisms of suppression of cardiomyocytes apoptosis might be through activating the PI3K/Akt and ERK1/2 signaling pathways (94).

Of our interest, among ATP synthase inhibitors, oligomycin A was identified in 1958 (95). Its presence is sensed by a subunit important for the functional and structural coupling between F_O and F_1: the OSCP. Recently, an important role of OSCP as a site of interaction with CYPD, a matrix protein that can modulate mPTP opening, was discovered. Intriguingly, in the early 2000s, a report described the potential of oligomycin A to inhibit mPTP opening induced by selenite, in fact it inhibited the selenite-induced cytochrome c release and $\Delta\psi_m$ loss, showing that F_1F_O ATPase was important in selenite or Ca^{2+}/P_i-induced MPT (96). Furthermore, oligomycin A has been showed an additive effect on cyclosporine A (CsA)-dependent mPTP activity (97).

Therefore, an high-resolution crystal structure model has defined a binding of oligomycin A to the c ring of yeast mitochondrial ATP synthase: the carboxyl side chain of Glu59, which is essential for proton translocation, forms an H-bond with oligomycin via a bridging water molecule but is otherwise shielded from the aqueous environment, in particular, the amino acid residues that form the oligomycin-binding site are 100% conserved between human and yeast (98).

With the aim of identifying a new pharmacological approach for the treatment of I/R-related damage, in the first chapter of this thesis, they are described the discovery, optimization, and structure−activity relationship (SAR) studies of the first small molecule mPTP inhibitors able to target the c subunit of the F_1F_O-ATP synthase complex. These compounds, which are based on a 1,3,8-triazaspiro[4.5]decane scaffold, may lead to the development of new cardio/neuroprotective agents for the clinical management of ischemic events.

2. Mitochondria in Ischemic Heart Diseases

Given mitochondria's importance in cellular physiology, mutations both in mitochondrial and nuclear DNA might lead to genetically heterogeneous group of mitochondrial disorders (99) as shown by the fact that the same mutation led to different pathological phenotypes in tissue specificity or age of patients, this situation is also linked to the level of heteroplasmy of mtDNA in mitochondria's pool (100).

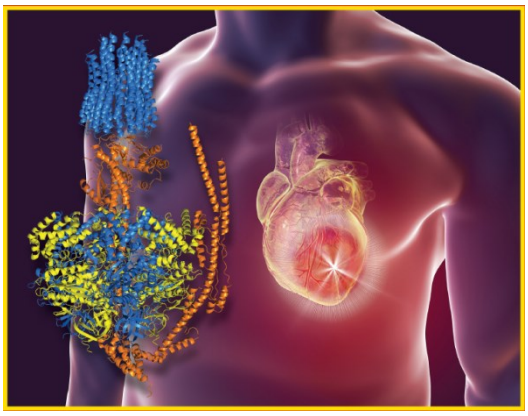

Figure 7. Cover journal of (101)

Furthermore mitochondrial dysfunctions have been found in a plethora of diseases, from metabolic disorders to neurodegenerative diseases: in particular this chapter has the purpose to explain the role of mitochondria in ischemic heart disease (IHD).
In cardiomyocytes about 35% of the total cell volume is constituted by the mitochondrial network (102), this is due to the large energetic consumption of this type of cell for their contractile capacity and to the meticulous regulation of electrical conduction depending from Ca^{2+} homeostasis. The strong importance of mitochondria in cardiomyocytes has been recently underlined by Hom and colleagues who found out a connection between mPTP and cardiomyocyte development: the state of opening of this pore can guide cardiac mitochondria maturation in structure and function and can control myofibrillar organization (103). Moreover, during ischemia a series of intracellular changes take place and they are accompanied by opening of the mPTP, loss of $\Delta\psi_m$ and impairment in ATP production.
Then nowadays it has been necessary to overcome existing therapies for heart failure (HF) in order to act directly on molecular impairment inside the cardiomyocytes: mitochondrial dysfunction has been identified as a target of study and an innovative way for patient treatment (104). Therefore studying mitochondria and mPTP in particular might produce advantageous information for the treatment of several pathologies, in particular cardiovascular diseases such as myocardial infarction, cardiomyopathies, hypertension, atherosclerosis, characterized exactly by an impaired mitochondrial function (105), (106).

- ## Ischemic heart diseases

According to the World Health Organization, ischemic heart diseases (IHD) are the leading cause of death, life-years lost and disability worldwide, contributing to over 7.2 million deaths annually (107), (108), (The World Health Organization, The top ten causes of death fact sheet. http://www.who.int/mediacentre/factsheets/fs310/en/index.html). IHD is not only a disease of the old people in rich countries, but also several studies indicate an impact on working-age adults and it is an increasing trouble in low- and middle-income countries (109), (110). A positive fact is that the mortality due to IHD has declined over the past four decades in western countries on the one hand thanks to significant progress in therapy and on the other linked to reduction of risk factors and to lifestyle improvements. In fact, this type of pathology is complex and multifactorial: several studies has linked IHD both to genetic and environmental factors such as physical activity, hyperlipidemia, hypertension, and smoking (111).

In Myocardial Infarction (MI), timely reperfusion strategies are the gold standard in the treatment of patients affected and most of the time are ensured by primary percutaneous interventions (PCI) (112). An ST elevation MI, also termed STEMI, mostly occurs when the thrombus formation promotes a complete occlusion of an important coronary vessel, leading to severe consequences as myocardial necrosis and cell death. This type of MI is life-threatening and despite in most cases is treated promptly and PCI is effective, a non-negligible amount of patients develop large MI and subsequent heart failure (HF).
Hausenloy and co-workers have demonstrated how important are the first minutes upon revascularization in limiting infarct size (IS) if mPTP inhibitors are timely perfused (i.e., sanglifehrin-A) (113), (114). This protection is lost if 15 minutes elapse without mPTP inhibitor administration defining a critical cardioprotective time window for interventions (115), (116).
The focus of this thesis is on mPTP, which opening causes an important collapse of the $\Delta\psi_m$, the depletion of adenosine triphosphate (ATP) stores and mitochondrial swelling (117) that accelerate tissues injury. For these reasons, the entity of mPTP opening may be considered as an adjunctive "risk factor" in the severity of reperfusion damage progression (118), (119) and it may differ among patients, thus it is important to be evaluated.

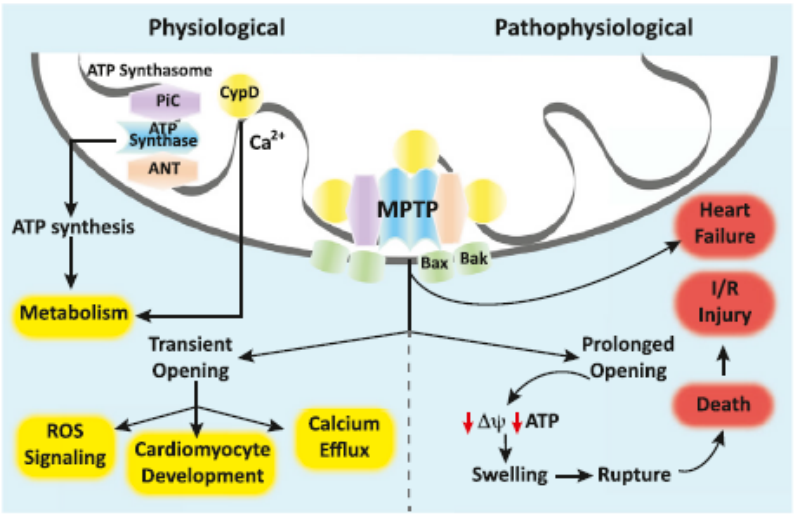

Figure 8. Physiological and Pathophysiological Roles of the mPTP in the Heart.
Transient opening of the mPTP is implicated in ROS signaling, cardiomyocyte development, and mitochondrial Ca^{2+} efflux that affects metabolism. Key components of the mPTP (PiC, ANT, and the F_1F_O ATP synthase) comprise the ATP synthasome, thereby providing a direct link to mitochondrial energy metabolism. Prolonged mPTP opening leads to loss of $\Delta\psi_m$, cessation of ATP synthesis, mitochondrial swelling, rupture, and death.

- ## Molecular mechanism of Ischemia and Reperfusion Injury

IHD occurs when cardiac myocytes are unable to obtain a sufficient oxygenated blood or in general in case of an increased myocyte metabolic demand and there is a failure of supply of oxygen delivery (120) caused normally by a plaque erosion or rupture or dissection of an atherosclerotic coronary artery. The detrimental effects of coronary occlusion depends on magnitude and duration of the arrest of blood flow and in order to defend the most part of tissue it is essential to restore the blood flow immediately: however reperfusion can exacerbate the damage leading to uncontrolled cell death, this event is usually known as ischemia-reperfusion injury (I/R Injury) and can have significant effects on clinical outcome of the patient (121), (122).

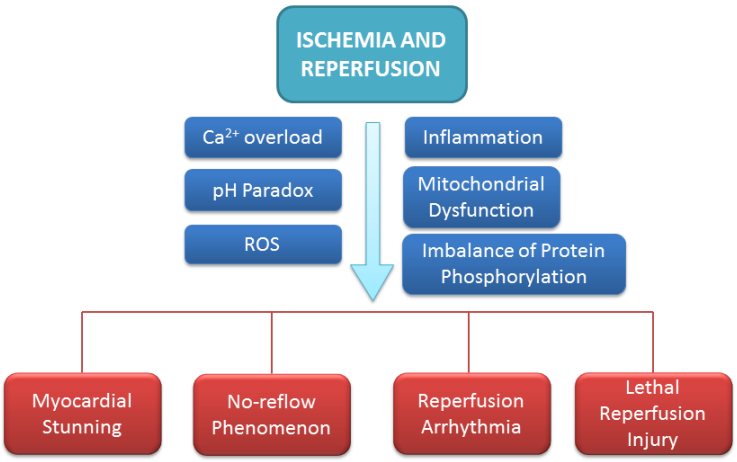

Figure 9: Schematic illustration of the mediators and consequences of ischemia/reperfusion injury

At molecular level in cardiomyocytes oxygen deprivation leads to mitochondrial respiratory chain function blockade, leading to a failed production of ATP, which is indispensable for cellular energy metabolism (123), (124). In this condition, it occurs the switch to anaerobic glycolysis to produce more ATP causing accumulation of lactate and hydrogen ions dropping down cellular pH and leading to metabolic acidosis. In order to restore physiological pH and ionic balance, progressively the plasma membrane Na^+/H^+ exchanger extrudes H^+ outside the cell and Na^+/K^+ ATPase try to remove excessive cytosolic Na^+ (125) but ATP shortage leads unavoidably to Na^+ accumulation, activation of the sarcolemmal Na^+/Ca^{2+} exchanger and intracellular Ca^{2+} overload (126). In particular, Ca^{2+} is buffered via mitochondrial calcium uniporter (MCU) thanks to negative ψ_m to drive uptake into the matrix: mitochondrial Ca^{2+} overload is an event deeply linked to myocardial I/R injury (127), (128). Also endoplasmic/sarcoplasmic reticulum Ca^{2+} handling is impaired: SERCA ATPase is unable to reuptake Ca^{2+} into ER/SR while ryanodine receptor release is augmented (129), (130), (128).

It is important to underline that it has been demonstrated that mPTP is closed during ischemia and its opening occurs only during reperfusion in response to ionic and metabolic changes (131).

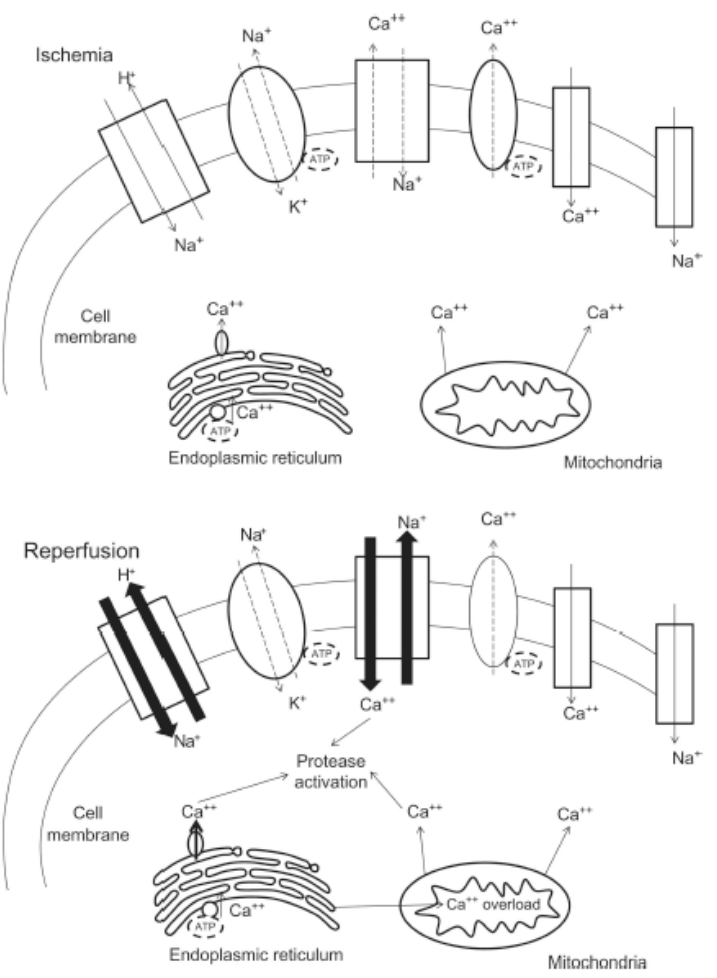

Figure 10: Major pathologic events contributing to ischemic components of tissue injury (132).

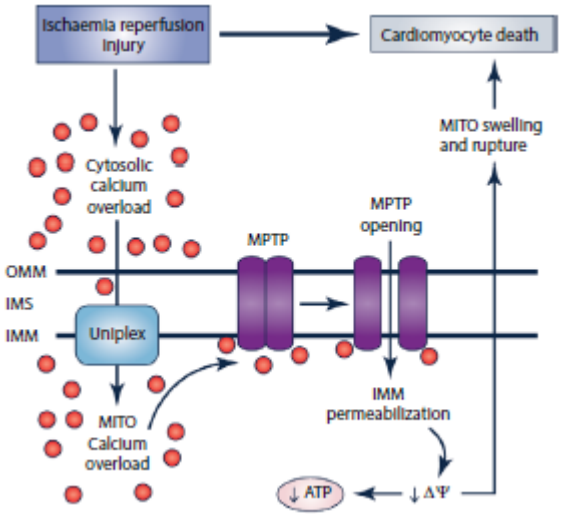

Figure 11. Ca^{2+} overload-induced cell death in the heart. Cardiac I/R injury results in cytosolic Ca^{2+} overload. The uniplex transports Ca^{2+} into the mitochondrial matrix, resulting in activation and opening of the mPTP. mPTP opening causes IMM permeabilization, loss of $\Delta\psi_m$ also causes mitochondrial swelling and rupture, which ultimately results in cardiomyocyte death.

Years ago, taking advantage from the tritiated glucose entrapment in mitochondria (also known as Hot-DOG technique), Griffiths and Halestrap discovered that mPTP is maintained closed during ischemia episodes and that opens only at the time of reperfusion; indeed, the key inhibitory effect exerted by acid pH generated during ischemia blocked the mPTP in its closed conformation despite the presence of other inducers.

In fact, ischemia condition is characterized by low pH that inhibits mPTP opening, restoration of blood flow causes a series of events after around 2 minutes of reperfusion that promote mPTP opening: intracellular pH returns to normal, mitochondria recover their function and Ca^{2+} is accumulated (133), (134), (135). mPTP is a pore of 1.5 kDa and during its opening H^+ can pass back into the matrix and ψ_m is dissipated, ATP synthesis is blocked and mitochondrial respiratory chain is uncoupled, finally, mitochondria start to swell because of water entry (136), (137).

Furthermore, upon reperfusion oxygen recovery determines oxidative stress by reducing nitric oxide (NO) bioavailability that consequentially reduces myocardial blood flow reperfusion through the coronary circulation.

Xanthine oxidase, NADPH oxidase (Nox) and mitochondria participate in reperfusion-induced oxidative stress producing reactive oxygen species (ROS) (138). Exactly oxidative stress and mitochondrial Ca^{2+} overload are found to participate intensively to I/R injury and are known activators of mPTP opening (139), conditioning cell death in response to I/R.

The implication of subunit c in MI is suggested by our findings showing the significant correlation between the circulating protein in the serum of STEMI patients and several surrogate markers of myocardial reperfusion (140) and that its selective targeting in the first 10 minutes of revascularization protected the ischemic rat heart from the impairment of the cardiac performance and the excessive apoptosis (101).

Therefore studying c subunit in order to found a therapeutic approach that limit I/R injury might be an innovative way to ameliorate STEMI patients clinical outcome.

- **Endogenous cardioprotection processes to reduce I/R Injury**

During the last decade, a great number of efforts has led to several clinical trials with the aim of limiting IS e and reducing I/R injury through different approaches.
A useful process of endogenous cardioprotection to decrease I/R injury in heart without using pharmacological interventions is to pre-condition with transitory ischemic episodes before undergoing to prolonged ischemia, this method is known as ischemic pre-conditioning (IPC) and it has been demonstrated in 1986 by Murry et al. (141). IPC has been associated to mPTP opening inhibition in Langendorff-perfused rat heart after global ischaemia enhancing pore closure as hearts recover (142), (143).
Similarly, short-term periods of ischemia performed just at the time of reperfusion can reduce IS, this method is called post-conditioning and its anti-ischemic protection has been linked to mPTP opening inhibition in *in vivo* experiments on rabbits (144) and it has been demonstrated to be as effective as IPC in reducing final IS in dogs (145). The first human study was performed in 2005 in a small group of STEMI patients and the results suggest a protective effect of post-conditioning treatment (146). A different study has demonstrated in STEMI patients that post-conditioning at the time of PCI reduce IS and edema (147). There are other small trials, but not all, that have reported beneficial effect on IS reduction by post-conditioning (148). However, protective effects of post-conditioning have not been demonstrated in a largest randomized clinical trial such has the POST (Effects of Postconditioning on Myocardial Reperfusion in Patients With ST-Segment Elevation Myocardial Infarction) of 2013 (149).

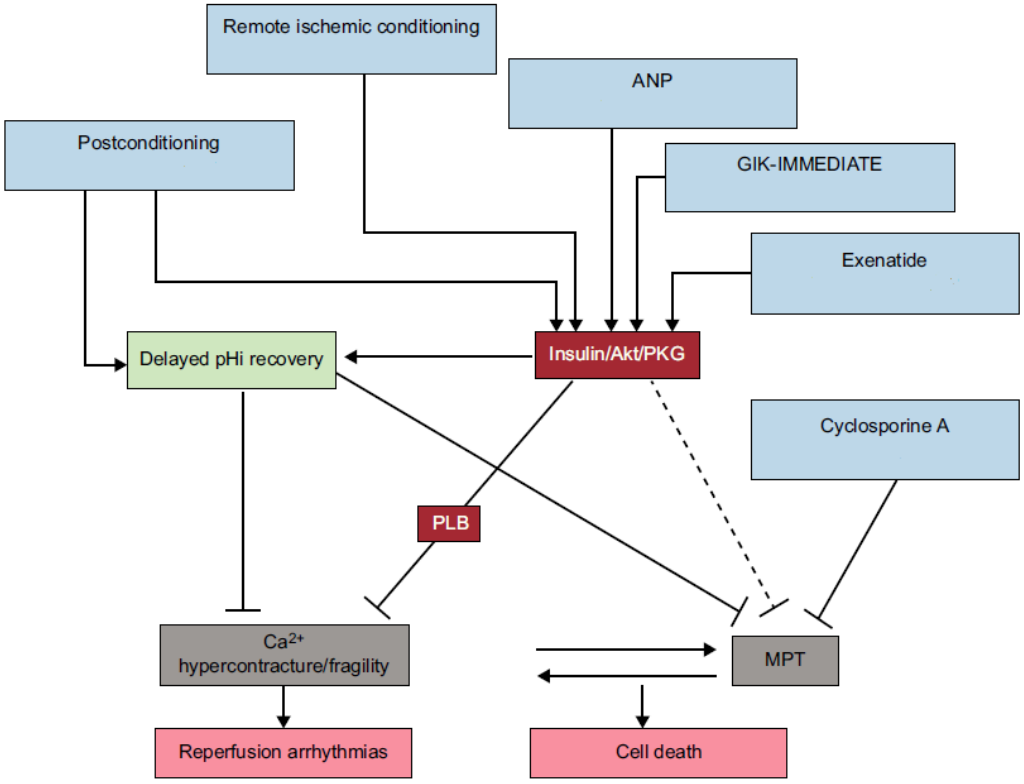

Figure 12. Some of the more promising strategies for combating reperfusion injury, by the mechanism of cell death interrupted. ANP, atrial natriuretic peptide; GIK, glucose-insulin-potassium; MPT, mitochondrial permeability transition; pHi, intracellular pH; PKG, protein kinase G; PLB, phospholamban.

At molecular level the cardioprotection of post-conditioning is linked to the delay of the normalization of intracellular pH during initial reperfusion, this acidosis inhibits hypercontracture, mPTP opening, calpain-mediated proteolysis, and gap junction-mediated spread of injury (150). This delayed normalization of intracellular acidosis during reperfusion after post-conditioning has been associated also to cGMP/PKG pathway, probably via PKG-dependent inhibition of Na^+/H^+-exchanger (151).
Another form of endogenous protection has been recently described: remote ischemic conditioning (RIC) consists in remote induction (generally in the extremities) of intermittent myocardial ischemia immediately before or in the first few minutes of reperfusion. It has been tested in animal models (152), (153) and compared to post-conditioning it is simpler, without the hazards and logistics of multiple coronary artery balloon inflations but molecular mechanisms involved in RIC cardioprotective effects are still unclear (154), (155). Furthermore, RIC's therapeutic potential has been tested against acute I/R injury in a number of different noncardiac organs and tissues including the kidneys, lungs, liver, skin flaps, ovaries, intestine, stomach and pancreas (156) and has shown protective effects after different types of cardiac surgery interventions (157), (158), (159), (160).

- ## Pharmacological treatments to reduce I/R Injury

In addition to endogenous protection of myocardial conditioning, it has been lately developed several pharmacological interventions to reduce I/R injury with different degrees of success.
For example among β-blockers, pre-clinical evidences of IV metoprolol on pig model of infarction with protective effects when administered before reperfusion (161), (162) has led to human METOCARD-CNIC (Effect of Metoprolol in Cardioprotection During an Acute Myocardial Infarction) trial which has shown significant smaller infarcts in early presenters (<6 h from STEMI onset) with long-term benefits (163), (164). In fact, in order to confirm these evidences, a much larger study named COMMIT (ClOpidogrel and Metoprolol in Myocardial Infarction Trial) on STEMI patients found out that early intravenous then oral metoprolol administration reduces the risks of reinfarction and ventricular fibrillation, but augments the occurrence of cardiogenic shock (165). A recent and in process trial (EARLY-BAMI) is going to figure out the effect of intravenous metoprolol administration before primary PCI for STEMI on myocardial infarct size as measured with MRI at 30 days (166).
As we described before, cGMP/PKG pathway controls the recovery of intracellular pH, but it has also direct effect on Ca^{2+} concentration and mPTP opening (167) and is deeply involved in post-conditioning protection. A pharmacological approach to modulate this pathway is through the activator of PKG: atrial natriuretic peptide (ANP) was used in a clinical trial on STEMI patients and it has shown protective effects such as lower infarct size, fewer reperfusion injuries, and better outcomes (168).
Several trials has studied the potential therapeutic role of glucose during myocardial infarction. *In vivo* administration of insulin in rats has been linked to Akt activation through the PI3-kinase-dependent mechanism and can reduce post-ischemic myocardial apoptotic death (169).
As a consequence of these evidences, it has been started several clinical trials with glucose/insulin/potassium (GIK) and the results indicate that GIK administered at the time of reperfusion, can reduce mortality in STEMI patients particularly in a high dose (170). Recently, the IMMEDIATE (Immediate Myocardial Metabolic Enhancement During Initial Assessment and Treatment in Emergency Care) trial tested a combined administration of GIK with beneficial effects on the subgroup of STEMI patients (171).

A different trial has tested exenatide, a glucagonlike peptide-1 analog, that has shown an effect at the time of reperfusion in patients with STEMI undergoing PCI with a significant increase in myocardial salvage (172) in particular, a *post hoc* analysis has shown that this effect occured only in patients with short-duration of ischemia (173). Also liraglutide, another glucagonlike peptide-1 analogue, administered to STEMI patients treated with PCI has improved left ventricular ejection fraction at 3 months (174).
On STEMI patients it has been developed a trial (INFUSE-AMI) to test the effect of abciximab, a glycoprotein IIb/IIIa inhibitor, and/or thrombectomy on IS: intracoronary administration of abciximab significantly reduced IS (175).
Also adenosine, a degradation product of adenosine monophosphate, acts via Akt activating cGMP/PKG pathway and several trials take advantage of its mechanism of action. For example, the Acute Myocardial Infarction STudy of ADenosine (AMISTAD) trial has tested adenosine as an adjunct to thrombolysis and it resulted in a significant reduction in IS (176) but AMISTAD-II, 6 years later, has investigated the effect of intravenous adenosine on clinical outcomes and IS in STEMI patients undergoing reperfusion therapy and it showed no significant differences on clinical outcomes between placebo and treated groups (177). Another trial (PROMISE) has investigated the intracoronary administration adenosine at the time of PCI with beneficial effect on IS, microvascular obstruction and post-infarction remodeling only in patients receiving primary angioplasty with shorter ischemic times (< 200 min) after the onset of pain (178).

- ## Translational aspects of mPTP inhibition to reduce I/R Injury

The essential involvement of mPTP opening in I/R injury (131) and in cardiac myocytes cell death has led to focused therapies on inhibition of mPTP opening in order to obtain a cardioprotective effect. Since 1991, a chemical inhibitor of CYPD, CsA, has been discovered involved in prevention of mitochondrial dysfunction induced *in vitro* by Ca^{2+} overload and protection against anoxia-induced injury mediated in isolated cardiac myocytes (179). A lot of pharmacological data have shown the protection of CsA pretreatment in different organs: for example CsA can significantly reduce apoptosis in liver following I/R injury (180); low-dose pretreatment has been shown a beneficial effect also on rat kidneys after I/R improving functional parameters by lowering oxidative stress (181). A pilot clinical trial of 2008 has shown that administration of CsA at the time of reperfusion attenuates lethal myocardial injury measured by different parameters such as the release of creatine kinase and troponin I and improving magnetic resonance imaging (MRI) results on day 5 after infarction (182). The same group of patients has been followed up at 6 months after infarction and the reduction in IS has been maintained 6 months post-treatment, moreover patients showed no negative effects on left ventricular (LV) remodeling (183). Furthermore, additional evidences have been added by a 2014 clinical study in patients undergoing aortic valve surgery: at time of reperfusion CsA administration has beneficial effect against I/R injury, reducing cardiac troponin I levels (184).
Lately, another CYPD binding compound, named Sanglifehrin A, has been identified as a potent inhibitor of the mPTP and I/R injury of the heart *in vivo*, via Langendorff perfused rat heart (185). Debio 025, another CYPD inhibitor has been demonstrated to improve dystrophic condition in a mouse model of Duchenne muscular dystrophy (DMD) thanks to its mPTP regulative activity (186).

Novel derivative of cyclosporin A, such as FR901459, has been shown to exert neuroprotective effects, via the inhibition of mPTP formation both for *in vitro* mitochondrial damage and for *in vivo* brain damage in cerebral ischemia models (187).
Baines et colleagues demonstrated that mice lacking CYPD gene are protected from I/R-induced cell death *in vivo* in addition their mitochondria extracted from liver, heart and brain are resistant to mitochondrial swelling and permeability transition; whereas mice CYPD-overexpressing show mitochondrial swelling and a strong cell death tendency (188). Others *in vivo* works on CYPD-deficient mice confirmed both functional and morphological protection in mice following I/R injury in several organs, such as kidney and brain (189), (190). Genetic *in vivo* studies have confirmed the inhibition of mPTP opening by inducible and cardiac-specific deletion of the mitochondrial phosphate carrier (PiC) leading to attenuated cardiac I/R injury (32).
Therefore component or regulators of mPTP can be putative targets for new pharmacological therapies for I/R injury treatment in order to reduce uncontrolled cell death.
In Chapter 1 is shown the discovery of a series of small-molecule mPTP opening inhibitors that targets the c subunit of the F_1F_O ATP synthase complex: these compounds have beneficial effects in a model of MI, with decreased apoptotic rate in the whole heart and overall improvement of cardiac function upon administration during reperfusion. Furthermore these compounds did not show off-target effects at the cellular and mitochondrial levels so they might be used in the treatment of reperfusion damage in myocardial infarction (101).
Since MI is a multifactorial disease in which both environmental factors and genetic profiles play a key role in its onset and development (191), (192), a genetic link between mPTP and reperfusion damage is a fascinating but still lacking topic.
In Chapter 2, to fill this gap, our purpose was to understand if the mPTP opening at reperfusion time could be also due to genetics determinants. In summary, because of the poor knowledge about mPTP and I/R injury in patients affected by MI and considering the need of additional therapies to support the standard clinical practice to reduce I/R injury, our aim was to investigate how mPTP is related to I/R injury in STEMI patients and how it can be easily assessed, as obtaining heart samples is extremely difficult or impossible. In addition, we also investigated whether genetic determinants of subunit c may contribute to the worsening of the mPTP-mediated I/R injury.

Chapter 1.

Discovery of Novel 1,3,8-Triazaspiro[4.5]decane derivatives that target the c Subunit of F_1F_O Adenosine Triphosphate (ATP) Synthase for the Treatment of Reperfusion Damage in Myocardial Infarction

Abstract

Mitochondrial permeability transition (MPT)-driven apoptosis is a type of programmed cell death during which the inner mitochondrial membrane (IMM) exhibits increased permeability with a consequent osmotic influx of solutes in the mitochondrial matrix. This event is mediated by the mitochondrial permeability transition pore complex (PTPC), a membrane multiprotein platform composed of pore-forming parts and modulators that contribute to its conformational state and, thus, to its mechanism of action.

In two previous studies, we provided experimental evidence that the c subunit of F_1F_O ATP synthase plays a pivotal role in mitochondrial permeability transition pore (mPTP) activity and mPTP formation, demonstrating first, a strong correlation between the mPTP functional state and c subunit expression; and second, the multi-step nature of the mPTP opening by ATP synthase dimers disassembly and c-ring conformational arrangements.

Recent cardiology research studies have reported a key role for mPTP opening in the progression of myocardial cell death secondary to reperfusion. Since up to 50% of the final infarct size is due to ischemia-reperfusion injury, targeting the PTPC could be a valuable adjunct in reducing infarct size.

In this first project, we validated a new pharmacological approach as an adjunct to reperfusion in myocardial infarction (MI) treatment and described the discovery, optimization, and structure−activity relationship (SAR) studies of the first small-molecule mPTP opening inhibitors based on a 1,3,8-triazaspiro[4.5]decane scaffold that targets the c subunit of the F_1F_O ATP synthase complex.

We identified three potential compounds with increased mPTP inhibitory activity at low concentrations, a specific localization to the mitochondrial compartment and beneficial effects in an *ex vivo* model of MI, they did not show off-target effects at the cellular and mitochondrial levels; moreover, the compounds preserved mitochondrial ATP content despite interacting with the ATP synthase complex.

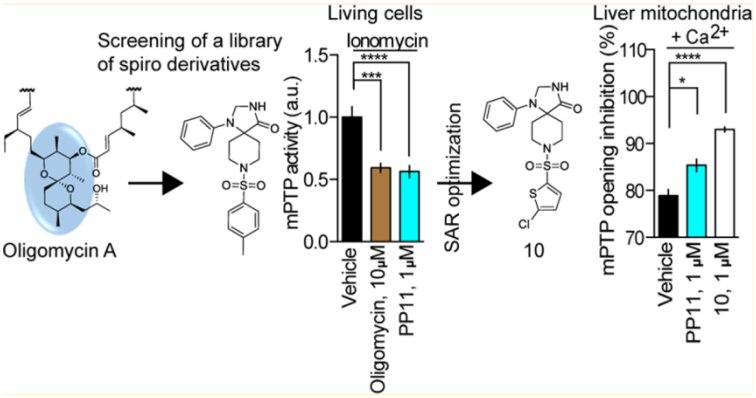

Figure 13. Rationale of the project.

Riassunto

Il processo di apoptosi provocata dalla transizione di permeabilità mitocondriale è un tipo di morte cellulare programmata durante il quale la membrana mitocondriale interna (IMM) mostra un'aumentata permeabilità con un conseguente influsso osmotico di soluti nella matrice mitocondriale. Questo evento è mediato dal complesso proteico del poro mitocondriale di transizione della permeabilità (PTPC), una piattaforma multiproteica di membrana composta da porzioni componenti il poro e da modulatori che contribuiscono allo stato conformazionale e al conseguente meccanismo di azione del poro stesso.
In due studi precedenti, il mio gruppo di ricerca ha dimostrato che la subunità c del complesso F_1F_O ATP sintasi ricopre un ruolo fondamentale nell'attività e nella formazione del poro di transizione mitocondriale (mPTP), prima di tutto dimostrando una forte correlazione tra lo stato funzionale dell'mPTP e l'espressione della subunità c, in particolare tra la modalità a diversi passaggi con cui avviene l'apertura dell'mPTP dovuta al disassemblaggio dei dimeri di ATP sintasi e da riarrangiamenti conformazionali del c-ring.
Studi recenti di cardiologia hanno riportato il ruolo chiave dell'apertura dell'mPTP nella progressione della morte delle cellule del miocardio in seguito a riperfusione. Infatti più del 50% dell'area finale dell'infarto è dovuta al danno da ischemia e riperfusione, quindi bersagliare il PTPC può essere un'ottima strategia per ridurre l'area infartuata finale.
In questo primo progetto, abbiamo validato un nuovo approccio farmacologico che può essere addizionato alla riperfusione nel trattamento dell'infarto del miocardio e qui vi si descrive la scoperta, l'ottimizzazione e gli studi di relazione struttura-attività (SAR) delle prime piccole molecole inibitrici dell'apertura dell'mPTP basate su uno 1,3,8-triazaspiro[4.5]decane scaffold che colpisce la subunità c del complesso dell' F_1F_O ATP sintasi. Abbiamo identificato tre potenziali composti che mostrano un'attività inibitoria dell'mPTP aumentata a dosi inferiori ai composti di riferimento, una migliore localizzazione nel compartimento mitocondriale e effetti positivi anche in un modello di MI *ex vivo*, inoltre non mostrano effetti collaterali né a livello cellulare né a livello mitocondriale preservando il contenuto mitocondriale di ATP nonostante la loro interazione diretta con il complesso dell'ATP sintasi.

Results

1. Identification of 1-phenyl-8-tosyl-1,3,8-triazaspiro[4.5]decan-4-one (PP11) as a novel small-molecule inhibitor of the mPTP.

Oligomycin A is classified as an mPTP opening inhibitor that targets the c subunit of F_1F_O ATP synthase (193); therefore, it was selected as the reference compound for this project. In particular, oligomycin has been investigated in mutagenesis studies: resistance to oligomycin in yeast implicate a target site residing at the interface of subunits a and c, with an involvement of both Gly23 and Glu59 of the N- and C-terminal transmembrane helices of subunit c, respectively (194), (195), (196). Yeast Glu59 of subunit c is equivalent to *E. coli* Asp61, located in the middle of the membrane, and is believed to be involved in proton translocation that drives ATP synthesis. Indeed, oligomycin A is known to establish several Van der Waals interactions with c subunits, forming a hydrogen bond with Glu59 through a water molecule bridge through which the carboxyl group of a leucine residue is also recruited (Figure 14A) (98). In particular, the southern part of oligomycin A (Figure 14B) is closely engaged by the binding cavity of the c-ring.

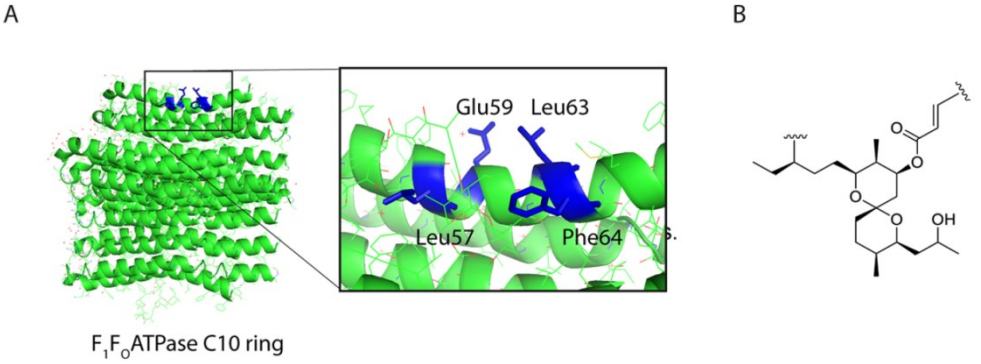

Figure 14. Discovery of PP11 as the first small-molecule inhibitor of the mPTP with a spirocenter template that mimics the spiroketal moiety of oligomycin A.
A: Graphical representation of the key amino acid residues defining the binding pocket of the known mPTP inhibitor oligomycin A to the c-ring.
B: Structure of the southern portion of oligomycin A showing a 1,7-dioxaspiro[5.5]undecan moiety that is closely involved in the interaction with the c-ring.

Considering this information and the need to simplify this natural compound to facilitate easy, accessible synthesis, we explored the activity of a series of small molecules mimicking the southern 1,7-dioxaspiro[5.5]undecane moiety of oligomycin A. To test the hypothesis that the spiro bicyclic fragment may be mandatory for mPTP inhibition, we initially screened a small internal library of spiro derivatives that somewhat resemble the functional structure of the natural compound. These preliminary investigations resulted in the identification of 1-phenyl-1,3,8-triaza-spiro[4,5]decan-4-one derivative 1 (PP11, Figure 14C).
To assess the efficacy of PP11 in inhibiting Ca^{2+}-mediated mPTP opening, we first measured its biological activity in HeLa cells by calcein-cobalt assay (34). mPTP opening was stimulated by the addition of the ionophore ionomycin, and the resulting kinetics were compared. As shown in Figure 14D, the addition of 1 µM ionomycin to cells pretreated for 15 minutes with 1 µM PP11 resulted in desensitization of mPTP opening by approximately 50% as assessed by the slope of the curve after stimulation, which was significantly less than that observed in vehicle-treated cells. Moreover, PP11 was able to inhibit the mPTP

opening in a manner very similar to that of oligomycin A (98), (197), (198) as a direct derivative but at a tenfold lower concentration. These data demonstrated that the small-molecule inhibitor derived from the known compound oligomycin A was able to efficiently inhibit mPTP opening.
PP11 inhibitory effect was comparable also with that of Cyclosporin A, another well-known mPTP inhibitor whose target protein is CYPD (199).
Therefore, PP11 was selected as the starting point for further studies.

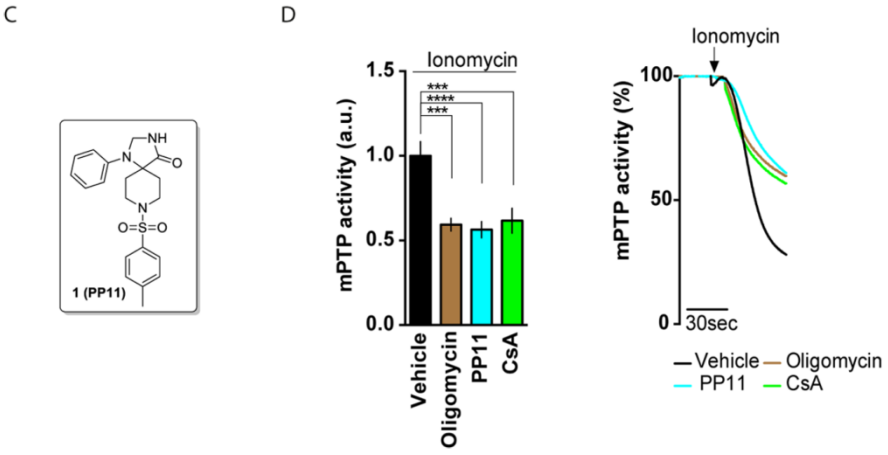

Figure 14. C: Structure of PP11, a novel small-molecule inhibitor of the mPTP with a 1,3,8-triaza-spiro[4.5]decan-4-one template.
D: Calcein-cobalt assay in living cells pretreated with vehicle, oligomycin A, PP11 and CsA. mPTP opening was stimulated by ionomycin administration, and representative kinetics data are reported. ***: p value<0.001; ****: p value<0.0001.

2. PP11 accumulates selectively in mitochondria.

To monitor and better characterize PP11's biological activity in cells, we investigated its subcellular localization, focusing on the amount localized within mitochondria, the hypothetical site of action. As illustrated in Figure 15A-C, fractionation (200) of living cells treated with vehicle (A) or PP11 (B) resulted in successful isolation of pure mitochondrial, cytosolic and endoplasmic reticulum (ER) fractions. Samples from each subcellular compartment were analyzed by HPLC-HRMS to detect the compound.

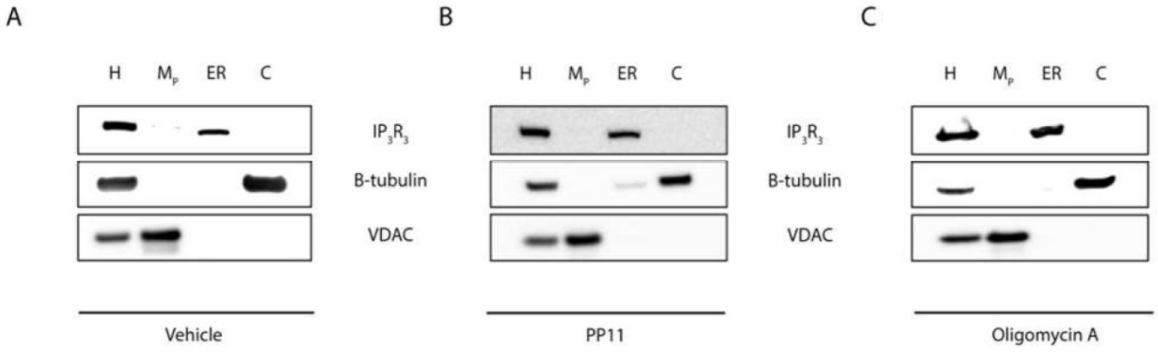

Figure 15. Intracellular localization studies.
A: Isolation and validation of mitochondrial, endoplasmic reticulum and cytosolic subcellular fractions from untreated cells.
B: Isolation and validation of mitochondrial, endoplasmic reticulum and cytosolic subcellular fractions from PP11-treated cells.
C: Isolation and validation of mitochondrial, endoplasmic reticulum and cytosolic subcellular fractions from oligomycin A-treated cells.

As shown in Figure 16C, PP11 selectively accumulated in the mitochondria without detectable traces in the other subcellular fractions (Figure 16D, E); however, a residual amount of the spiro derivative was detectable in the supernatant fraction (Figure 16F). The same investigation performed after administration of oligomycin A revealed a less selective distribution of the compound, with significant amounts detected in all the isolated subcellular compartments (data not shown).

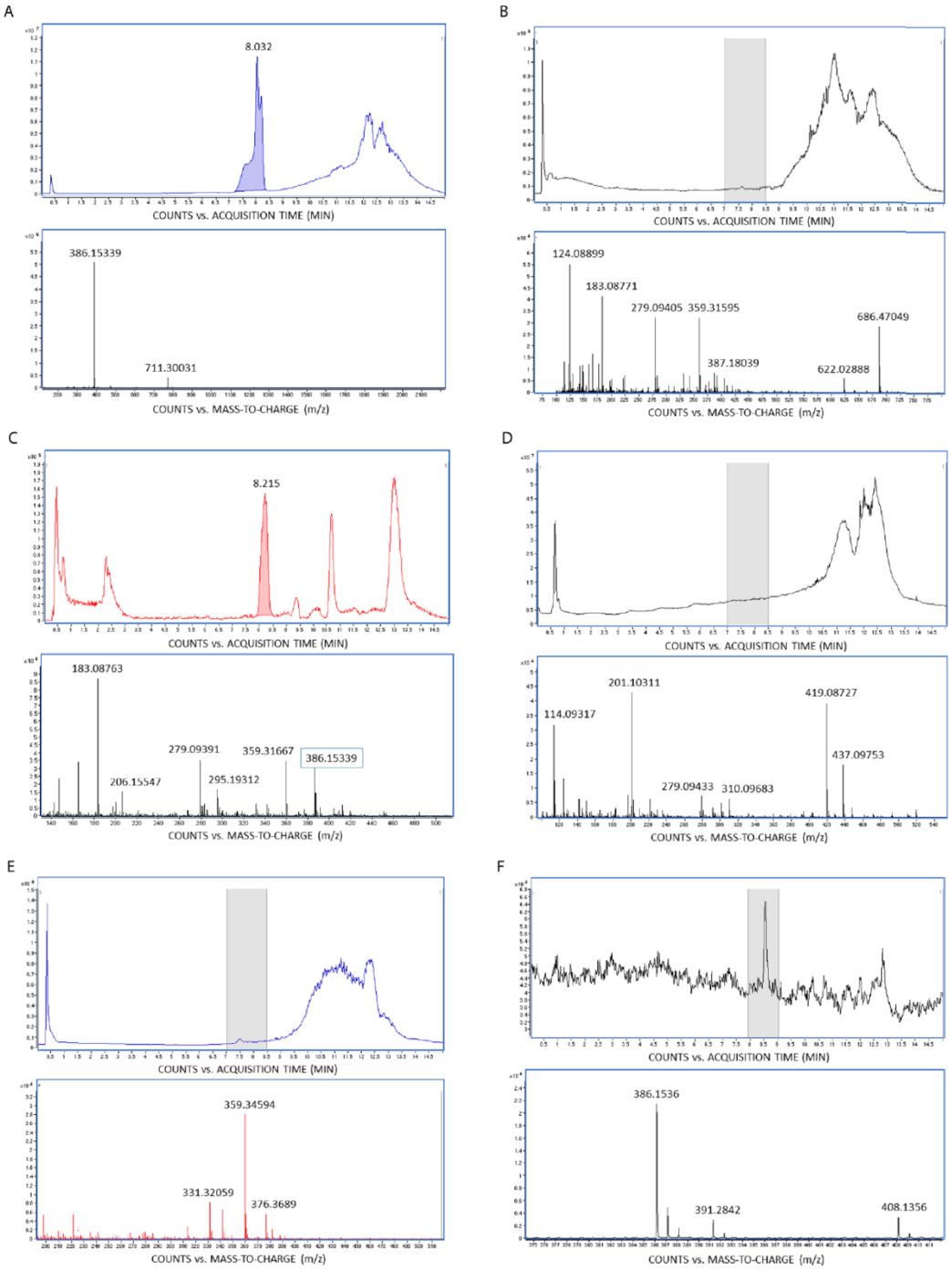

Figure 16. PP11 selectively localizes in mitochondria.
Subcellular localization of PP11 was investigated via HPLC-HRMS analysis of samples from different cellular compartments before and after treatment with the compound.
A: The HPLC-HRMS profile of PP11 analyzed in physiological solution revealed broad band absorption (7-8.5 min) with maximum absorption at a retention time of 8.03 min (top panel). The

blue region of the HPLC spectrum corresponds to a unique mass peak at [M+H]+ m/z of 386.15339 (bottom panel, [M+H]+ calculated for PP11 386.1533).
B: The HPLC profile of the mitochondrial fraction isolated from untreated cells revealed a relatively clean zone in the detection region of PP11 (from 7 to 8.5 min, top panel). The gray band on the HPLC spectrum corresponds to the mass spectra area between the retention time of 7 to 8.5 minutes enlarged in the bottom panel.
C: The HPLC-HRMS profile of the mitochondrial fraction isolated from cells pretreated with PP11 clearly indicated the presence of the PP11 compound with an HPLC band at a retention time of 8.2 min (top panel). The red area of the signal corresponds to the enlarged TIC signal for the mass peaks (bottom panel), among which the [M+H]+ m/z of 386.15339 indicated that the presence of PP11 was not detectable in the corresponding untreated fraction (panel B).
D: No detectable amount of PP11 was found by HPLC-HRMS in the cytosolic fraction of PP11-treated cells.
E: The HPLC profile of the ER fraction isolated from PP11-treated cells revealed a relatively clean zone in the detection region of PP11 (from 7 to 8.5 min, top panel). The gray band of the HPLC spectrum corresponds to enlargement of the TIC signals of mass peaks detected by HRMS analysis (bottom panel).
F: The HPLC-HRMS profile of the supernatant fraction isolated from cells pretreated with PP11 indicated the presence of the compound.

Moreover, to directly monitor target engagement inside cells, we performed a cellular thermal shift assay (CETSA) (201), (202) using a protocol based on ligand-induced thermal stabilization of the target protein, the c subunit of F_O ATP synthase. Thermal shifts at high compound concentrations are known to correlate with median inhibitory concentration (IC_{50}) values and affinities, as measured by other methods (203), (204); therefore, by using higher concentrations of PP11, we were able to detect its binding with the c subunit of F_O ATP synthase (Figure 15D) between 60-80°C. Despite the low sensitivity of the assay and an inability to perform any molecular docking assays, Figure 15D shows that the c subunit protein was thermally stabilized by PP11 pretreatment (red-dashed line) and that this effect was absent in other mitochondrial proteins, such as ATP5A (black-dashed line).

D

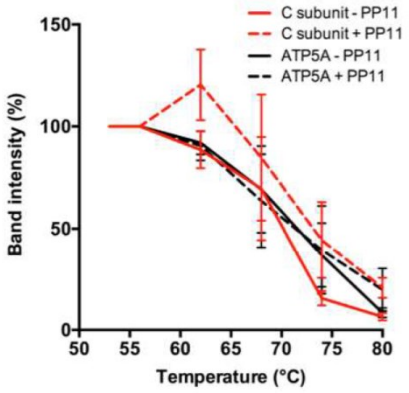

Figure 15. D: CETSA assay in HeLa cells to evaluate the thermal stabilization of two mitochondrial proteins (ATP5A and the c subunit) in the presence or absence of the PP11 compound.

To further confirm the putative selective PP11-c subunit binding, a UPLC-XEVO-TQD (Waters, UK) mass spectrometry investigation of the c subunit protein overexpressed in and immunoprecipitated from isolated mitochondria of PP11-pretreated cells was performed. The results from this experiment are reported in Figure 17 and indicate that a significant amount of PP11 was clearly detectable and bound to the c subunit. Together, these data confirm the ability of PP11 to selectively enter mitochondria and bind the c subunit to inhibit mPTP opening.

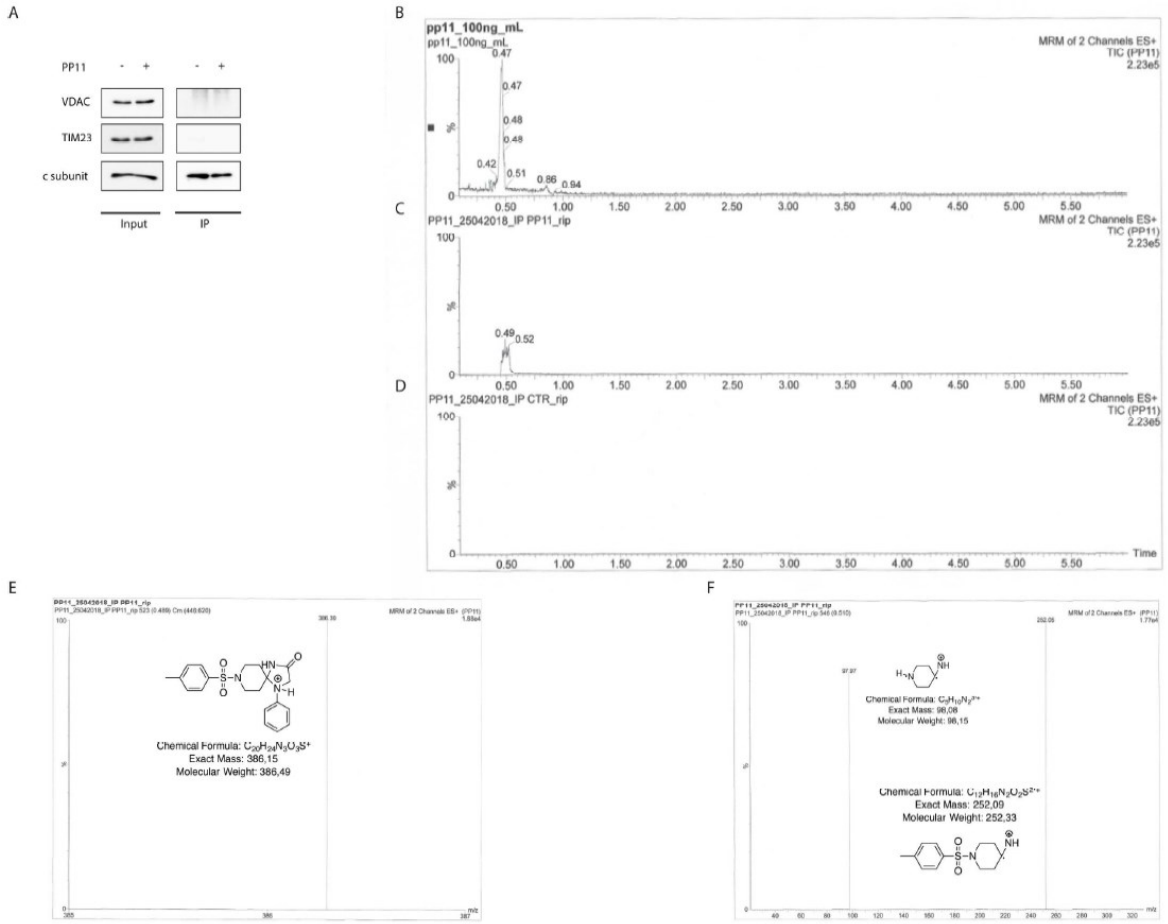

Figure 17. UPLC-XEVO-TQD investigation of the c subunit protein immunoprecipitated from cells pretreated with PP11.

A: Immunoprecipitation of the c subunit of F_O ATP synthase in isolated mitochondria from vehicle- and PP11-treated HeLa cells. Input lysates as well as IPs used for the UPLC-XEVO-TQD investigation are shown. VDAC and TIM23 mitochondrial proteins have been used as negative controls.

B: UPLC-XEVO-TQD profile of PP11 as a reference compound. Typical band absorption at a retention time of 0.47 minutes was observed.

C: UPLC profile of the c subunit obtained through immunoprecipitation from cells pretreated with PP11. The presence of the compound is indicated by the UPLC band at a retention time of 0.49 min.

D: The UPLC profile of the c subunit immunoprecipitated from untreated cells does not show significant band absorption, confirming that the signal observed in panel B can be ascribed to PP11.

E: Mass profile of the molecular ion peak [M+H]+ of PP11. F: MS/MS profile of PP11 revealing two typical fragments. Both molecular ion and fragment peaks were detected via band absorption at a retention time of 0.49 min, as shown in panel B.

3. Design, synthesis and biological characterization of PP11 analogs as inhibitors of the mPTP.

Encouraged by the promising biological profile of PP11 and considering the higher chemical stability of the aza-spiro moiety compared with the spiro-ketal function of oligomycin A, we initiated an SAR investigation of a new bicyclic core to improve compound potency. We applied a versatile synthetic approach that resulted in a series of PP11 derivatives that were differentially substituted at the N^1 and N^8 positions (Figure 18). We first investigated the effect of replacing the tosyl function at the N^8 position of PP11 with a benzyl group (compound 6a) or with different sulfonamide (8-10), carboxamide (13, 14), urea (15 and 16) or thiourea (17) moieties.

The results of the biological assay indicated that the compounds with the benzyl group or (hetero)arylsulfonamide N^8 substitutions exhibited the best performance; these compounds were therefore combined with N^1 phenyl rings at the para/meta positions with both electron donating or withdrawing groups (compounds 6b-g, 11, 12). The common synthetic pathway for the preparation of all the investigated final compounds is depicted in Figure 18.

α-Aminonitriles 3a-g were synthesized by a Strecker reaction from the commercially available N-benzylpiperidone 2, which was reacted with (substituted) anilines in the presence of trimethyl silyl cyanide (TMSCN). The nitrile group was then hydrolyzed to the corresponding amide function (4a-g) by treatment with concentrated sulfuric acid. Spirocyclization was then performed with dimethylformamide dimethyl acetal (DMF-DMA), which resulted in the generation of the unsaturated intermediates 5a-g. The latter derivatives were also screened as mPTP inhibitors to evaluate the effect of the C^2-N^3 double bond constraining the 5-membered ring of the bicyclic template. Subsequently, the imidazolinone ring was efficiently reduced with $NaBH_4$ to yield the final compounds 6a-g.

Debenzylation at the N^8 position of 6a and 6b was performed via hydrogenation under Pd/C catalysis and yielded 7a and 7b, respectively, which were employed as key intermediates for the selective functionalization of the N^8 position. Specifically, the sulfonamide derivatives 1 and 8-12 were obtained by treatment of 7a-b with appropriate sulfonyl chlorides, while N^8 acetylation (13) or benzoylation (14) was achieved by standard treatment with acetic anhydride or benzoylchloride, respectively. In addition, the urea derivatives 15-16 and the thiourea 17 were prepared from 7a and the properly substituted isocyanates or isothiocyanates.

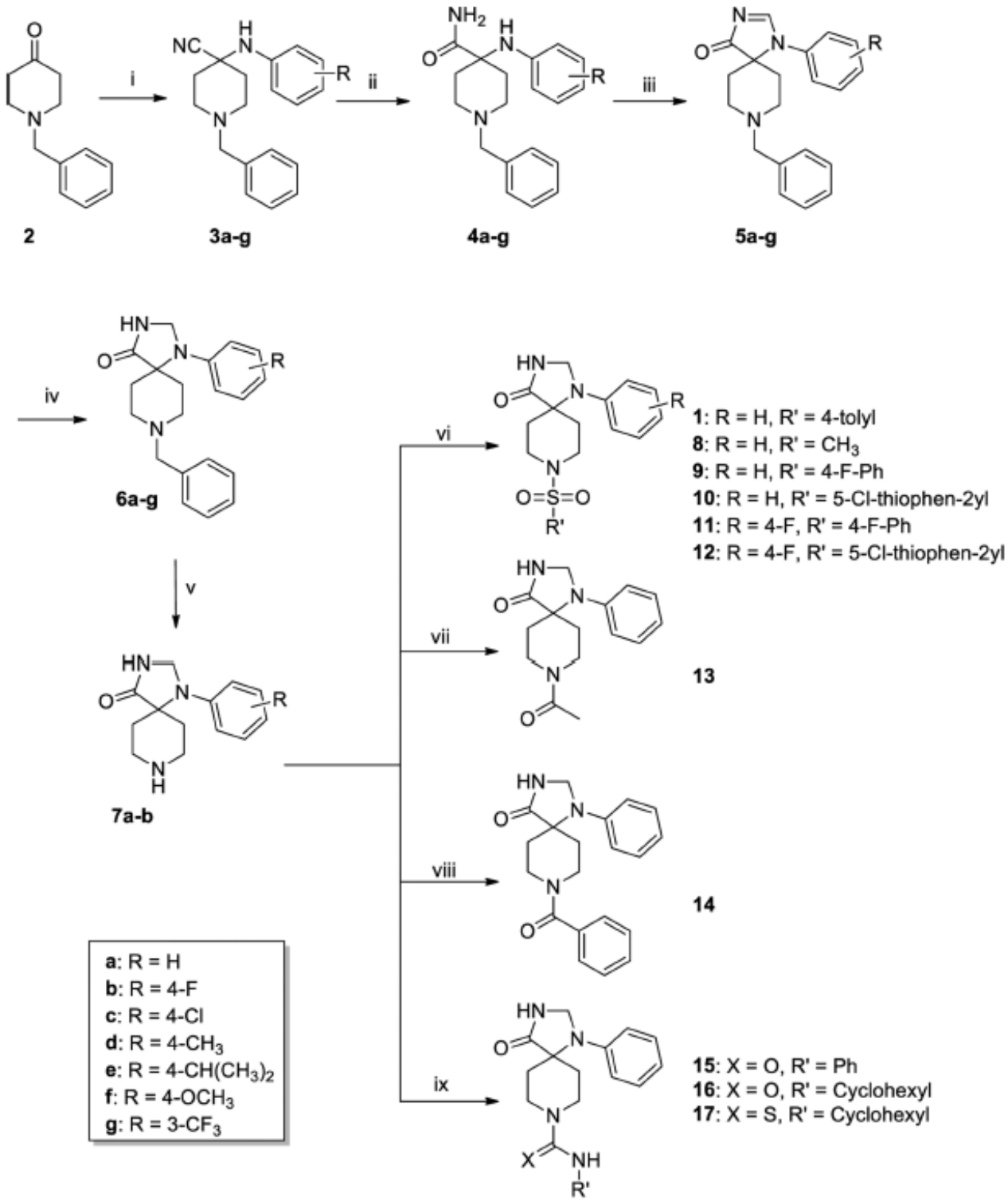

Figure 18. Synthesis of PP11 and related spiro bicyclic derivatives.

To investigate the effectiveness of the new, synthesized PP11 analogs against mPTP opening, we used the mitochondrial swelling assay as previously described (205); this protocol is faster than microscopy analysis for the screening of multiple compounds. It was confirmed that PP11 significantly inhibited mPTP opening both with calcein-cobalt assay and mitochondrial swelling assay (Figures 14D and 19B). To demonstrate specificity in measuring Ca^{2+}-induced mPTP opening, we added two positive controls, CsA and ruthenium red (RR), a known mPTP inhibitor and a mitochondrial calcium uptake blocker, respectively. Freshly isolated mouse liver mitochondria were first evaluated to ensure high purity (Figure 19A) and were then stimulated with 500μM Ca^{2+}, and absorbance at 540 nm, at which a decrease was indicative of swelling, was monitored for 10 minutes (Figure 19B, C). Under these conditions, mitochondria treated with vehicle exhibited marked membrane swelling (red bar), which was significantly prevented by pretreatment with 1μM CsA and 5μM RR (green and blue bars, respectively). As shown in Figure 19B, most of the small molecules showed good inhibitory potential compared to the control mitochondrial sample (red bar). In particular, compounds 5c, 6g and 10 were significantly more potent than PP11 in inhibiting mPTP opening. Additional details are shown in panel 19D, including the mean percentages of mPTP inhibition. Figure 19E showed a dose-response for the selected compounds and confirmed that 1μM was the lowest dose with the best effectiveness in inhibiting mitochondrial swelling for each molecule.

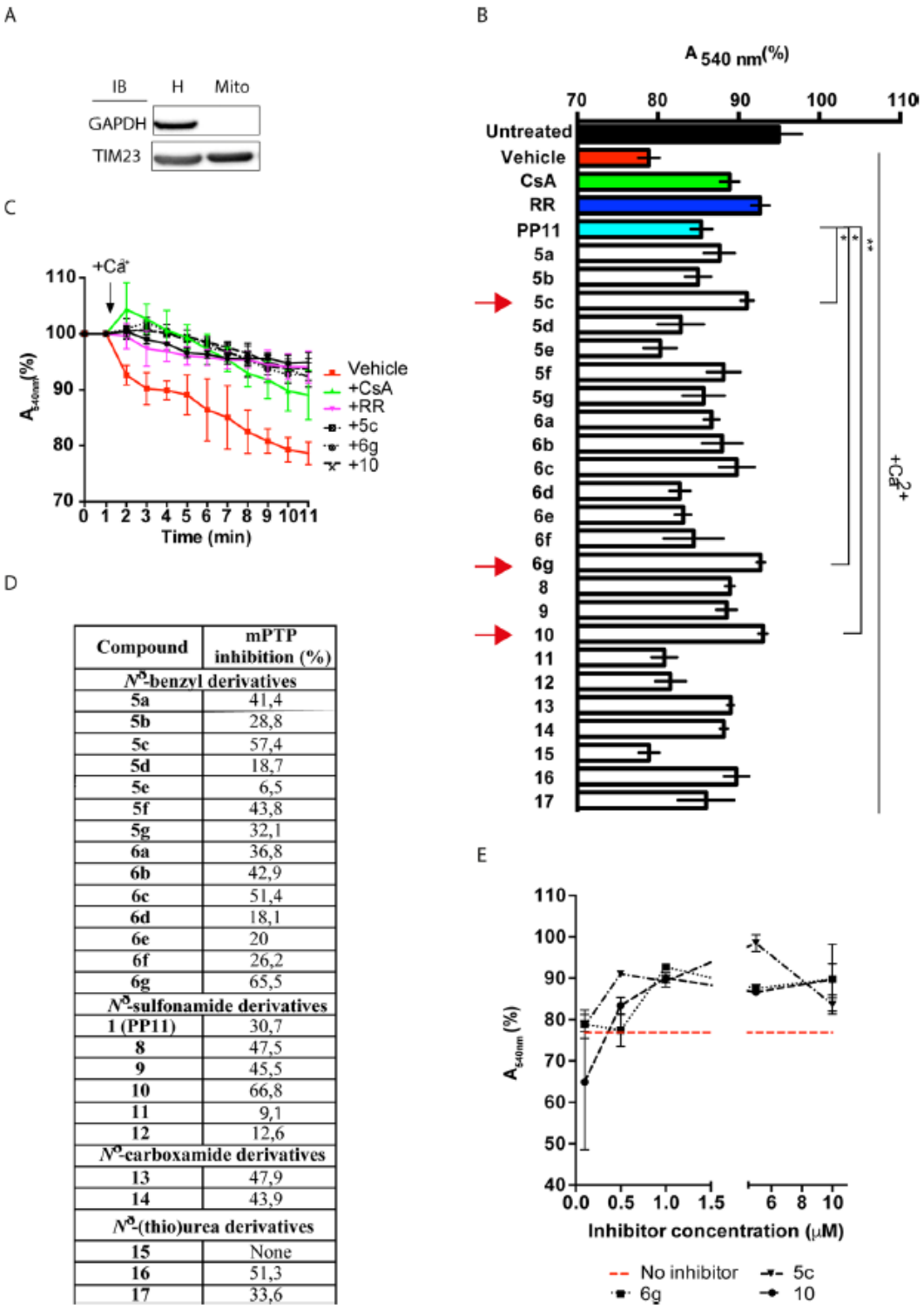

Compound	mPTP inhibition (%)
N^{δ}-benzyl derivatives	
5a	41,4
5b	28,8
5c	57,4
5d	18,7
5e	6,5
5f	43,8
5g	32,1
6a	36,8
6b	42,9
6c	51,4
6d	18,1
6e	20
6f	26,2
6g	65,5
N^{δ}-sulfonamide derivatives	
1 (PP11)	30,7
8	47,5
9	45,5
10	66,8
11	9,1
12	12,6
N^{δ}-carboxamide derivatives	
13	47,9
14	43,9
N^{δ}-(thio)urea derivatives	
15	None
16	51,3
17	33,6

Figure 19. Screening of PP11 analogs.

A: Immunoblot detection of GAPDH (cytosolic marker) and TIM23 (mitochondrial marker) proteins in the homogenate (H) of the whole liver and in the mitochondrial (Mito) fraction.

B: Mitochondrial swelling assay for the screening of compounds in freshly isolated mouse liver mitochondria. Data were obtained by recording changes in absorbance (540 nm), and then, the data were converted into percentages. Black bar: untreated and unstimulated mitochondria; red bar: untreated mitochondria stimulated with 500μM Ca^{2+}; green bar: pretreatment with 1μM CsA and stimulation with 500μM Ca^{2+}; blue bar: pretreatment with 5μM RR and stimulation with 500μM Ca^{2+}; cyan bar: pretreatment with 1μM PP11 and stimulation with 500μM Ca^{2+}; and white bars: pretreatment with 1μM PP11 analogs and stimulation with 500μM Ca^{2+}. Red arrows indicate the three selected compounds.

C: Kinetics and statistical data from the mitochondrial swelling assay for the vehicle, CsA, RR, 5c, 6g and 10 experimental conditions.
D: Mean percentages of mPTP inhibition with the tested compounds.
E: Dose-responses for the 5c, 6g and 10 compounds. One-way ANOVA was used for statistical analysis; *: p value<0.05; **: p value<0.01; CsA: cyclosporine A; RR: ruthenium red.

4. Biological profile of the most promising compounds.

Overall, mPTP assays revealed a set of three very potent inhibitors (5c, 6g and 10) with the greatest effects on reducing mitochondrial swelling (Figure 19B) compared to PP11. Given the crucial role of the c subunit in ATP synthase assembly and cellular energy production as a component of the membrane rotor, the basal mitochondrial ATP content and agonist-induced ATP production were monitored by the luciferin-luciferase assay (206). Treatment of living cells with 1µM PP11 slightly but significantly depleted mitochondrial ATP levels in resting conditions (Figure 20A); similarly, the relative amount of ATP remained low even upon histamine-induced Ca^{2+} uptake (207) (Figure 20B).

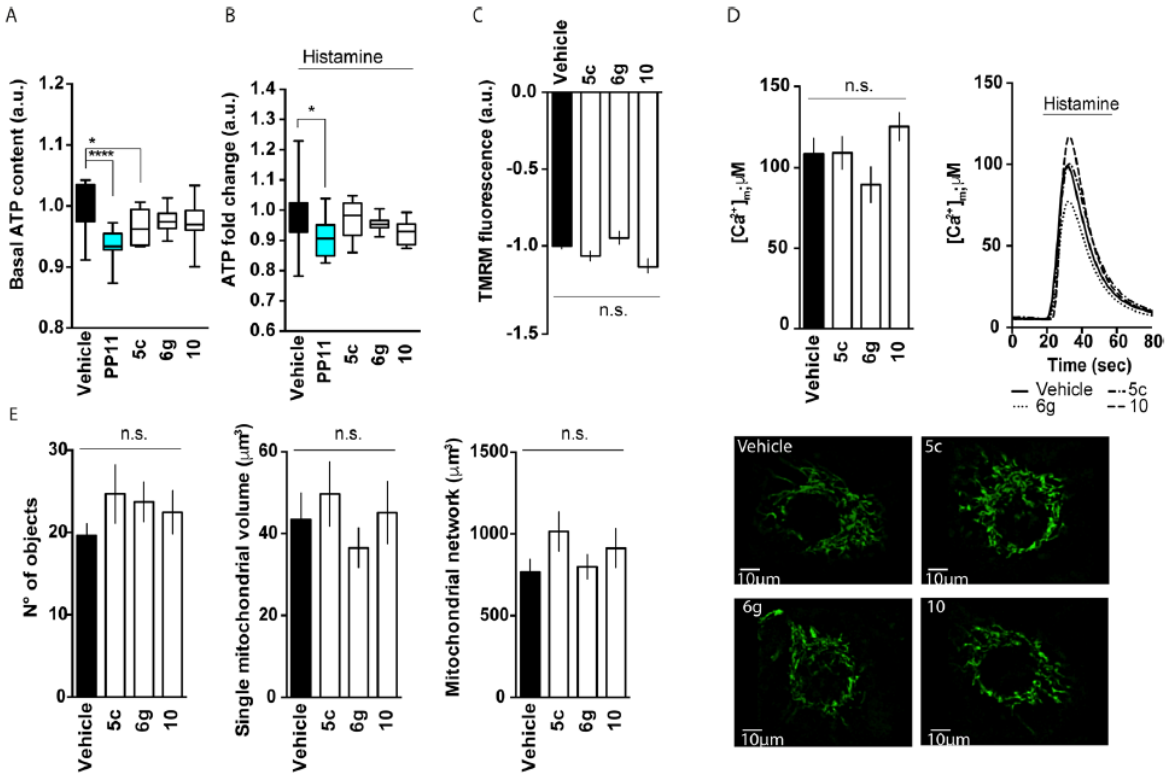

Figure 20. Biological profile of the most promising compounds.
A: Mitochondrial ATP content in living cells at resting conditions using the luciferase-luciferin method.
B: Mitochondrial ATP generation upon agonist-induced Ca^{2+} uptake in living cells using the luciferase-luciferin method. His indicates 100µM histamine, the agonist used to induce Ca^{2+}-dependent ATP production.
C: TMRM fluorescence as an index of $\Delta\psi_m$ changes in living cells.
D: Mitochondrial calcium uptake in living cells using a mitochondrially-targeted aequorin probe; histograms of statistical and representative kinetics data; 100µM histamine (His) addition is indicated.
E: Evaluation of mitochondrial morphology parameters using an mtCHERRY probe.

It is not recommended that a compound developed in order to inhibit uncontrolled mPTP opening in I/R injury leads to an impairment of ATP basal concentration and production after stimulus.

The PP11 derivatives 5c, 6g and 10 synthesized with various specific chemical groups, such as electron withdrawing atoms (Cl) or moieties (CF_3) in the aromatic substituents in positions 1 and 8 of the spirodecane scaffold, allowed us to successfully overcome this drawback and step-limiting factor. Indeed, use of the 6g and 10 inhibitors did not affect ATP levels, but treatment with compound 5c induced a small decrease in the basal mitochondrial ATP content, which was completely recovered upon Ca^{2+}-induced ATP generation (Figure 20A, B). To identify possible side effects of the compounds on living cells that may preclude their use in future studies, we evaluated other important mitochondrial parameters. $\Delta\psi_m$ and Ca^{2+} homeostasis are critical factors for the maintenance of physiological functions in cells, including proper respiratory chain function and a wide range of intracellular signaling pathways, respectively.

As shown in Figure 20C and D, pretreatment of cells with the 5c, 6g and 10 inhibitors did not affect basal MMP or mitochondrial Ca^{2+} uptake. Moreover, mitochondrial morphology, the number of mitochondria in cells and their network volume were unchanged (Figure 20E).

In addition, the results previously described were further confirmed by the 3-(4,5-Dimethylthiazol-2-yl)-2,5-diphenyltetrazolium bromide (MTT) assay, which showed that treatment of living cells with micromolar concentrations of 5c, 6g and 10 for 24 h and 48 h did not induce significant MTT reduction compared with treatment with vehicle (Figure 20F). Only prolonged (72 h) treatment slightly but significantly decreased cell viability *in vitro* (Figure 20F).

The permeability transition pore has been postulated to play an important role in cytochrome c (CytC) release (188); therefore, we explored the ability of the selected compounds to prevent CytC release from mitochondrial cristae. To correlate mPTP desensitization with apoptotic cell death prevention, we detected the amount of CytC in the cristae of mitochondrial fractions from the mitochondrial swelling assay upon Ca^{2+} stimulation. Pretreatment with 5c, 6g and 10 prevented CytC release and preserved it into mitochondria as assessed by immunoblot analysis (Figure 20G).

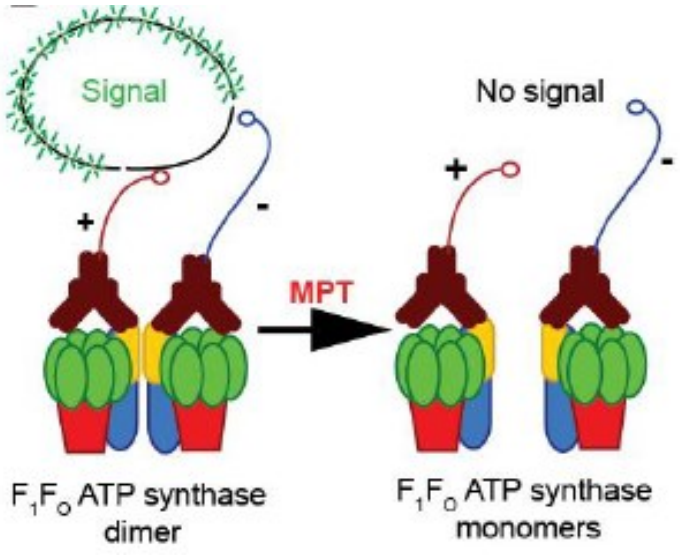

Figure 21. Schematic representation of PLA assay setting. In physiological conditions (left), the mitochondrial F_1F_O ATP synthase can form dimers or higher order oligomers. In this setting, antibodies specific for ATP5H can bring + and – PLA probes in proximity to each other, allowing for rolling-circle amplification of a detectable DNA product. In the course of MPT (right), as F_1F_O ATP synthase dimers dissociate, the distance between + and – PLA probes conjugated to ATP5H-targeting antibodies is excessive for rolling-circle amplification to occur. In this specific system, detection is highly conservative as both the + and the – PLA probes are conjugated with ATP5H-targeting antibodies, but + and + (or – and –) probes in proximity do not allow for rolling-circle amplification.

Taken together, these findings demonstrated that inhibition of mPTP opening may inhibit CytC release to the cytosol and consequently prevent apoptotic cell death (Figure 22E).
Next, to understand the molecular mechanism by which the selected compounds inhibit mPTP complex activity, we used a previously tested proximity ligation assay (PLA)-based procedure (75) to verify the F_1F_O ATP synthase dimerization grade in living cells. Vehicle-treated cells exhibited a considerable amount of reddotted staining that colocalized with the mitochondrial protein translocase of outer mitochondrial membrane 20 (TOM20). We showed the F_1F_O ATP synthase dimerization status via a PLA intensity profile upon ionomycin administration alone or in the presence of small-molecule inhibitors. As recently published by our lab, the MPT was accompanied by a significant decrease in the PLA signal following 1µM ionomycin treatment; however, the MPT did not occur with the same intensity in the presence of 1µM 5c, 6g and 10 (Figure 20H). These findings suggest that mPTP desensitization by the synthesized compounds is correlated with stabilization of F_1F_O ATP synthase dimers.

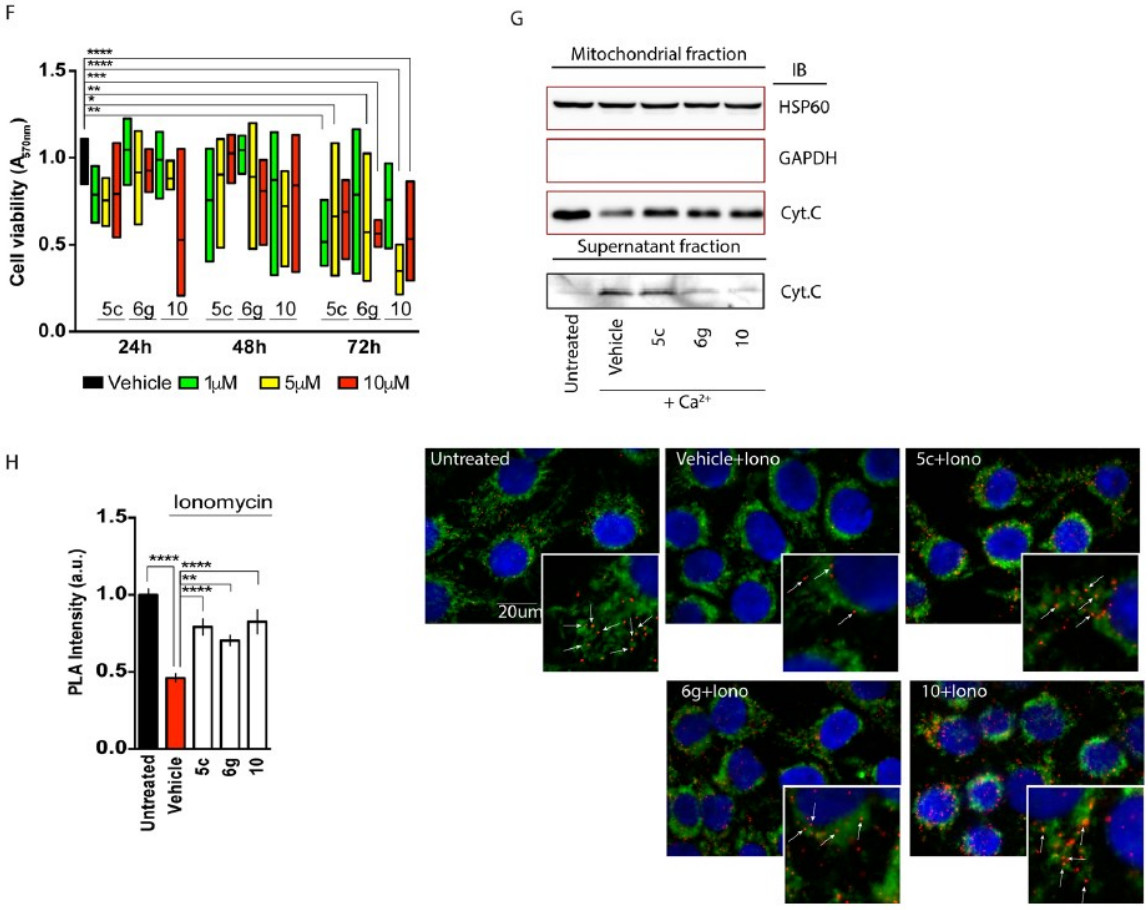

Figure 20. F: MTT assay in living cells to evaluate the toxicity of compounds at 24 h, 48 h and 72 h and at different concentrations. Black bar: cells treated with vehicle; and green bar: 1µM compound; yellow bar: 5µM; red bar: 10µM. The data were standardized to the vehicle condition.
G: Immunoblot detection of cytochrome c in both mitochondrial cristae and respiration buffer from the mitochondrial swelling assay. HSP60 was used as a mitochondrial marker, and GAPDH was used as a cytosolic marker.
H: PLA-based assay for assessment of the ATP synthase dimerization status. Blue: nuclei by DAPI detection; green: mitochondria by TOM20 detection; red spots: ATP5H detection as described in the methods.

5. Cardioprotective effect of compound 10 in a model of reperfusion injury.

Considering the ability of these inhibitors to desensitize mPTP opening (Figure 19B) by stabilizing ATP synthase dimers (Figure 20H) and prevent CytC release (Figure 20G) without affecting long-term cell viability (Figure 20F) and the mitochondrial ATP content (Figure 20A, B), we investigated the effects of compound 10 in an animal model of cardiac reperfusion injury. We isolated beating rat hearts and placed them in a Langendorff system, which was continuously perfused with Krebs-Henseleit buffer (KHB) bubbled with oxygen at 37°C. The *ex vivo* protocol included stabilization of the heart for 20 min, and then, retrograde perfusion was progressively stopped to induce 30 min of global ischemia followed by 1 hour of reperfusion (Figure 22A). After stabilization, the left ventricular developed pressure (LVDP) was 89.8±3 mmHg in the I/R vehicle group. Following reperfusion, the LVDP decreased to 66±5 mmHg, with a mean reduction of 36±9%, indicating successful induction of ischemia (as previously reported in (208)). No difference in LVDP was identified among the experimental groups during stabilization. As indicated in figure 22A, compound 10 was administered in the reperfusion phase during the first 10 minutes of reflow. The dose of 10µM of compound 10 was selected based on previous experiments to identify the highest dose that could be perfused in the heart without toxicity (data not shown). In isolated hearts, perfusion with a constant volume of derivative 10 resulted in decreases in coronary perfusion pressure (CPP) (-17.5±3.4%) and end-diastolic pressure (EDP) (-72±9.86%) (Figure 22B, D) with an increase in LVDP (+36.4±3.9%) (Figure 22C), indicating reduced diastolic stiffness, vasoconstriction and deterioration of myocardial performance, respectively.

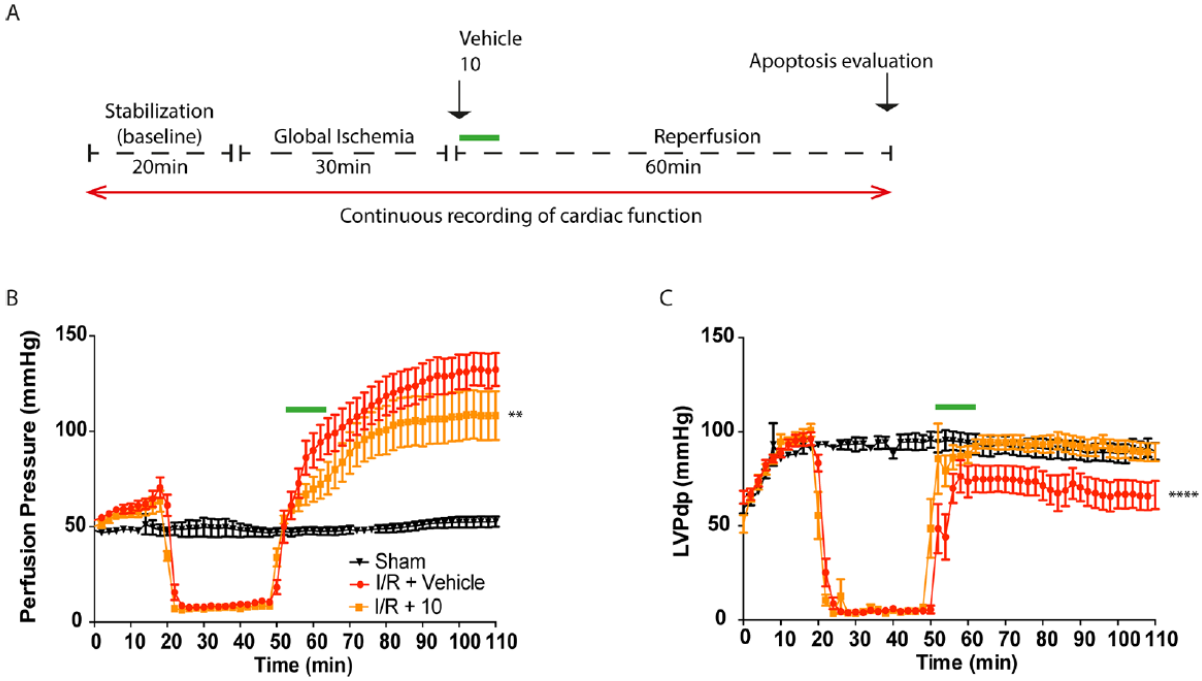

Figure 22. Beneficial effects of compound 10 in a cardiac reperfusion injury model.
A: Diagram depicting the standard Langendorff *ex vivo* protocol.
B: Coronary perfusion pressure recording of a rat heart in the stabilization, ischemia and reperfusion phases. Compound 10 is used at a concentration of 10µM.
C: Left ventricular peak developed pressure recording of a rat heart in the stabilization, ischemia and reperfusion phases.
The green bar in panels A-D indicates vehicle or compound administration time.

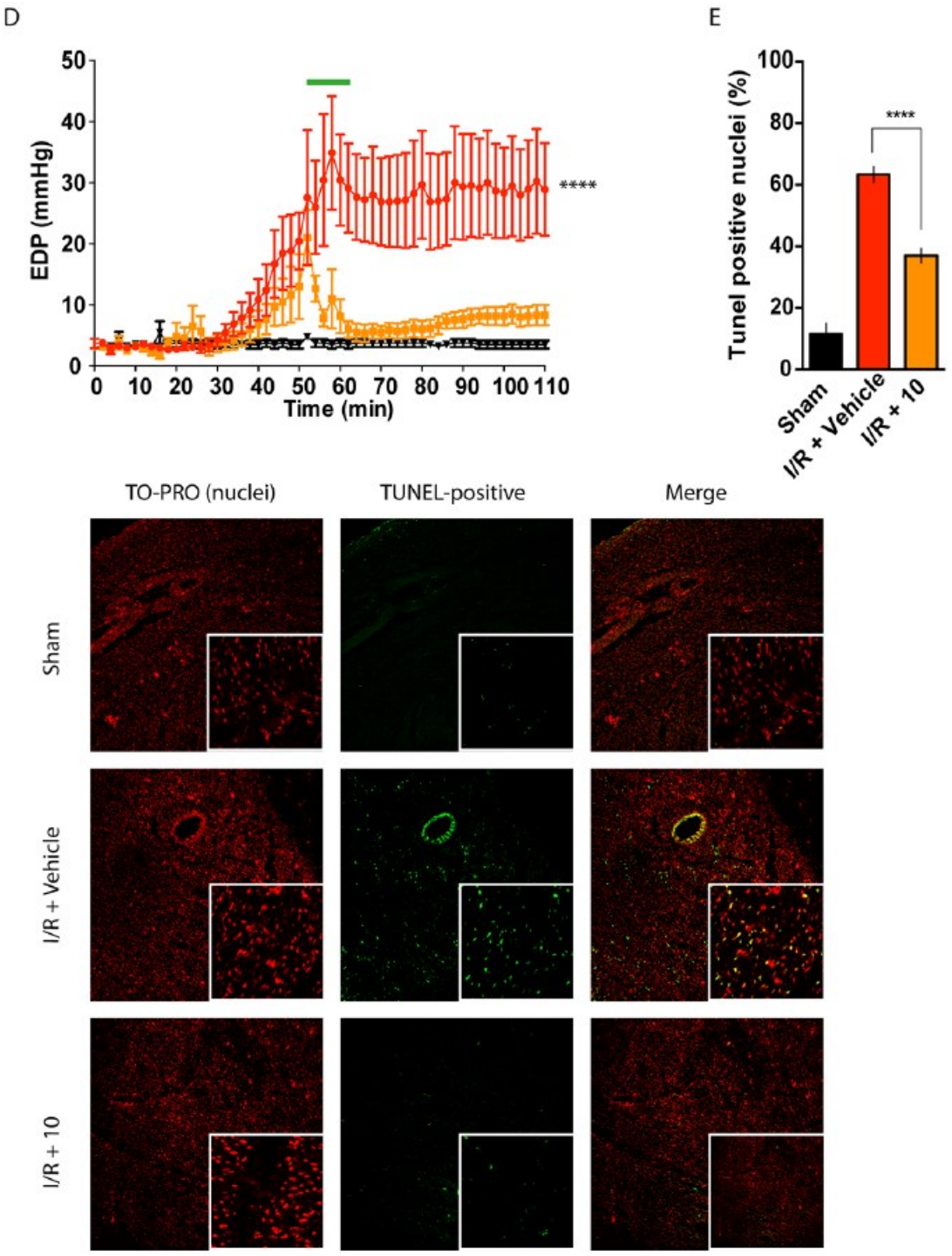

Figure 22. D: End-diastolic pressure recording of a rat heart in the stabilization, ischemia and reperfusion phases.
E: TUNEL assay for apoptosis evaluation under experimental conditions and representative images. Red: nuclei detected by TO-PRO; green: apoptotic nuclei detected by TUNEL enzyme. **: p value<0.01; and ****: p value<0.0001.

At the end of the procedure, cell death was analyzed in the hearts by terminal deoxynucleotidyl transferase dUTP nick-end labeling (TUNEL) assays. In the I/R+vehicle group, 64% of the cardiomyocytes were TUNEL-positive; however, the number of TUNEL positive cardiomyocytes was significantly reduced in the presence of spiro derivative 10 (Figure 22E). These findings confirmed the ability of c-ring-targeting agents to inhibit mPTP opening and to protect against cell death in an *ex vivo* animal model of cardiac reperfusion injury.

Discussion

Myocardial infarction is an ischemic heart disease in which mPTP opening is widely accepted as a crucial step in the development of myocardial damage, which is better known as ischemia-reperfusion injury (209). Since up to 50% of the final infarct size is due to I/R injury, targeting the mPTP complex may be a valuable pharmacological adjunct to reduce infarct size. Currently, although satisfying results have been achieved in *in vitro* and *in vivo* animal models, manipulation of the PTPC and, more generally, mitochondrial targeting do not appear to influence the mortality of affected patients, but they reduce hospital readmission for heart failure (118). Instead, drugs with a broad-spectrum mechanism of action are currently utilized in clinical practice (119). The apparent lack of translational value among mitochondrial-targeting drugs can be ascribed first to limited knowledge regarding the exact molecular structure of mPTP; therefore, the appropriate mitochondrial target possibly has not yet been considered. Second, the multifactorial nature of MI should be considered, and the adoption of combined strategies targeting multiple intracellular signaling pathways is always recommended (210). Based on our previous studies on the role of the c-ring in mPTP opening (36), (75) and to validate a new pharmacological approach for the treatment of I/R-related damage, in this project, we describe the discovery, optimization and SAR studies of the first small-molecule mPTP opening inhibitors that target the c subunit of the F_1F_O ATP synthase complex. To the best of our knowledge, this is the first attempt to inhibit the mPTP by targeting the eukaryotic c subunit of ATP synthase using novel small molecules for therapeutic purposes. Indeed, treatment during reperfusion with one of the most promising screened compounds (10) showed beneficial effects in an *ex vivo* model of MI, with a reduction of apoptotic cell death upon I/R injury (Figure 22E). The decreases in CPP and EDP (Figure 22B, D) with an increase in LVDP (Figure 22C) in the isolated heart reflected significant reductions in diastolic stiffness, vasoconstriction and deterioration of myocardial performance. Moreover, the *ex vivo* beneficial effects of compound 10 together with strong inhibition of mPTP opening by the selected compounds *in vitro* can be achieved without altering mitochondrial parameters (Figure 20A-E) or short-term toxicity in living cells. Indeed, these compounds weakly but significantly disrupted cell viability only with 72 h of treatment (Figure 20F). The compounds were derived using the scaffold of the known c subunit inhibitor oligomycin A; we first identified PP11, a compound with a strong desensitization effect on mPTP opening (Figure 14D) and an inhibitory effect comparable to that of oligomycin A, but it is functionally active at a tenfold lower concentration (Figure 14D). The increased performance at lower concentrations can be ascribed to its better localization to the mitochondrial compartment (Figure 16), the putative site of action, as assessed by HPLC-HRMS.

Indeed, PP11 accumulates exclusively in the pure mitochondrial fraction (Figure 15 and 16) without detectable traces in other subcellular compartments. In contrast, although oligomycin A is present in the mitochondrial compartment where it exerts known biological effects, a significant amount diffuses into the cytoplasm and ER organelles (data not shown), likely lowering its potency and conferring a better drug-like profile to PP11. In addition, given its effectiveness in targeting the c subunit for mPTP inhibition (36), (75), (82) and the exclusive mitochondrial localization of its ligand, PP11 (and derivatives) use led to fewer side effects compared to other known mPTP inhibitors, such as CsA. Indeed, CsA off-target effects (211), (212) are derived from a diffuse intracellular localization pattern characterized by cytosolic (211), (212) and nuclear interactions (213), thus prompting research on alternative methods to target the mPTP. Criticism could arise from

the use of putative ATP synthase disruptors as ligands of the membrane rotor components, as confirmed here by the suboptimal effect of PP11, a preliminary derivative of oligomycin A, on the mitochondrial ATP content (214). Indeed, although PP11 is considered a good mPTP opening inhibitor (Figure 14D), it has a slight deleterious effect on the production of basal ATP (Figure 20A); however, this effect is reduced upon Ca^{2+}-dependent stimulation in the mitochondria (Figure 20B). When designing PP11 derivatives, we tried to evaluate different chemical modifications at several positions of the parent compound to identify possible structural determinants that can abolish any undesired effects. Among the most promising compounds screened in Figure 19B, 6g and 10 did not affect the basal mitochondrial ATP content; only compound 5c promoted a small decrease in the basal mitochondrial ATP content, which was completely recovered upon Ca^{2+}-induced ATP generation. A possible explanation for such experimental evidence may be faster reversibility of the interaction of 6g and 10 with the postulated cellular target compared to PP11. The main findings of this work are consistent with those of our previously published studies and those of independent groups (37), (81), (82), (215) confirming the importance of the roles of i) the c-ring as a core component in mPTP activity and ii) the dimer versus monomer transition of ATP synthase linked to the mPTP and the resulting apoptotic cell death. Indeed, a PLA-dedicated assay suggested dimer stabilization upon Ca^{2+}-triggered mPTP opening when cells were pretreated with the 5c, 6g and 10 compounds (Figure 20H) as a molecular mechanism by which these inhibitors may exert anti-apoptotic effects. We are aware that our data appear to disagree with the hypothesis from Walker JE's group on the persistence of the MPT in a cell clone lacking the c subunit of human ATP synthase (85); however, as a very exhaustive commentary on this discrepancy explains (216), in the absence of the primary mechanisms in mPTP opening (e.g., c subunit expression), the MPT can presumably occur through other pathways involving misfolded proteins of the mitochondrial membrane (216), (217).
In conclusion, we propose small-molecule c subunit inhibitors as a new pharmacological approach for the treatment of I/R injury.

Future perspectives

Future perspectives will be oriented towards the study of ATP synthase conformational changes (if detectable) in terms of modulation of its dynamic assembly into supercomplexes upon inhibitor treatment (for instance, by using native gels) and understanding the exact binding sites between inhibitors and mitochondrial proteins. Photoaffinity labeling of the most promising compounds identified here may lead to useful tools that will facilitate future binding site deconvolution studies, advancing structure-based drug design approaches in this field.

Furthermore, with the aim to understand which aminoacid is involved in c subunit-inhibitors interaction it will be a good approach to perform a mutagenesis study of c subunit sequence, creating point mutations supposing that amino acids involved may be the same or close to those participating in oligomycin bound to ATP synthase detected in yeast.

Finally, it must be very useful and interesting to search if these mutations are involved in potential pathologies in order to find an additional therapeutic implication of the use of these compounds.

Obviously, the development of these inhibitors has to be implemented with *in vivo* studies, in order to confirm the protective activity after I/R also in animal models before to progress to clinical studies.

Materials and methods

Chemistry

Reaction progress and product mixtures were monitored by thin-layer chromatography (TLC) on silica gel (precoated F254 Macherey-Nagel plates) and visualized with a UV lamp (254 nm light source). The organic solutions from extractions were dried over anhydrous sodium sulfate. Chromatography was performed on Merck 230−400 mesh silica gel or using Isolera One (Biotage Sweden). 1H, 13C, DEPT, bidimensional (gCOSY), and heterocorrelated (gHMQC, gHMBC) NMR spectra were recorded on a VARIAN Mercury Plus 400 MHz spectrometer. Chemical shifts (δ) are reported in parts per million (ppm) using the peak of deuterated solvents as an internal standard, and coupling constants (J) are reported in Hertz. Splitting patterns are designed as follows: s, singlet; d, doublet; t, triplet; q, quartet; m, multiplet; and b, broad. Melting points for purified products were determined in a glass capillary on a Stuart Scientific electrothermal apparatus SMP3 and are uncorrected. Mass spectra were recorded by an ESI single-quadrupole mass spectrometer Waters ZQ 2000 (Waters Instruments UK). For analytical controls, Beckmann System Gold 168 HPLC was used with an LC column Kinetex 5-µm EVO C18 100 Å (250 × 4.6 mm) and a variable-wavelength UV detector fixed to 220 nm. The analysis was conducted using two solutions, A and B, containing 100:0.1 H2O:TFA and 40:60:0.1 H2O:CH3CN:TFA, respectively, with a gradient elution of 0−50% solution B over 30 min. The purity of all compounds was determined by HPLC and was greater than 95%. LC-HRMS analysis of crude mitochondria and cytosol of PP11-treated cells and final compounds was performed with an ESI-Q-TOF Nano HPLC-CHIP Cube Agilent 6520 instrument (Agilent Technologies USA) using a linear gradient (0.4 µL/min) from 0%
solvent A (97% water/3% acetonitrile/0.1% formic acid) to 80% solvent B (97% acetonitrile/3% water/0.1% formic acid) over 10 min and from 80% to 5% solvent B over 5 min using a Zorbax C18
Column (43 mm × 75 µm, 5 µm) equipped with an enrichment column (4 mm, 40 nL). The UPLC-MS analysis was performed in an Acquity UPLC equipped with a triple-quadrupole mass spectrometer XEVO-TQD (Waters UK). Chromatographic separation was carried out using a BHE C18 column (50 mm × 2.1 mm i.d. 1.8 µm) from Waters (Waters, Milford, USA) heated at 40 °C. The mobile phase consisted of water with 0.1% formic acid (solvent A) and acetonitrile with 0.1% formic acid (Solvent B). An 8 min gradient elution at 0.3 mL/min was performed as follows: from 100% solvent A to 80% solvent A over 4 min, from 80% A to 20% A over 2 min, and from 20% A to 0% A over 2 min. Mass spectrometric detection was carried out using an electrospray interface (ESI) operated in positive ionization mode with multiple reaction monitoring (MRM) for the PP11 analyte. Nitrogen was used as a desolvation gas at a 650 L/h flow rate with the desolvation temperature set at 200 °C and the source temperature set at 150 °C. The collision gas (argon) flow was set at 0.1 mL/min. The capillary voltage was set at 4 kV; the collision energy and con voltage were optimized to maximize the signal corresponding to the major transition observed in the MS/MS spectra following fragmentation of the [M + H]+ ion corresponding to the PP11 molecule.

Cell culture and transient transfection

HeLa cells were grown in Dulbecco's Modified Eagle Medium (DMEM, Euroclone) supplemented with 10% fetal bovine serum (FBS, Gibco™, Thermo-Fisher), in 75-cm^2 flasks (Corning). All cells were maintained at 37°C and 90% relative humidity in 5% CO2. Before transfection, cells were seeded onto 13-mm glass coverslips for intracellular Ca^{2+} measurements and onto 24-mm glass coverslips for microscopic analysis. Next, plasmid transfections with Lipofectamine 2000 (Thermo-Fisher) were performed. All experiments were performed 24 h after transfection. In experiments involving compounds cells were pre-treated for 15 min in complete medium.

Calcein−Cobalt Assay

HeLa cells were pretreated with DMSO (vehicle), 10μM oligomycin A, 1μM CsA, or 1μM PP11 and then loaded with 1μM calcein acetoxymethyl ester (Thermo-Fisher) and Co^{2+} as described in Bonora et al. of 2016 (34). Staining solution was added to the cells for 15 min at 37 °C in a 5% CO_2 atmosphere. Image acquisitions were performed with a motorized Olympus IX81-ZDC inverted microscope with a 40 × /1.30-N.A. UPlanFLN oil-immersion objective and Cell MT20E xenon lamp. Ionomycin (1μM, Sigma-Aldrich) was administered 30 sec after the beginning of the experiment to induce mPTP opening. Finally, images were analyzed and quenching rates were determined as the slopes of the fluorescence trace over a period of 60 sec post-stimulation.

Mitochondrial Isolation and Swelling Assay

Mitochondria were isolated by conventional procedures involving differential centrifugation. Freshly excised SV129 mouse livers were washed and then homogenized in medium containing 50 mmol/L Tris-HCl, 25.67 g/L sucrose, and 40.98 g/L D-Mannitol (pH 7.4) supplemented with 0.5 mmol/L EGTA and 5 g/L bovine serum albumin (BSA, Sigma-Aldrich). The homogenate was then transferred to microcentrifuge tubes and centrifuged at 0.8 rcf for 5 min for at least 2 cycles; the supernatants were collected, and the pellets were discarded. Subsequently, the sample was centrifuged at 10.0 rcf for 10 min to separate the mitochondrial fraction; the pellet was resuspended and ground in a loose-fitting glass Potter Elvehjem omogenizer for a fixed number of times. Samples were then centrifuged at 10.0 rcf for 10 min, and the pellet (mitochondria) was resuspended in 1 mL of Respiration Buffer (pH 7.4, Tris-HCl 50 mmol/L; 25.67 g/L sucrose; 40.98 g/L D-Mannitol) supplemented with 5 mmol/L succinate. Mitochondria were quantified and diluted to a final concentration of 1 mg/mL for each mitochondrial swelling assay to monitor the changes in absorbance at 540 nm as previously described. Incubations with small molecules were carried out at 25 °C, and mPTP opening was induced by the addition of 500μM Ca^{2+}.

Immunoblotting

Immunoblotting was performed to prove purity of the homogenate of the whole mice liver and to quantify the amount of cytochrome c release after compounds treatment.

Thereafter, protein extracts (15 μg/lane) were separated on precast 4-12% SDS-PAGE gels (Bio-Rad), electrotransfered onto nitrocellulose membranes and probed with antibodies specific for GAPDH (Cell Signaling) as cytosolic marker, TIM23 (BD Biosciences) or HSP60 (Cell Signaling) as mitochondrial markers, Cytochrome c (BD Biosciences) as signal of mPTP opening and apoptosis induction. Finally, membranes were incubated with appropriate HRP-labeled secondary antibodies (Thermo-Fisher). A conventional chemiluminescent substrate (Bio-Rad) and the ImageQuant LAS 4010 were employed for detection.

Luciferase−Luciferin Method

HeLa cells expressing a mitochondrially-targeted variant of the *Photinus pyralis* luciferase were perfused with a modified Krebs–Ringer buffer containing 125 mM NaCl, 5 mM KCl, 1 mM Na_3PO_4, 1 mM $MgSO_4$, 1 mM $CaCl_2$, 20 μM luciferin, and 20 mM HEPES buffer (pH 7.4) at 37°C, and luciferin-dependent luminescence was monitored in basal condition and after agonist-induced Ca^{2+} uptake, with a customized luminometer (Elettrofor), as previously described (218).

Mitochondrial parameters measurements

$\Delta\psi_m$ was assayed as described in Bonora et al. of 2016 (34). Briefly HeLa cells were loaded with 1nM TMRM (Thermo-Fisher) in Krebs-Ringer buffer supplemented with 250 μM sulfinpyrazone, then placed in a humidified chamber at 37°C and imaged with a LiveScan Swept Field Confocal Microscope (Nikon Instruments, Inc.) equipped with a 60× oil immersion (N.A. 1.4, from Nikon Instruments, Inc.) every 30 sec for 30 min. TMRM fluorescence was analyzed by means of the NIS Elements software package (Nikon

Instruments, Inc.), and depolarization rate were calculated as the slope of the fluorescence trace over a period of 10 min after stimulation.
For mitochondrial Ca^{2+} uptake measurements, for mtAEQmut at 24 h post-transfection, the coverslips were incubated with 5μM coelenterazine for 1.5 h in Krebs-Ringer modified buffer (KRB) supplemented with 1mM $CaCl_2$ (KRB: 125mM NaCl, 5mM KCl, 1mM Na_3PO_4, 1mM $MgSO_4$, 5.5mM glucose, and 20mM Hepes, pH 7.4, at 37°C). Aequorin signals were measured in KRB supplemented with either 1mM $CaCl_2$ using a purpose-built luminometer. The agonist (histamine at 100μM) was added to the same medium. The experiments were terminated by lysing the cells with Triton X-100 (Sigma-Aldrich) in a hypotonic Ca^{2+}-rich solution (10mM $CaCl_2$ in H_2O), thus discharging the remaining aequorin pool. The light signals were collected and calibrated with [Ca^{2+}] values.
Mitochondrial morphology was assayed as described in Bonora et al. of 2016 (34). Briefly, HeLa cells expressing a mitochondrially-targeted variant of mCherry, were imaged with an IX-81 automated epifluorescence microscope (Olympus) equipped with a 60X oil immersion objective (N.A. 1.35, from Olympus) and an ORCA-R2 CCD camera (Hamamatsu Photonics K.K.). Selected cells were followed over time, and z-stacks were subjected to digital deconvolution by means of a Wiener deconvolution filter and a theoretical point-spread function provided by the Xcellence software package (Olympus). GFP+ objects were quantified with the “3D object counter” plug-in of the open-source Fiji software (freely available at http://fiji.sc/), whereas 3D representations were obtained with the “3D Viewer” plug-in.

MTT assay
Cells were treated for 3 h at 37 °C with 0.5 mg/ml Thiazolyl Blue Tetrazolium Blue (MTT, Sigma-Aldrich) solution; after this incubation MTT solution was removed and was added extraction solution (90% isopropanol, 10% DMSO), extraction was at 37 °C for 15 min. After this passage the absorbance of the formazan solution is read spectrophotometrically at 570 nm.

Proximity Ligation Assays
Cells were fixed in 4% PFA for 10 min at 37 °C, washed in PBS, placed in a jar containing 1 mmol/L EDTA buffer (pH 8.0) for 20 min at 100 °C (to improve epitope antibody binding), and then placed at room temperature for an additional 10 min. Then the cells were permeabilized with 0.05% Triton X-100 for 10 min at 37 °C, and unspecific binding sites were blocked by incubating the cells in 0.05% Triton X-100 supplemented with 2% BSA for 45 min at 37 °C. Upon overnight incubation with ATP5H-specific antibodies that were previously conjugated to + or − PLA oligonucleotide probes per the instructions of the Duolink In Situ Probemaker kits (Sigma-Aldrich), detection was performed as follows. A ligation−ligase solution was added to each sample for 30 min at 37 °C followed by 2 washes for 2 min each with Duolink In Situ Wash Buffer A; an amplification-polymerase solution was added and incubated for 100 min at 37 °C followed by 2 washes for 10 min each with 1× Duolink In Situ Wash Buffer B and 1 wash for 1 min with 0.01× Duolink In Situ Wash Buffer B. Cells were fixed again in 4% PFA for 10 min at 37 °C and then blocked in 0.05% Triton X-100 supplemented with 2% BSA for 10 min at 37 °C. Finally, the samples were incubated overnight with primary anti-TOM20 (Cell Signaling) antibody, and the next day, the primary antibodies were revealed by incubation with the appropriate goat anti-rabbit Alexa Fluor 488 secondary antibody (Thermo-Fisher). The slides were then stained with Duolink In Situ Detection Reagent Red and mounted using DAPI-containing Duolink In Situ Mounting Medium. Protein proximity was evaluated on an Axiovert 200 M fluorescence microscope equipped with a 40× water immersion objective (N.A. 1.2, from Carl Zeiss Microscopy, LLC) as a function of mitochondrial-localized red signal intensity.

TUNEL (terminal deoxynucleotidyl transferase dUTP nick end labeling) assay
After I/R experiments through Langendorff model hearts are frozen and sectioned by a cryostat and stored at -20°C. After defreezing heart slices are fixed with 4% PFA for 20 min at RT, washed 3 times with PBS and permeabilized with 0.1% Triton X-100 in milliQ

water for 20 min at RT. After 3 washes slices are incubated for 1h at 37°C with TUNEL reaction mixture, made of label solution and enzyme solution (DNase I recombinant, grade I, 1000U/ml) that works in condition of 50mM Tris-HCl, pH 7.5, 10mM $MgCl_2$ and 1mg/ml BSA. 3 more washes precede the addition of TO-PRO diluted 1:25000 for 10 min at RT, after this passage there are washes too. Slices were imaged with an IX-81 automated epifluorescence microscope (Olympus) equipped with a 60X oil immersion objective (N.A. 1.35, from Olympus) and an ORCA-R2 CCD camera (Hamamatsu Photonics K.K.).

Statistical Analysis

The statistical method included one-way ANOVA with multiple comparisons performed by GraphPad Prism. P values are reported in the figure legends.

Ex Vivo Model

I/R was studied *ex vivo* using the Langendorff model with minor modifications (75). In brief, upon euthanasia, the hearts of Wistar rats weighing 270−280 g at inclusion into the study were rapidly excised, immediately arrested in ice-cold KHB (pH 7.4; 4°C), cannulated, and retrograde perfused at a fixed-flow rate (11 mL/min) through the aorta with warm KHB (37 °C) bubbled with 95% O_2 and 5% CO_2. Upon removal of the left atrial appendage, a latex fluid-filled balloon was inserted into the left ventricular chamber through the atrium to obtain an isovolumetrically beating preparation and connected to a pressure transducer (APT300, Hugo-Sachs, Grünstrasse, Germany) by a fluid-filled polyethylene catheter to monitor performance. An additional transducer above the aortic cannula monitored the CPP. At the start of each experiment, the fluid in the balloon was increased incrementally to achieve a constant EDP of 4 ± 1 mmHg. The LVDP was then measured. The LVDP, EDP, and CPP were continuously recorded using a programmable acquisition system (HSE Isoheart Software for Isolated Heart, Hugo-Sachs, Grünstraße, Germany).

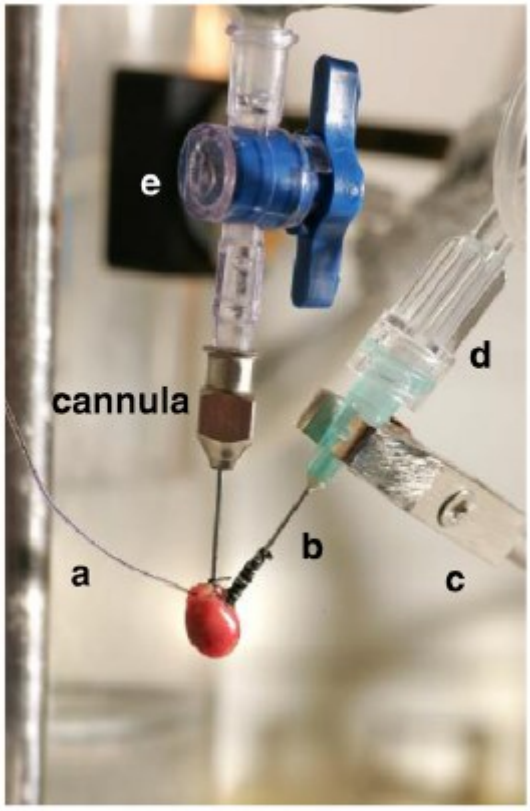

Figure 23. A Langendorff-perfused mouse heart. During the perfusion protocol, the heart would normally be immersed in an organ bath.
a: thermal couple for continual temperature monitoring;
b: intraventricular balloon inserted in the left ventricle and mounted on a 21-gauge non-bevelled needle;
c: a micromanipulator which helps placing and keeping the balloon in the left ventricle;
d: one end of the non-pliable tubing that provides the hydraulic line to a pressure transducer mounted at the same height as the heart;
e: a 2 way tap placed between the bubble trap and the cannula, which serves to switch off the buffer during global ischemia (208).

Chapter 2.

Permeability Transition Pore function correlates with reperfusion damage in STEMI patients and a novel nucleotide transition in C subunit genes is associated to increased cell death at reperfusion time

Abstract

In vitro and pre-clinical models have demonstrated the deleterious effects of mitochondrial Permeability Transition Pore (mPTP) opening in the first few minutes upon reperfusion, becoming a key player in the acceleration of the injury process.

According to this, targeting mPTP might be a valid adjuvant strategy to counteract the reperfusion damage. Hitherto, no evidences are present in a clinical scenario.

Recent studies hypothesized that one of the pore-forming proteins of the mPTP is the F_O ATP synthase c subunit. Its circulating levels had been found to be associated with surrogate endpoints of myocardial reperfusion in patients with ST-segment elevation myocardial infarction (STEMI).

No data about genetic determinants in c subunit have ever been related to reperfusion injury in patients with MI. Overall in this project, the CROFT clinical study showed how mPTP activity measured in fibroblasts significantly correlates with that monitored in myocytes from the same patient, so in those conditions where cardiac biopsies are impossible to be taken, mPTP function in fibroblasts from STEMI patients may be predictive of the mPTP activity in myocytes.

Moreover, for the first time we provided a proof of mPTP correlation to reperfusion injury developed upon MI in patients. In addition, a new polymorphism found in ATP5G1 gene encoding for c subunit in two STEMI patients was responsible for worsening reperfusion injury *in vitro*.

Riassunto

Sia modelli *in vitro* che preclinici hanno dimostrato l'effetto deleterio dell'apertura dell'mPTP nei primi minuti dopo la riperfusione, giocando un ruolo chiave nell'accelerazione del processo di danno tissutale.
In accordo con ciò, colpire il mPTP può essere una valida strategia adiuvante per contrastare il danno da riperfusione. Fino a questo momento infatti, non ci sono evidenze nello scenario clinico dell'infarto del miocardio.
Studi recenti hanno ipotizzato che una delle proteine componenti il poro dell'mPTP è la subunità c della porzione F_O dell'ATP sintasi. I suoi livelli circolanti sono stati associati con endpoints surrogati della riperfusione miocardica in pazienti con infarto miocardico con sopraslivellamento del tratto ST (STEMI).
Non sono mai stati correlati dati sui determinanti genetici nella subunità c al danno da riperfusione in pazienti con infarto del miocardio (MI).
Complessivamente in questo capitolo, lo studio clinico CROFT ha mostrato come l'attività dell'mPTP misurata nei fibroblasti correli in modo significativo con quella monitorata nei cardiomiociti dello stesso paziente, in questo modo in quelle condizioni in cui le biopsie cardiache sono impossibili da ottenere, la funzione dell'mPTP nei fibroblasti di pazienti STEMI può essere predittiva dell'attività dell'mPTP nei cardiomiociti.
Inoltre, per la prima volta abbiamo dimostrato una correlazione tra l'mPTP e il danno da riperfusione dopo infarto in pazienti. In aggiunta, un nuovo polimorfismo è stato trovato nel gene ATP5G1 che codifica per la subunità c in due pazienti STEMI ed è stato associato ad un peggioramento nel danno da riperfusione *in vitro*.

Results

1. Skin fibroblasts are an alternative model to study mPTP in patients affected by cardiovascular diseases.

Obtaining heart samples or myocytes for cardiovascular research purposes is extremely difficult and sometimes impossible, also considering the progressive development of mini-invasive or percutaneous procedures. To provide for the first time an alternative and feasible way to obtain information on mPTP function in cardiovascular diseases (i.e., MI), we performed a pilot study (named CROFT) involving 16 patients undergoing cardiac surgery (Figure 24a) from which we collected both cardiomyocytes and fibroblasts from left atrial appendage and skin biopsies at the level of surgery access, respectively. In these samples, we performed mPTP functional analysis by analyzing $\Delta\psi_m$ under Ca^{2+}- and oxidative stress-dependent conditions as previously published (134), (34) (Figure 24b). Interestingly, we reported first, an important variability in the mPTP opening among patients ($p < 0.0001$ as result from ANOVA test applied to both fibroblasts and myocytes measures, Figure 24b) and second, a significant correlation between mPTP activity measured in fibroblasts and that recorded in myocytes of the same patient (Spearman's $r = 0.51$, $p = 0.04$, Figure 24c). Overall, as showed in Figure 24d, patients with lower mPTP activity recorded in fibroblasts (mPTP value below the median) have also a lower mPTP activity in myocytes compared to the others. Taken together, these data suggest an interesting variability in the mPTP function among different individuals and confirm that fibroblasts obtained from skin biopsy are a feasible model to obtain crucial information on the mPTP function in patients (i.e., MI).

a

Variable	Summary statistics	Patient Population N=16
Age (years)	Mean ± SD; Median (min-max)	64.8 ± 13.1; 67(33-83)
Male sex	N (%)	12 (75%)
Body Mass Index (kg/m^2)	Mean ± SD; Median (min-max)	27.8 ± 5.6; 26.2 (19.6-39.5)
Extracardiac arteriopathy	N (%)	1 (6%)
Sinusal rhytm	N (%)	15 (88%)
Urgent indication	N (%)	5 (29%)
Etiology:		
Mitral/Aortic valve disease	N (%)	9 (53%)
Coronary artery disease	N (%)	5 (29%)
Valvular and ascending aorta	N (%)	2 (12%)
Valvular and coronary disease	N (%)	1 (6%)
Family history	N (%)	6 (35%)
Hypertension	N (%)	12 (71%)
Diabetes mellitus	N (%)	4 (23%)
Smoker	N (%)	3 (18%)
COPD	N (%)	1 (6%)
Renal failure	N (%)	2 (12%)
Cerebrovascular accident	N (%)	2 (12%)
Leukocyte	Mean ± SD; Median (min-max)	6.3±2; 6.3 (3.1-10.4)
Creatinine (mg/dL)	Mean ± SD; Median (min-max)	1.0.1 ± 0.33; 0.89 (0.65-1.77)
C-Reactive protein (mg/dL)	Mean ± SD; Median (min-max)	0.3±0.2; 0.3 (0-0.7)
Hemoglobin (g/dL)	Mean ± SD; Median (min-max)	13.4±1.9; 13.3 (10.5-16.5)
NYHA III - IV	N (%)	2 (12%)
Ejection fraction (%)	Mean ± SD; Median (min-max)	56.8 ± 10.4; 60 (35-75)
euro SCORE I	Mean ± SD; Median (min-max)	4.8±3.5; 5 (0-11)
euro SCORE II	Mean ± SD; Median (min-max)	6.2 ± 7.1; 3.98 (0.88-24.9)
Logistic EuroSCORE	Mean ± SD; Median (min-max)	3.1 ± 3.9; 1.98 (0.56-15.81)

5.

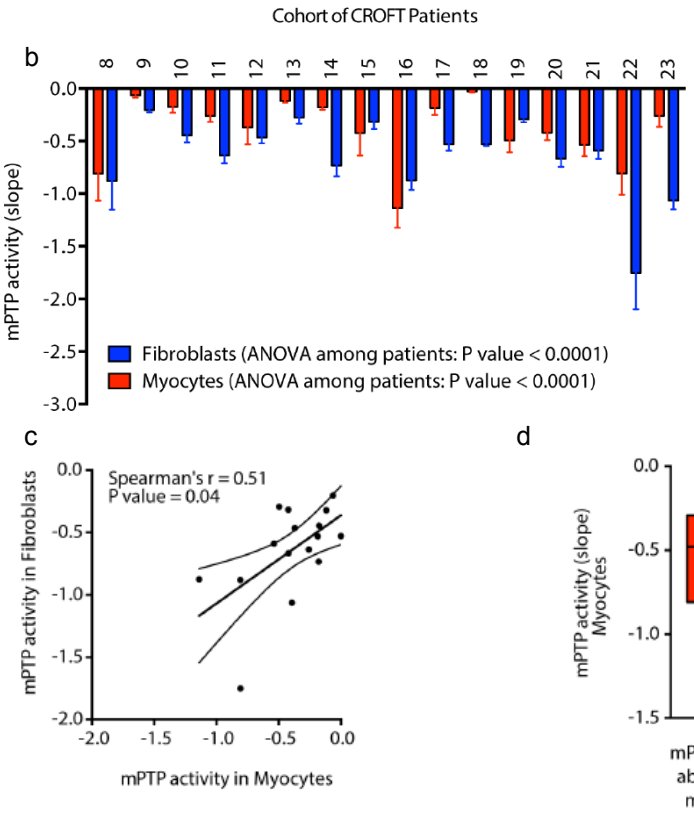

Figure 24. Study A: results from CROFT clinical study.
a: table containing statistics and information on the 16 patients enrolled in the CROFT study.
b: $\Delta\psi_m$ assay by the use of TMRM probe in both myocytes (red) and fibroblasts (blue) from the same patients.
c: graph showing the correlation (as Spearman's r) between $\Delta\psi_m$ measured in both myocytes and fibroblasts for each patient of the CROFT study.
d: stratification of mPTP function measured in myocytes according to fibroblasts mPTP median value.
P values reported next to the legend of the graph in b refer to the ANOVA test performed first, among mPTP measures in fibroblasts (blue rectangle) and second, to those of myocytes (red rectangles).

	MSI			
	All (n=14)	**below the median (n=7)**	**Above the median (n=7)**	**p**
Age (years)	58 [52-66]	58 [54-62]	60 [51-66]	0.4
Male sex, no. (%)	13 (93)	7 (100)	6(86)	0.9
CV risk factors, no. (%)				
Diabetes	4 (29)	2 (29)	2 (29)	1
Hypertension	9 (66)	5 (71)	4 (57)	0.7
Dyslipidemia	6 (43)	3 (43)	3 (43)	1
Smokers	4 (20)	2 (29)	2 (29)	0.7
Clinical presentation,				
OS-balloon time (min)	245 [190-300]	240 [185-300]	250 [200-305]	0.8
FMC-balloon time (min)	55 [40-80]	55 [45-90]	58 [40-80]	0.9
SBP (mmHg)	140 [120-160]	130 [110-170]	145 [130-155]	0.9
HR (beats/min)	90 [85-100]	90 [80-100]	91 [85-100]	0.6
Killip class ≥2, no. (%)	3 (21)	2 (29)	1 (14)	
Angiographic features, no. (%)				
Proximal LAD, no. (%)	11 (79)	5 (71)	6 (86)	0.9
MVD, no. (%)	7 (50)	3 (43)	4 (57)	0.8
RVD (mm)	3.2 [3-3.5]	3.2 [2.8-3.7]	3.1 [3-3.3]	0.7
MLD post (mm)	3 [3-3.3]	3 [2.7-3.8]	3 [2.8-3.7]	0.6
Thrombectomy, no. (%)	9 (64)	4 (57)	5 (71)	0.8
Predilatation, no. (%)	11 (79)	5 (71)	6 (86)	0.7
Number of stent, no.	1 [1-2]	1 [1-2]	1 [1-2]	0.9
Stent diameter (mm)	3 [3-3.5]	3 [3-3.5]	3 [3-3]	0.9
Stent lenght(mm)	24 [18-30]	20 [18-28]	24 [29-30]	0.9
At discharge,				
CK-MB at peak (ng/dl)	210 [145-300]	189 [75-309]	210 [150-334]	0.3
Troponin T at peak (ng/dl)	5.3 [2.9-9]	7.6 [0.8-14]	4.8 [3.3-6.8]	0.4
WMSI,	1.25 [1.2-1.8]	1.4 [1.2-1.9]	1.2 [1.1-1.7]	0.4
LVEF (%)	45 [38-53]	42 [35-50]	47 [40-60]	
Aspirin, no. (%)	14 (100)	7 (100)	7(100)	1
Clopidogrel, no. (%)	9 (64)	4 (57)	5 (71)	0.9
Ticagrelor , no. (%)	5 (36)	3 (43)	2 (29)	0.7
ACE inhibitors, no. (%)	13 (93)	6 (86)	7 (100)	0.9
B-blockers, no. (%)	13 (93)	7 (100)	6 (86)	0.8
Statins, no. (%)	14 (100)	7 (100)	7 (100)	0.9

Figure 25. Study B: Study population for mPTP function and reperfusion damage tests, stratified according to median value of myocardial salvage index.
OS: onset of symptoms.
FMC: first medical contact.
SBP: systolic blood pressure.
HR: heart rate.
LAD: left anterior descending.
MVD: multivessel disease.
RVD: reference vessel diameter.
MLD: minimal lumen diameter.
WMSI: wall motion score index.
LVEF: left ventricle ejection fraction.
ACE: angiotensin II converting enzyme.

2. mPTP activity is significantly related to reperfusion injury in STEMI patients.

Supported by the evidences of previous data (Figure 24), we conducted a second pilot study in a cohort of 14 patients with anterior MI undergoing primary PCI (Figure 25 and Methods for details) with the aim to investigate the correlation between mPTP activity and the so-called reperfusion damage. Thus, skin biopsies from the forearm of patients have been used to obtain fibroblasts for functional analysis and cardiac magnetic resonance imaging (cMRI) was performed to assess reperfusion damage. Figure 26 a and b reported mPTP opening in fibroblasts for each STEMI patient as evaluated by both calcein-cobalt and TMRM techniques under Ca^{2+}- and ROS-dependent conditions, respectively. For a better understanding of mPTP variations among individuals, in panel c we reported representative kinetics for both ID4 (hyper-responsive mPTP) and ID30 (hypo-responsive mPTP) patients.

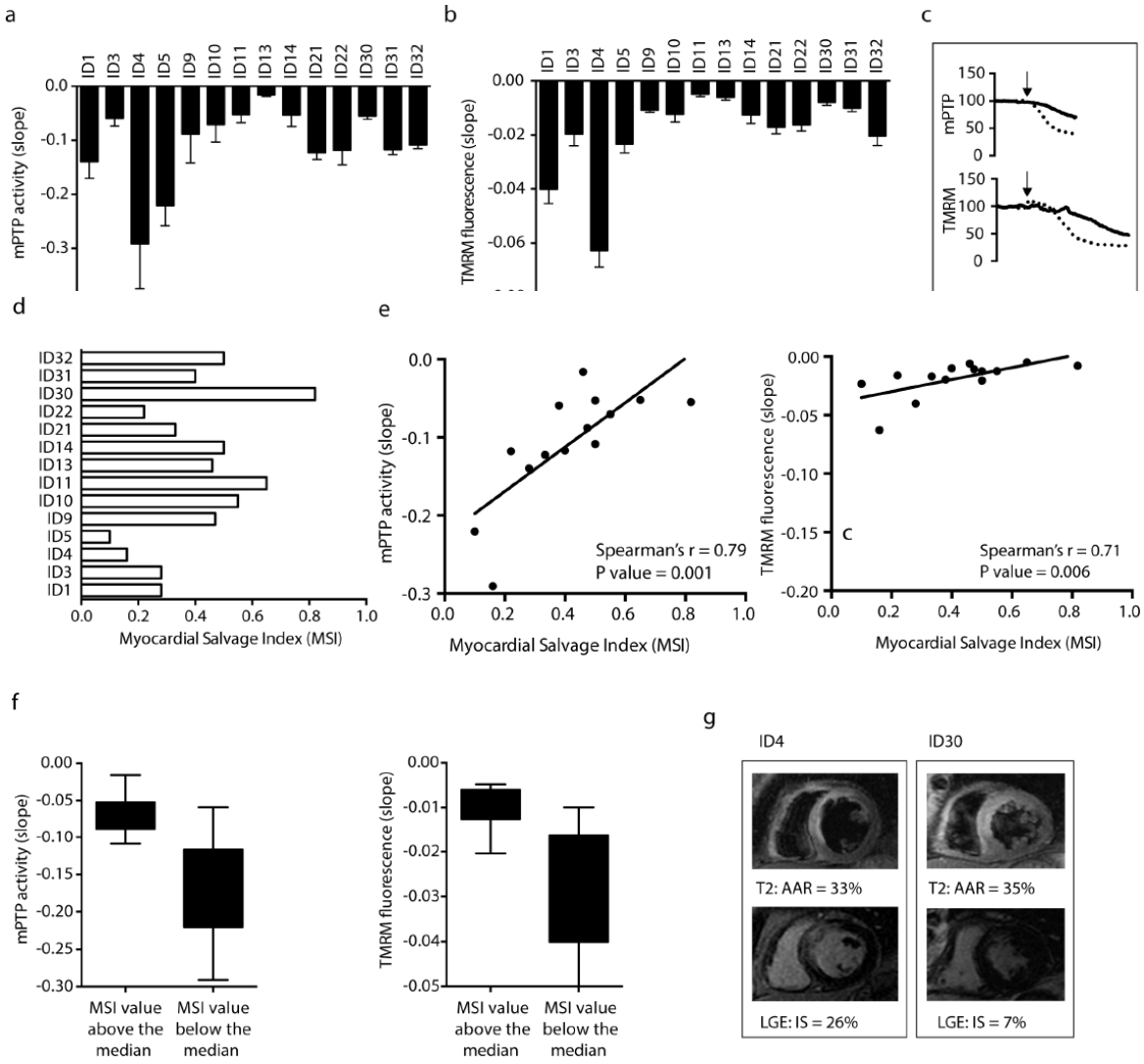

Figure 26. Correlation between mPTP function and reperfusion damage in STEMI patients.
a: calcein-cobalt quenching assay in fibroblasts from skin biopsy of STEMI patients where mPTP activity is reported as slope of the kinetics following ionomycin administration, as indicated.
b: $\Delta\psi_m$ in the same cells of a by using TMRM assay; it is reported as slope of the kinetics following hydrogen peroxide administration, as indicated.
c: representative kinetics on the difference in mPTP activity between two STEMI patients: ID4 and ID30

d: MSI from cMRI.
e: graphs explaining correlation between mPTP activity and MSI (on the left) and $\Delta\psi_m$ and MSI (on the right) measured in fibroblasts from STEMI patients; Spearman's r and p value have been reported in the panel.
f: stratification of mPTP and $\Delta\psi_m$ values according to MSI median value.
g: representative cMRI images of two STEMI patients: ID30 with hypo-responsive mPTP opening and limited IS (7%), ID4 with hyper-responsive mPTP opening and extensive IS (26%).

At cMRI evaluation, the Myocardial Salvage Index (MSI) has been calculated and reported in Figure 26d. We observed a significant correlation between MSI and mPTP activity (Spearman's r = 0.79, p = 0.001) and $\Delta\psi_m$ (Spearman's r = 0.71, p = 0.006) values (Figure 23e). Median value of MSI was 0.44 [0.21-0.55]. We did not observe significant differences in baseline characteristics in patients stratified according MSI median value (Figure 25). Out of all variables listed in Figure 25, none is related to mPTP activity and $\Delta\psi_m$ values. Overall, in patients with larger reperfusion damage (MSI below the median value), we found significantly heightened mPTP activity and $\Delta\psi_m$ values as compared to the others (Figure 26f). Figure 26g showed representative images for cMRI between two STEMI patients: ID4 who experienced a hyper-responsive opening of the mPTP (Figure 26c) owns a final infarct size (IS) of 26%; ID30 who has been subjected to a hypo-responsive mPTP opening (Figure 26c) owns a final IS of 7% (Figure 26g). Taken together these data describe in patients the strong relationship between mPTP activity and reperfusion damage and confirmed, in a second cohort of individuals (as for Figure 24b), the overall inter-subject variability in mPTP function ($p < 0.0001$ from ANOVA test applied to mPTP and $\Delta\psi_m$ measures).

3. A novel nucleotide transition in F_O ATP synthase c subunit-encoding genes of two STEMI patients is predicted to be probably damaging.

It is known that MI is a multifactorial disease in which both environmental factors and genetic profiles play a key role in its development; a given signature of gene expression or mutations are already reported to be associated to incident MI or an increased risk of cardiovascular death (191), (219). Despite this, no genetic links between the mPTP complex and the impact on reperfusion injury progression have ever been reported in MI.

Since we recorded differences in mPTP activity among individuals (Figure 24b and 26a,b) and that c subunit has been found to be an important regulator of the mPTP (75), (36), we wondered if, in some cases, a hyper- or hypo-responsive opening of the mPTP can be determined also by genetic alterations in genes encoding for c subunit and whether they further contribute to reperfusion damage in STEMI patients by altering mPTP activity.

For this purpose, we started to randomly select one third (N=52, Figure 27 and Methods for details) of STEMI patients from those already enrolled in our previous study (140) to perform a complete genetic screening for all three ATP5G1-3 genes encoding for c subunit of the mPTP; results have been summarized in Figure 28.

	All (n=52)
Age (years)	63±11
Male sex, no. (%)	39 (75)
CV risk factors, no. (%)	
Diabetes	7 (14)
Hypertension	36 (70)
Dyslipidemia	28 (55)
Smokers	29 (56)
Clinical presentation,	
Symtom-balloon time (min)	130 [90-200]
FMC-balloon time (min)	85±39
Angiographic features, no. (%)	
Proximal LAD, no. (%)	26 (51)
MVD, no. (%)	27 (52)
Thrombectomy, no. (%)	20 (40)
Number of stent, no.	1 [1-2]
Stent diameter (mm)	3 [3-3.5]
Stent lenght(mm)	24±8
At discharge,	
CK-MB at peak (ng/dl)	110 [30-260]
Troponin T at peak (ng/dl)	2.1 [0.9-8]
WMSI,	1.5 [1.2-1.8]
LVEF (%)	45 [36-55]
Aspirin, no. (%)	52 (100)
Clopidogrel, no. (%)	10 (20)
Ticagrelor, no. (%)	34 (66)
Prasugrel, no. (%)	7(13)
ACE inhibitors, no. (%)	42 (80)
B-blockers, no. (%)	47 (90)
Statins, no. (%)	50 (97)

Figure 27. Study B: Study population for genetic analysis in c subunit encoding genes of mPTP

Figure 28.

a: Primers' name and sequences for the amplification of the genes ATP5G1-3. The size of each amplicon is reported in base pairs together with the specific annealing temperature.

a

Primers ATP5G1	Forward	Reverse	Amplicon size	Annealing T°C
ATP5G1-5'UTR	tacaccttggtcgccatctt	gagcagtgggtcttcaaagc	721	56
ATP5G1-1	cctttcgcaacatttccttc	gctgtctctatggccaggac	544	54
ATP5G1-2	tgattaaagctgtgcccaaa	ggagtgcagtggcatagtca	612	56
ATP5G1-3	ccaaagtgggaggagagttg	aggacacaggagggtgaggt	759	60
ATP5G1-4	ggaggagctcccttcagga	actcagacaaacccatattcctc	650	54

Primers ATP5G2	Forward	Reverse	Amplicon size	Annealing T°C
ATP5G2-1	atccagtgatgccagagtcc	gactgggtggaacaggtgaa	765	54
ATP5G2-2	aagtcttgagaagcgttccttt	ctgttgcctcagcctcct	680	56
ATP5G2-3	tgttgagtgaggcaaatgct	tgaggccctagtctattcttgc	732	56
ATP5G2-4	cctgtgcactgctgctaact	atcgcttgaacccagaggta	733	60
ATP5G2-5	gggccaagaggtcttaatttg	ttcgggccttgtactctcac	626	58

Primers ATP5G3	Forward	Reverse	Amplicon size	Annealing T°C
ATP5G3-1	ccggctagttgccaataaag	aaagggccactcctggtcta	757	54
ATP5G3-2	ttcaaggtagcaagcgttacaa	gtcaagcaatcctccctcct	656	54
ATP5G3-3	tgacagaccaggtgagacctt	gacctgggcaagtaatgtgg	713	58
ATP5G3-4	cagatggataagaatgtcagaacc	gcttcctctgaatgggacag	600	60

b: Results from next generation sequencing applied to all ATP5G1-3 genes in the study population B.

b

ATPG1	Variation	Coordinates	Functional position	dbSNP
Exon 1	G>T	chr17:46970684	intronic	rs573172017
Exon 3	ΔCTCT	chr17:46972481-46972484	intronic	rs3080082
	G>A	chr17:46972660	exonic (missense)	–
Exon 4	C>T	chr17:46972865	intronic	rs832410
	T>C	chr17:46973103	exonic (missense)	–

ATPG2	Variation	Coordinates	Functional position	dbSNP
Exon 1	ins.CA	chr12:54070063	5 UTR	rs4020138
	C>T	chr12:54069803	intronic	rs916134
Exon 2	C>G	chr12:54066271	intronic	rs10876480
	T>C	chr12:54066378	exonic (synonymous)	rs57929423
Exon 3	C>T	chr12:54063501	intronic	rs1800633
	A>G	chr12:54063493	intronic	rs1800634
	C>T	chr12:54063869	intronic	rs79533383
Exon 4	ins GTTTGTTT	chr12:54062799	intronic	–
Exon 5	ins. C	chr12:54059441	intronic	–
	C>T	chr12:54059281	intronic	rs71455254

ATPG3	Variation	Coordinates	Functional position	dbSNP
Exon 1	C>A	chr2:176046483	5 UTR	–
	C>T	chr2:176046415	5 UTR	rs268228
	C>T	chr2:176046408	5 UTR	rs2217675
	C>A	chr2:176046392	5 UTR	–
	ins. C	chr2:176046365	5 UTR	–
	G>T	chr2:176046363	5 UTR	rs147943553
	G>A	chr2:176046257	5 UTR	rs268227
	G>T	chr2:176046167	5 UTR	rs41270205
	G>A	chr2:176046007	intronic	rs73039765
Exon 3	A>T	chr2:176044136	intronic	rs268224
	C>A	chr2:176044008	intronic	rs12615406
	G>A	chr2:176043618	3' UTR	rs268223
Exon 4	C>T	chr2:176042877	3' UTR	rs189393963
	G>A	chr2:176042819	3' UTR	rs2288960
	T>C	chr2:176043097	3' UTR	rs8106

In detail, we found 23 known polymorphisms and 6 unknown variations (not reported in the gnomAD, dbSNP and 1000genomes databases) where, 4 of them fell in non-coding genomic regions like introns and 5'UTR and 2 of them were missense mutations. The first one was a G>A nucleotide transition found in the exon 3 of the ATP5G1 gene of 2 out of 52 patients, apparently a very high recurrence considered the little cohort of patients analyzed (Figure 29a). This variation led to a missense mutation (a glycine substitution with a glutamic acid, G87E) in the exon 3 of the gene at position 87 ($ATP5G1^{G87E}$). Given that the amino acid substitution occurred in an important and highly conserved glycine-rich domain of the c subunit coding-sequence (Figure 29b) and that consensus to obtain biological samples from those patients took a long time, we first conducted a bioinformatics analysis to predict if the variation, once expressed, may induce damaging phenotypes *in vivo*. By querying PolyPhen-2 software (220), it predicted $ATP5G1^{G87E}$ as

probably damaging with a score of 0.993 in a scale from 0 to 1 (Figure 29c). To consolidate this finding, we investigated other 6 prediction softwares known in the literature and all returned similar readouts: once expressed, this mutated protein would be probably damaging with a score ranging between 60% and 90% (Figure 29c). Additional bioinformatics studies based on the RaptorX web server (221) also predicted that ATP5G1^{G87E} would exhibit a structural deformation at the level of the first helix of c subunit (Figure 29d).

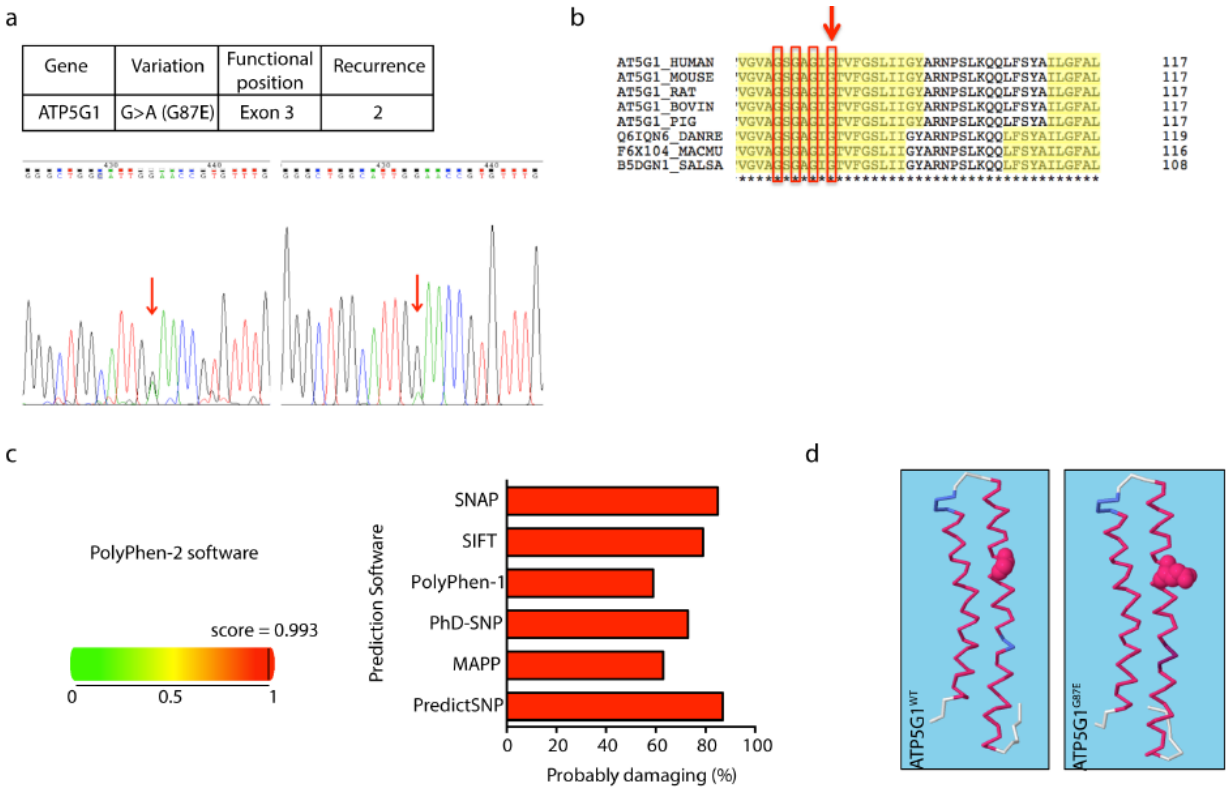

Figure 29. ATP5G1^{G87E} variation alters mPTP activity and cell death pathway during I/R in fibroblasts collected from the patient carrying mutation

a: genetic profile of ATP5G1^{G87E} variation (up) and capillary electrophoresis of the DNA sequencing of 2 patients carrying mutation (down): arrows indicate the presence of the variation in heterozygosis.

b: c subunit coding sequence alignment among different species: glycine-rich region has been highlighted by 4 red rectangles and the arrow indicate the site of amino acid substitution.

c: data output from the PolyPhen 2 software (on the left) in which green color indicate the probability of a benign variation while the red one damaging. The black line indicates the score predicted by the software. On the right, data output of other 6 different predictive softwares (Y axis) where red color indicates that the variation is damaging, on the X axis its probability.

d: data output from the RaptorX software: highlighted the steric hindrance of the amino acid substitution.

4. ATP5G1^{G87E} expression worsens in vitro mPTP-mediated ischemia/reperfusion damage.

Given the interesting biological prediction outlined by bioinformatics tools (Figure 29a-d), we were interested to confirm in cells the putative harmful effects of ATP5G1^{G87E} in terms of mPTP function and cell death in I/R conditions. To this aim, we tried to enroll both STEMI-patients carrying the mutation, but we were able to recall only one, because the second one died following MI. Functional analysis on fibroblasts of the enrolled STEMI-patient (Id 24) unveiled an altered mPTP activity and $\Delta\psi_m$ under Ca^{2+}- and ROS-dependent stimuli, respectively, when compared to control counterparts Id C1 and Id C2 (Figure 29e,f). These differences were statistically significant with a $p < 0.01$. In addition, under I/R insult, we noticed decreased cell viability in Id 24 cells as evaluated by the propidium iodide (PI) uptake ($p < 0.001$ for Id C1 vs. Id 24; $p < 0.0001$ for Id C2 vs. Id 24) and crystal violet ($p < 0.05$ for Id C1 vs. Id 24; $p < 0.01$ for Id C2 vs. Id 24) approaches (Figure 29g). Cell death at reperfusion time was due to a greater activation of the apoptotic pathway in Id 24 cells compared to the control counterparts, as measured by quantification of cleaved PARP, once detected in fluorescence by the use of a monoclonal specific antibody ($p < 0.01$ for Id C1 vs. Id 24; $p < 0.001$ for Id C2 vs. Id 24; Figure 29h).

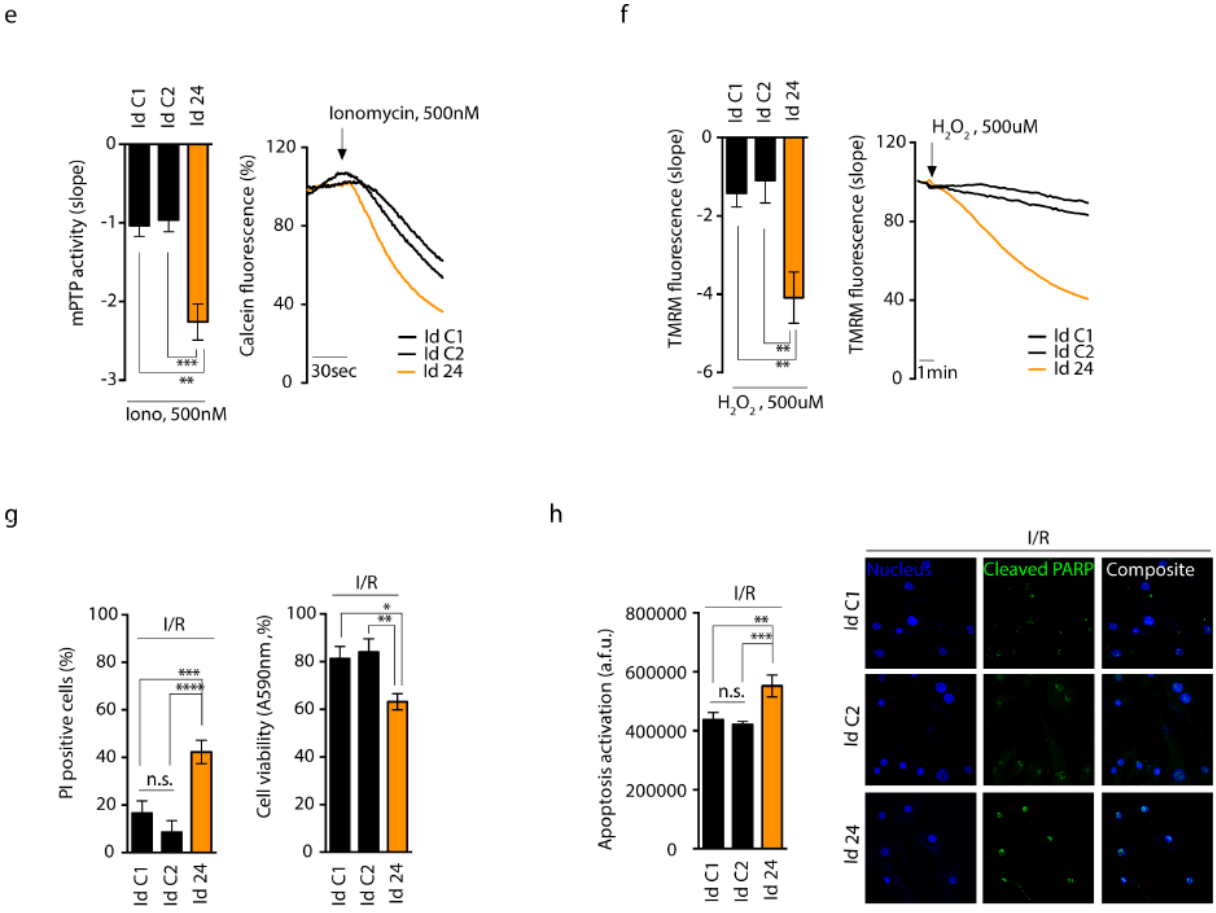

Figure 29. e: calcein-cobalt quenching assay in fibroblasts from skin biopsy of the STEMI patient carrying mutation (Id 24, orange bar) and the control counterparts (Id C1 and Id C2, black bars), mPTP activity is reported as slope of the kinetics following ionomycin administration.
f: $\Delta\psi_m$ in the same cells of E by using TMRM assay, it is reported as slope of the kinetics following hydrogen peroxide administration.

g: quantification of cell viability by reporting both cells that have incorporated propidium iodide (PI) (on the left) and cells remained alive upon I/R, stained with crystal violet (on the right). Results have been reported as percentage.
h: cleaved PARP detection and quantification by immunofluorescence in confocal microscopy: statistics and representative images under I/R are reported. Results have been represented as arbitrary fluorescence units (a.f.u.)

Moreover, in the absence of stressors, fibroblasts from Id C1, Id C2 and Id 24 patients shared similar mitochondrial parameters in terms of morphology, $\Delta\psi_m$ and mitochondrial Ca^{2+} handling (Figure 30a-c), they own similar expression levels of proteins that could be directly or indirectly involved in mPTP opening (Figure 30d), as well as unchanged was the dimerization status of ATP synthase complex at resting state (Figure 30e). The findings reported up to here highlighted once again a critical role for c subunit in mPTP opening, but taking into consideration genetic determinants.

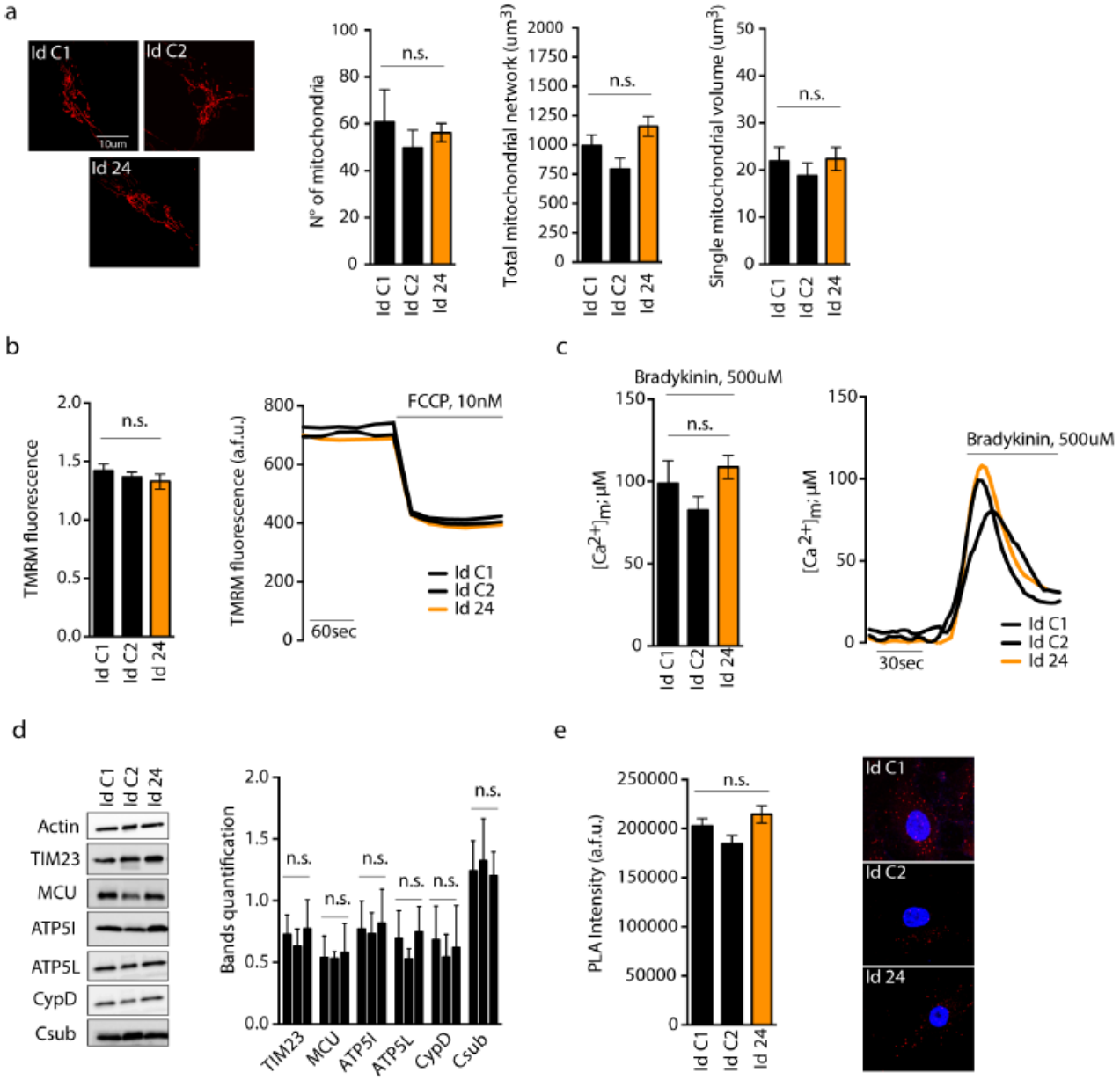

Figure 30. Mitochondrial parameters of fibroblasts in normoxia conditions
a: analysis of mitochondrial morphology performed in Id C1, Id C2 and Id 24 cells by the use of Mitotracker Deep Red and confocal microscopy: representative images on the left and statistics about the number of mitochondria and their volume, the total mitochondrial network (Y axis) on the right.
b: analysis of basal $\Delta\psi_m$ performed by the use of TMRM probe and fluorescence microscopy.
c: analysis of mitochondrial Ca^{2+} handling upon agonist (Bradykinin) administration.
d: detection (on the left) and quantification (on the right) of proteins directly or indirectly involved in mPTP modulation by western blot analysis. Actin: loading marker; TIM23: mitochondrial loading marker; MCU: mitochondrial calcium uniporter; ATP5I: ATP synthase subunit e, involved in ATP synthase dimerization; ATP5L: ATP synthase subunit g, involved in ATP synthase dimerization; CYPD: mitochondrial cyclophilin D, mPTP modulator.
e: ATP synthase dimerization status of fibroblasts in resting conditions assessed by proximity ligation assay (PLA) with the use of ATP5H specific antibody and confocal microscopy.
n.s.=not significative.

In order to evaluate and confirm the deleterious effects of $ATP5G1^{G87E}$ expression in a cardiac environment, the wild type ATP5G1 cDNA has been mutated and overexpressed in human ventricular cardiomyocytes (AC16 cell line, Figure 31a), to mimic the effect of the heterozygous mutation. As seen in Figure 31b, the mutated protein is expressed and localized to mitochondrial compartment in AC16 cells. As expected, the expression of $ATP5G1^{G87E}$ strongly altered mPTP opening upon Ca^{2+}-dependent stimulus in three different types of cardiac myocytes: AC16 ($p < 0.01$), neonatal rat cardiomyocytes (NRCMs, $p < 0.01$) and HL-1 ($p < 0.05$) (Figure 31c). In details, $ATP5G1^{G87E}$ promoted a mPTP opening that was double to that seen by overexpressing c subunit WT ($ATP5G1^{WT}$), the reference control (36). For the experiments reported below, AC16 was the cell line taken into account to perform the study since it has human origin and it is easy to handle. In Figure 31d we reported $\Delta\psi_m$ measures upon ROS-dependent stimulus that reproduced data seen in panel c for AC16.

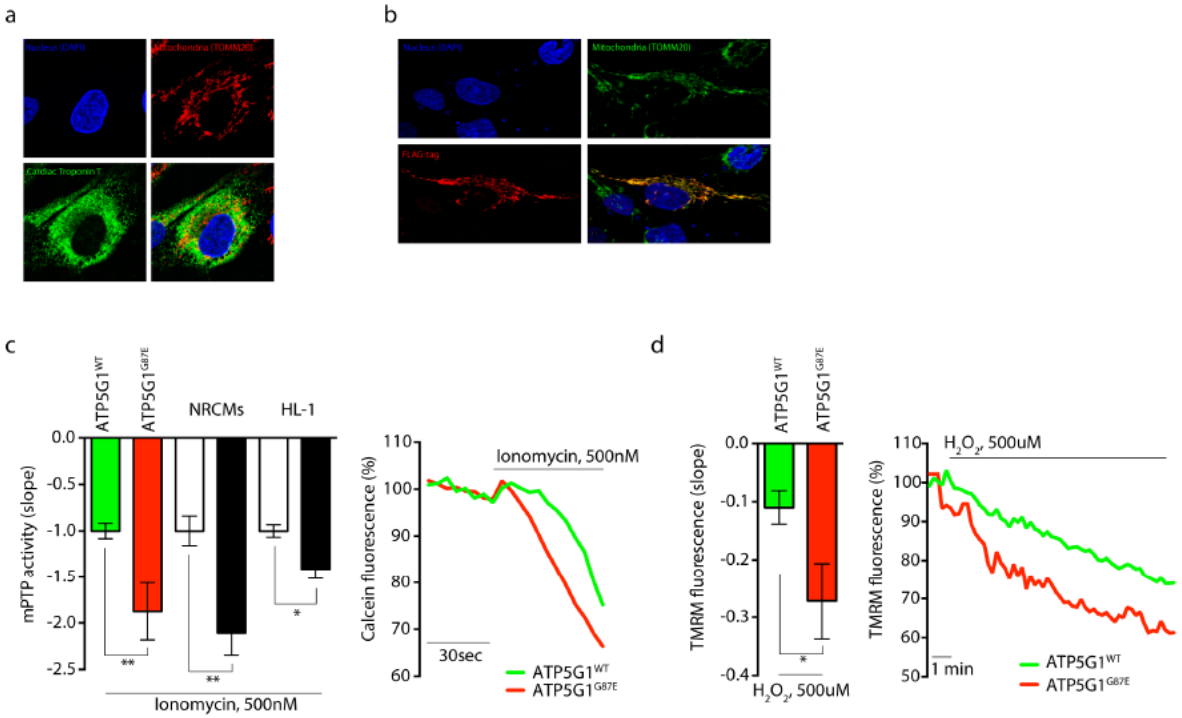

Figure 31. ATP5G1^{G87E} variation alters mPTP activity and cell death pathway during I/R in human ventricular cardiomyocytes

a: cardiac troponin T (in green) detection in AC16 cell line by immunofluorescence in confocal microscopy; in the image can be seen also the nucleus (in blue) and the mitochondrial network detected by TOM20 antibody (in red)

b: expression and localization of ATP5G1^{G87E} mutated protein (in red, with the use of an anti-FLAG antibody as tag of the plasmid) in AC16 cell line.

c: calcein-cobalt quenching assay in AC16, neonatal rat cardiomyocytes (NRCMs, white bar for ATP5G1^{WT} and black bar for ATP5G1^{G87E}) and HL-1 cells (white bar for ATP5G1^{WT} and black bar for ATP5G1^{G87E}) where mPTP activity is reported as slope of the kinetics following ionomycin administration.

d: $\Delta\psi_m$ in AC16 cells by using TMRM probe; it is reported as slope of the kinetics following hydrogen peroxide administration.

In the attempt to validate the hypothesis that genetic determinants of c subunit and thus of mPTP are crucial in I/R conditions in the heart, we have reproduced ischemia and reperfusion by the use of a hypoxic chamber in which we evaluated kinetics of mPTP and cell death onset at the time of reperfusion. Even in this case, cells expressing ATP5G1^{G87E} resulted in a hyper-responsive mPTP opening ($p < 0.01$, Figure 31e) compared to those expressing ATP5G1^{WT}.

To better describe the effect of ATP5G1^{G87E} in experiments involving cell population rather than single-cell analysis, two AC16 clones stably expressing ATP5G1^{WT} and ATP5G1^{G87E} proteins have been used. In cardiomyocytes, the altered mPTP channel activity promoted by ATP5G1^{G87E} led to decreased cell viability ($p < 0.0001$, Figure 31f) due to greater apoptosis activation as detected by cleaved PARP specific antibody in western blot and immunofluorescence analysis ($p < 0.01$, Figure 31g,h).

Taken together these findings suggest that ATP5G1^{G87E} is responsible for a significant and exacerbated I/R damage in both fibroblasts from patient and in ventricular cardiomyocytes.

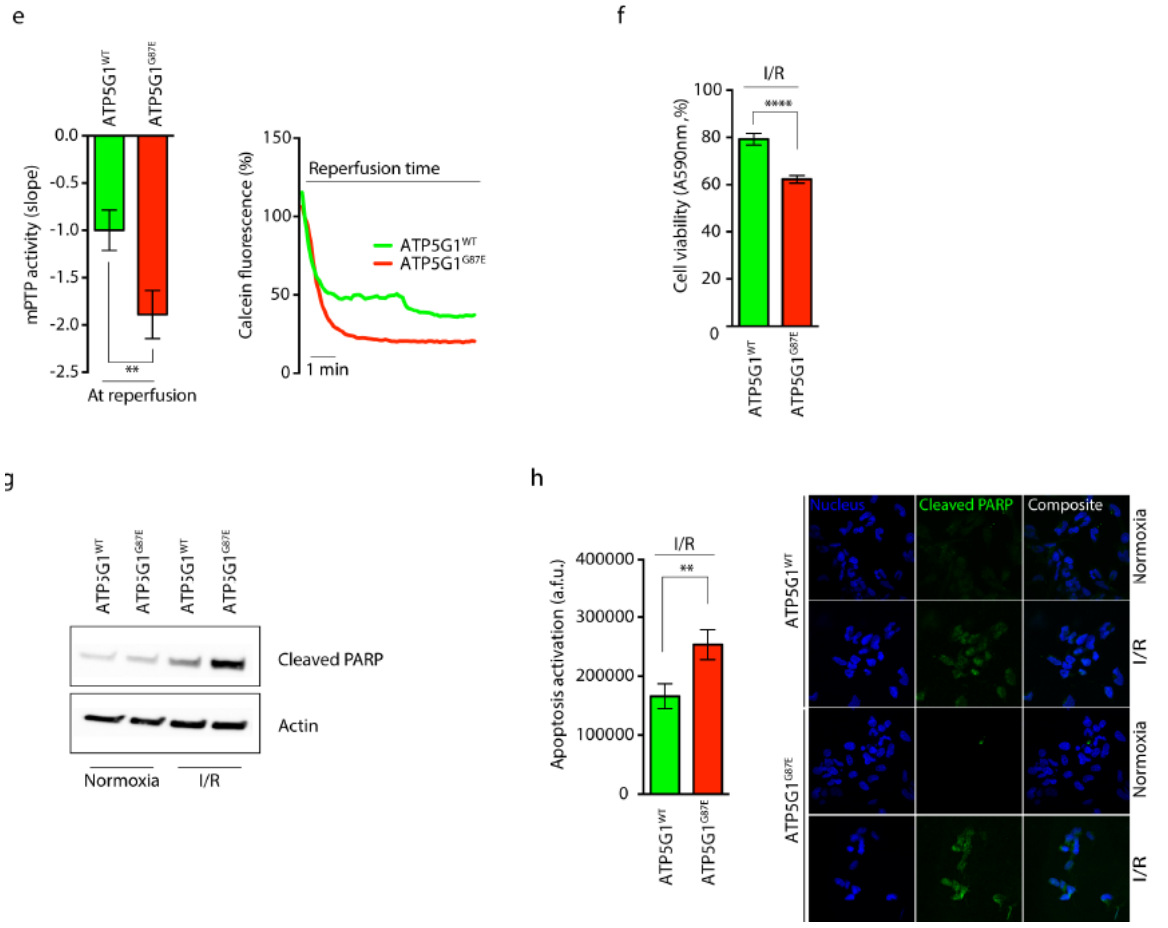

Figure 31. **e:** calcein-cobalt quenching assay in AC16 at reperfusion time upon hypoxic chamber where mPTP activity is reported as slope of the kinetics.
f: quantification of cell viability by crystal violet assay in AC16 clones stably expressing ATP5G1^{WT} and ATP5G1^{G87E} in I/R conditions. Results have been reported as percentage.
g: detection of the cleaved PARP activation by western blot analysis in I/R conditions in AC16 clones stably expressing ATP5G1^{WT} and ATP5G1^{G87E}
h: cleaved PARP detection and quantification by immunofluorescence in confocal microscopy in AC16 clones stably expressing ATP5G1^{WT} and ATP5G1^{G87E}: statistics and representative images under normoxia and I/R are reported. Results have been represented as arbitrary fluorescence units (a.f.u.). .

5. C subunit selective targeting reduces deleterious effects of ATP5G1^{G87E} expression.

With the aim to counteract the deleterious effects of ATP5G1^{G87E} in I/R injury and to understand if they are dependent mainly from cell genotype, we performed most of the experiments showed in Figure 31 in the presence of compound 10, a selective c subunit inhibitor known to have cardioprotective roles (101). Figure 32a,b reported the presence of an altered mPTP opening also in AC16 clone stably expressing ATP5G1^{G87E} mutation upon ionomycin administration and I/R induction (at reperfusion time); in addition, compound 10 treatment desensitized channel activity lowering the slope of the kinetics ($p < 0.05$ for ATP5G1^{WT} vs. ATP5G1^{WT} + c.10 and $p< 0.01$ for ATP5G1^{G87E} vs. ATP5G1^{G87E} + c.10). Upon I/R, living cells were significantly more than those untreated ($p < 0.05$ for ATP5G1^{WT} vs. ATP5G1^{WT} + c.10 and $p< 0.01$ for ATP5G1^{G87E} vs. ATP5G1^{G87E} + c.10, Figure 32c). Indeed, compound 10 reduced apoptosis activation as detected by cleaved PARP specific antibody (Figure 32d). Taken together these findings suggest first, that ATP5G1^{G87E} variation is sensible to c subunit inhibitors at the time of reperfusion; second, harmful effects previously described were dependent form the expression of ATP5G1^{G87E}.

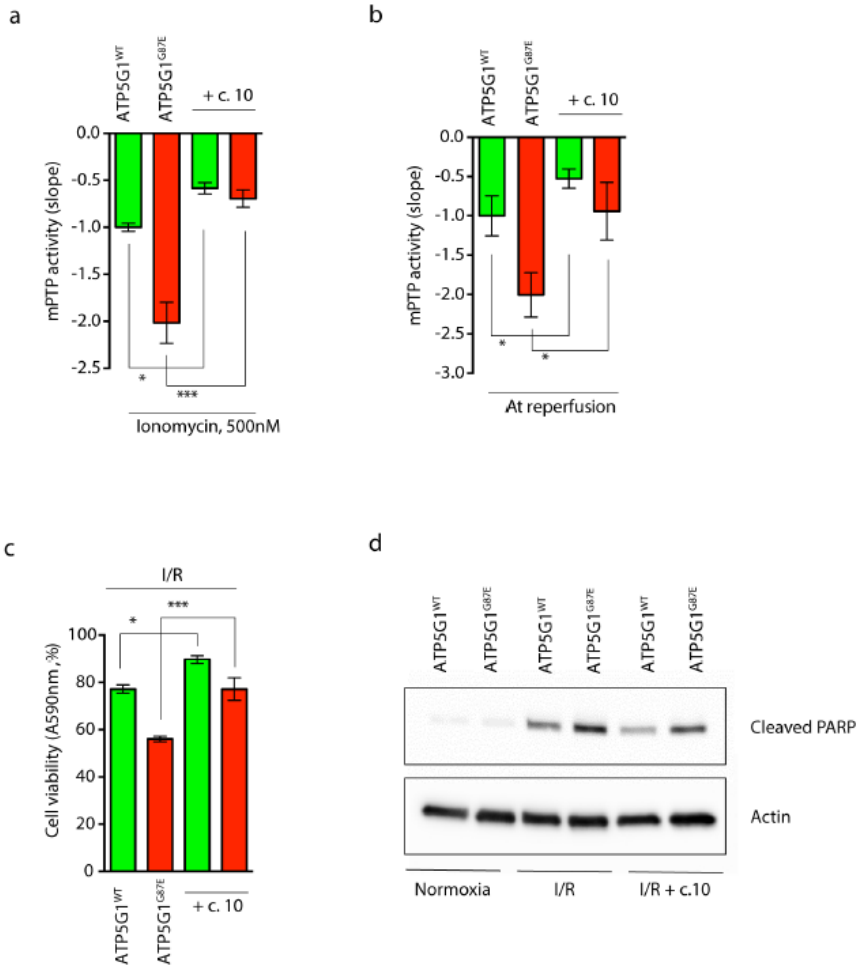

Figure 32. Selective targeting of c subunit reduces harmful effects of ATP5G1^{G87E}
a: calcein-cobalt quenching assay in AC16 clones stably expressing ATP5G1^{WT} and ATP5G1^{G87E}, where mPTP activity is reported as slope of the kinetics following ionomycin administration.
b: calcein-cobalt quenching assay in AC16 clones stably expressing ATP5G1^{WT} and ATP5G1^{G87E}, where mPTP activity is reported as slope of the kinetics at reperfusion time after ischemia.
c: quantification of cell viability by crystal violet assay in AC16 clones stably expressing ATP5G1^{WT} and ATP5G1^{G87E} in I/R conditions. Results have been reported as percentage.
d: cleaved PARP detection by western blot assay in AC16 clones stably expressing ATP5G1^{WT} and ATP5G1^{G87E}.

Discussion

At the best of our knowledge there are no translational studies that report evidences of a link between mPTP opening and its effects in reperfusion injury progression in patients affected by I/R-related pathologies; as well as one important question still remains to be solved, how mPTP function varies and how it can be assessed in MI patients. Given these premises, the first part of this study was planned and carried out to fill those gaps in evidence.

Thus, we performed the following two-step study: first, to understand how mPTP activity can be assessed in patients affected by cardiovascular diseases, we collected fibroblasts and cardiomyocytes in a cohort of 16 patients undergoing cardiac surgery (Figure 24a). We evaluated and compared mPTP function in both cell lines for each patient where we reported a significant positive correlation in mPTP activity between fibroblasts and myocytes (Figure 24b-d). Surprisingly, the findings suggested that differences between fibroblasts and myocytes in terms of mPTP activity are negligible, thus skin biopsy can be considered as a feasible cell model to study mPTP activity, with the advantage of being a collection of tissue less invasive than a conventional cardiac biopsy.

Second, given the still lacking direct correlation between mPTP activity and RI in STEMI patients undergoing successful PCI, we performed a second pilot study (Figure 25) in which, the clinical outcome of 14 STEMI patients expressed in terms of MSI (detected by cMRI, Figure 26d) and mPTP function measured in fibroblasts (Figure 26a-c), have been related. With a strong statistical significance, we found a direct correlation between the opening of the pore and the reperfusion damage developed upon PCI (Figure 26e).

Thus, for the first time in patients, we reported the important correlation between mPTP and RI upon PCI and that, hyper-responsive mPTPs are one among signaling players involved in a worse reperfusion damage in patients undergoing the same MI type (Figure 25 and Figure 26f,g). In addition, the fact that inter-individuals differences of mPTP function exist (Figures 24a and 26a,b), strengthens the concept that the analysis of mPTP function is a crucial step to be evaluated.

Recently, c subunit has been identified as an important regulator of the mPTP and what is known is that the protein expression in cells regulates the opening of the pore and cell death (36), circulating c subunit levels in serum vary between acute myocardial infarction patients and are significantly related to several surrogate markers of myocardial reperfusion (140); moreover, mPTP involves dissociation of ATP synthase dimers and a proper c-ring conformation (75) and that c subunit targeting is known to be a valid cardioprotective strategy in pre-clinical animal models as an adjunct therapy for the treatment of reperfusion injury (101). Since MI is a multifactorial disease in which both environmental factors and genetic profiles play a key role in its development and progression (191), (219), we wondered if mPTP function (that varies among patients) at the time of reperfusion might be dependent also by genetic variations in proteins that modulate it, such as c subunit. Indeed, the link between genetics of mPTP and reperfusion damage progression is still lacking. For this reason, in the third part of the study we sequenced all three c subunit-encoding genes in a cohort of 52 STEMI patients (Figure 27) where we detected the new ATP5G1^{G87E} variant, a heterozygous missense mutation found in exon 3 of ATP5G1 gene with a recurrence of 2 individuals out of 52 (Figure 28 and Figure 29a). This mutated glycine at position 87 is part of a glycine-rich and highly conserved domain of c subunit (Figure 29b) (222); it has been reported that modifications in this site determine c-ring conformational changes (75) that may impact on mPTP opening. *In silico* approaches by the use of the highly established predictive software PolyPhen 2, classified ATP5G1^{G87E} variant as probably damaging once

expressed with a score of 0.993 in a scale ranging from 0 to 1. Other 6 softwares have confirmed this prediction (Figure 29c); as well as functional analysis performed in fibroblasts from one of the two STEMI patients carrying mutation (the second one died following MI). These cells own a hyper-responsive mPTP opening (Figures 29e,f) that, in I/R experimental conditions led to a significant decrease in cell viability due to a greater extend of apoptotic pathway activation and when compared to control counterparts (Figures 29g,h). These important findings have been replicated in an *in vitro* model of human ventricular cardiomyocytes subjected to I/R (Figure 31). Considered that cells used in this study did not highlighted differences in mitochondrial parameters in absence of stressors and in normoxia conditions (Figure 30), we can speculate that ATP5G1^{G87E} variant may be deleterious only at reperfusion time, once MI has developed. The fact that targeting c subunit by the use of the selective inhibitor compound 10 limited mPTP alteration and reduced cell death (Figure 32), suggested us first, that patient(s) carrying mutation could be still ideally treated with c subunit inhibitors (101) at the time of reperfusion; second, that harmful effects previously reported were dependent from the expression of ATP5G1^{G87E} genotype.

We are aware that this study contains limitations including the little cohorts of patients analyzed (mainly due to ethical concerns), but it was important to do the groundwork in improving the knowledge about mPTP in I/R injury both in the clinical practice and how it can be used as pharmacological target in current strategies; for these reasons in the future we will extend the study to bigger population size.

Materials and Methods

Study A: Study population for analysis about PTP function in different human cells

The CROFT (Simultaneous evaluation of levels and sub-unit function components of the mitochondrial permeability transition pore (mPTP) in CaRdiOmyocytes, Fibroblasts and Thymocytes in patients undergoing cardiac surgery) was a single centre, investigator driven, prospective study conducted at the Cardiac surgery unit of Maria Cecilia Hospital of Cotignola, Ravenna, Italy. Patients were enrolled between July and December 2019. The trial was performed according to the Declaration of Helsinki and approved by the local ethics committee (Comitato Etico Area Vasta Emilia Romagna). Patients with a surgical indication for cardiac revascularization or heart valve surgery, >18 years old, previous coronary angiography with documentation of coronary artery disease were enrolled. Exclusion criteria were: refused informed consent; contra-indication to statin therapy, known haemorrhagic disease, known disease of mitochondria, neoplasia treated <5 years ago, chemotherapy < 5 years ago, life expectancy < 1 year, suspected neoplasia, use of oral contraceptives, pregnancy or feeding. All patients enrolled underwent skin biopsy to obtain a fibroblast culture and myocardial biopsy to obtain atrial cardiomyocytes cultures. As a basic research pilot study, the sample size calculation is not feasible. Considering similar studies (223), (224) and the poor performance of cardiomyocytes once they are put into culture, we enrolled 20 patients in which the two-fold biopsy (skin fibroblasts and atrial cardiomyocytes) was performed.

Skin biopsy and fibroblasts extraction protocol

Patients undergoing coronary artery bypass graft need the packaging of one or more saphenous or autologous mammary bypass. Thus a skin biopsy was performed at the site of the autologous saphenous bypass or at the level of the thoracic skin incision. The skin tissue was collected with a clamp and introduced in a sterile container, pre-filled with an adequate quantity of preservative solution. Fibroblasts were isolated from the epidermis, dermis and hypodermis.

After the surgical intervention, the skin biopsy was stored overnight in HBSS containing 3% PS and 1% amphotericin B. After washings and mincing, the pieces were arranged in 25-cm^2 with a thin layer of FBS and every day added with 500 µL of DMEM with 50% FBS. After around 10 days from the pieces came out fibroblasts that were trypsinized and amplified.

Myocardial biopsy and cardiomyocytes extraction protocol

A single tissue sample was collected at the level of the left atrial appendage where the tobacco-pouch was made for venous cannulation. The tissue was collected with a clamp and introduced in a sterile container, pre-filled with an adequate quantity of preservative solution. Cardiomyocytes were isolated from myocardium. The procedure was performed in accordance with standard procedure widely described in the literature (223), (224).

Briefly, within 20 min after myocardial biopsy, atrial appendages have been digested using a double step protocol involving first 30 min of Protease XXIV and then 60 min Collagenase II digestion in a buffer with low calcium, at 37°C and continuously oxygenated. The digestion product was filtered with a 300 µm nylon mesh and carefully centrifuged at 100 g for 5 min. Cells were counted and seeded onto 24-mm glass coverslips characterized by a laminin coating. Experiments were performed within 6 hours.

Cell culture and transient transfection

AC16 Human Cardiomyocyte Cell Line was grown in DMEM/F12 containing 2mM L-Glutamine, 12.5% fetal bovine serum (FBS) and 1x Penicillin-Streptomycin (PS) Solution in 75-cm^2 Corning flasks. AC16 stable clones overexpressing wild-type or mutated c subunit were grown in the same DMEM/F12 supplemented with 0,4 mg/ml G418 selection. Human primary fibroblasts were grown in Dulbecco's Modified Eagle Medium (DMEM) supplemented with 20% FBS, 2mM L-Glutamine and 1x PS in 100mm Petri dishes. All cells were maintained at 37°C and 90% relative humidity in 5% CO_2. Before transfection or infection, cells were seeded onto 13-mm glass coverslips for intracellular Ca^{2+} measurements and onto 24-mm glass coverslips for microscopic analysis. All experiments were performed 24 h after plasmid transfections with Lipofectamine 2000. In experiments involving compound 10, cells were pre-treated for 15 min with a concentration of the compound of 5μM in complete medium

Ischemia/Reperfusion protocol

Where needed, cells were rinsed with PBS and culture medium changed according to the oxygen-glucose deprived protocol as described in (225) with little variations. Cells were exposed at 37°C, to 1% O_2 for 3 h to simulate ischemia condition. At reperfusion time cells were cultured with complete fresh medium and measured.

mPTP measurements

For calcein-cobalt quenching assay all cells were loaded with 1μM calcein acetoxymethyl ester and 2mM Co^{2+}, staining solution was added to cells for 15 min at 37 °C in a 5% CO_2 atmosphere (34). Image acquisitions were performed with Nikon Eclipse Ti confocal microscope with a 40×/0.60 SPlanFluor objective. Openings of mPTP rates were determined as the slopes of the fluorescence of calcein trace over a period of 60 sec post-stimulation with 500nM ionomycin, administered 30 sec after the beginning of the experiment to induce mPTP opening. For $\Delta\psi_m$ measurements cells were loaded with 20 nM tetramethyl rhodamine methyl ester (TMRM) for 30 min at 37°C. Stimulation with 500 μM H_2O_2, a pro-oxidant that induced mPTP opening, mitochondrial depolarization, and reduced TMRM signal intensity (34). Image acquisitions were performed with Nikon Eclipse Ti confocal microscope with a 40×/0.60 SPlanFluor objective.

Mitochondrial parameters measurements

For basal $\Delta\psi_m$, cells were loaded with 20nM tetramethyl rhodamine methyl ester (TMRM) for 30 min at 37°C. To obtain and analyse basal levels, cells were stimulated with 10nM carbonyl cyanide p-trifluoromethoxyphenylhydrazone (FCCP), a strong uncoupler of oxidative phosphorylation.

For mitochondrial morphology primary fibroblasts were stained with 20nM MitoTracker Deep Red FM for 30 minutes at 37°C and imaged with Nikon Eclipse Ti confocal microscope using a 60 × 1.4 NA Plan-Apochromat oil-immersion objective. The analysis was performed with IMARIS software.

For mitochondrial Ca^{2+} measurements fibroblasts were infected with mtAEQmut, 48 h later the coverslips were incubated with 5μM coelenterazine for 1.5 h in Krebs-Ringer modified buffer (KRB) supplemented with 1mM $CaCl_2$ (KRB: 125mM NaCl, 5mM KCl, 1mM Na_3PO_4, 1mM $MgSO_4$, 5.5mM glucose, and 20mM Hepes, pH 7.4, at 37°C). Aequorin signals were measured in KRB supplemented with 1mM $CaCl_2$ using a purpose-built luminometer. The agonist (500μM Bradykinin for fibroblasts) was added to the same medium. The experiments were terminated by lysing the cells with Triton X-100 in a hypotonic Ca^{2+}-rich solution (10mM $CaCl_2$ in H_2O), thus discharging the remaining

aequorin pool. The light signals were collected and calibrated with [Ca^{2+}] values. Further experimental details have been previously described in (226).

Immunofluorescence

AC16 cells were grown onto 13-mm coverslips and transfected as described previously, were washed with PBS and fixed in 4% formaldehyde for 10 min at 37°C. After washing three times with PBS, cells were permeabilized with 0.1% Triton X-100 in PBS (PBS-T) for 2 h at room temperature and then blocked with PBS-T containing 2% BSA at room temperature for 1 h. For fibroblasts permeabilization lasts 10 min with 0.05% PBS-T. Cells were then incubated with primary antibodies overnight at 4°C, washed 3 times with PBS-T, and incubated with the appropriate isotype matched, AlexaFluor-conjugated secondary antibodies. Coverslips were mounted with mounting medium with DAPI reagent at room temperature, and images were acquired with Nikon Eclipse Ti confocal microscope using a 60 × 1.4 NA Plan-Apochromat oil-immersion objective. Acquired images were then analyzed by using open source software Fiji.

Propidium iodide (PI) uptake assay

Primary fibroblasts were stained with 1.5mM PI for 5 min at room temperature, then washed and fixed in 4% formaldehyde. After another wash, coverslips were mounted with mounting medium reagent, and images were acquired with Nikon Eclipse Ti confocal microscope using a 60 × 1.4 NA Plan-Apochromat oil-immersion objective. Acquired images were then analyzed for PI positivity by using open source software Fiji. For further details see (36).

Proximity Ligation Assay (PLA)

After fixation, cells were exposed to 1mM EDTA buffer (pH 8.0) for 20 min at 100°C (antigen retrieval) then the procedure was started. The PLA protocol to detect F_1F_O ATP synthase dimers is described in detail in (75). Protein proximity was evaluated on Nikon Eclipse Ti confocal microscope using a 60 × 1.4 NA Plan-Apochromat oil-immersion objective.

Immunoblot

For immunoblotting, cells were lysed in RIPA buffer, then quantified by the Lowry method and 10 µg of proteins were loaded on a 4–20% precast gel. After electrophoretic separation, proteins were transferred onto nitrocellulose membranes that were incubated overnight with primary antibodies as Actin (1:5000), TIM23 (1:1000), MCU (1:1000), ATP5I (1:1000), ATP5L (1:1000), CYPD (1:1000), c subunit (1:1000), Cleaved PARP (1:1000). The revelation was assessed by specific HRP-labeled secondary antibodies, followed by detection by chemiluminescence using ChemiDoc™ Touch Gel Imaging System.

Cell viability assay (Crystal violet)

Cells seeded in 12-well plates were treated with I/R protocol in the presence or absence of compound 10, then the cells were washed with PBS, fixed in 4% paraformaldehyde, and stained with 0.1% crystal violet. Crystal violet was dissolved with 1 mol/L acetic acid, and absorbance at 590 nm was measured with spectrophotometer.

Study B: Study population for mPTP function and reperfusion damage tests and c subunit genetic screening

Based on findings of study A, study B is carried out to investigate, in humans, the correlation between PTP activity as measured on fibroblasts and reperfusion damage as measured by cMRI. It was a single centre, investigator driven, prospective study conducted at the Cardiology Unit of the Azienda Ospedaliero-Universitaria di Ferrara (Ferrara, Italy). Patients were enrolled between February 2019 and March 2019. The trial was performed according to the Declaration of Helsinki and approved by the local ethics committee (Comitato Etico Unico della Provincia di Ferrara). Inclusion criteria for the enrolment were: i) first-time acute anterior ST-segment elevation myocardial infarction (STEMI) treated with successful percutaneous coronary intervention (PCI); ii) time from onset of symptoms to balloon <6 hours; iii) culprit lesion in the proximal or mid portion of left anterior descending artery (LAD); and iv) baseline thrombolysis in myocardial infarction (TIMI) flow 0–1. Major exclusion criteria were: prior myocardial infarction and/or percutaneous or surgical coronary revascularization and/or prior angina and/or evidence of ischemic heart disease, previous heart failure, cardiac arrest and/or cardiogenic shock, atrial fibrillation, pacemaker, concurrent inflammatory, infectious or malignant disease, liver and/or renal failure, recent significant bleeding and/or major surgery (<4 weeks), use of oral anticoagulants or contraceptive. PCI procedure, antithrombotic drugs and all other medications were administered according to standard clinical practice, institutional protocols and current guidelines. The study flow consists in a skin biopsy to obtain fibroblasts and in a cMRI to assess the reperfusion injury.

Skin biopsy

Skin biopsies (3 mm punch) were collected from the volar side of the forearm (227). Each biopsy was cut into small pieces (around 0.5 mm) and seeded in 25 cm^2 flasks. The tissue was collected with a clamp and introduced in a sterile container, pre-filled with an adequate quantity of preservative solution.

Cardiac MRI

All cMRI studies were performed with a 1.5-T scanner (Signa HDX, GE Medical Systems, Milwaukee, Wisconsin) using a dedicated cardiac software, phased-array surface receiver coil and ECG triggering. Patients underwent cMRI in two different timepoints: the first one within 4+-1 days and the second one after 180+-20 days after successful primary PCI, respectively. Data were analyzed using Segment software (Medviso, Svezia) by a fully blinded operator. After acquisition of localizer images, cine images were obtained using breath-hold single-phase steady-state free precession (SSFP) sequences in multiple short-axis and 3 long-axis views (slice thickness 10 mm, no gap in identical slice positions). Black-blood T2-weighted short inversion time inversion-recovery fast spin echo sequence was performed in the same views as the cine sequences in order to evaluate myocardial edema. Ten minutes after intravenous injection of contrast agent (0.15 mmol/kg Gadobutrol, Scering, Germany), late gadolinium enhancement (LGE) images were acquired using breath-hold segmented T1-weghted inversion-recovery gradient-echo sequence in the same long-axis and short-axis views of cine images. The inversion time was individually adjusted to null normal myocardium. T2-weighted and LGE images were semi-automatically analyzed. Infarct related edema was defined by a signal intensity >2 SD the mean single intensity of the non-infarcted myocardium, identifying the area at risk (AAR) expressed as percentage of LV mass. Infarcted myocardium was quantified on

LGE images as myocardium with a signal intensity exceeding the mean signal intensity of remote myocardium by at least 5 SD and was expressed as percentage of LV mass. Finally, the myocardial salvage index (MSI) was calculated according to the following equation (AAR-infarct size at LGE)/AAR) and it was expressed as value ranging between 0 and 1 (228).

Study C: C subunit genetic screening

To investigate the potential role of genetic determinants in the inter-subject variability a complete analysis of the gene coding for c subunit of the mitochondrial permeability transition pore is performed in patients of a previous published trial (140). It was a single centre, investigator driven, prospective study conducted at the Cardiology Unit of the Azienda Ospedaliero Universitaria di Ferrara, Ferrara, Italy. Patients were enrolled between December 2013 and January 2015. Inclusion and exclusion criteria have been previously reported (229). Briefly, as the population of the study B, patients with a first-time acute anterior STEMI treated with successful primary PCI were considered eligible. Overall, 158 patients have been enrolled. The aim of the study was to measure the values of serum subunit c and to correlate them with surrogate markers of reperfusion injury. In 52 of these patients, whole blood was available for DNA extraction and were considered for the present analysis. DNA was extracted and full sequencing of the subunit c genes was performed.

Blood sample collection

Blood withdrawal was performed 6–18 h after the end of successful PCI (median 10 hours). Blood samples were collected from an antecubital vein using a 21-gauge needle. The first 2 to 4 mL of blood was discarded. The remaining blood was collected in empty tubes and, after 45 min, centrifuged at 1700 xg at 4 °C for 15 min. The serum obtained was stored at −20 °C.

DNA extraction

Genomic DNA was extracted from whole blood of selected patients after informed consent using the Wizard® Genomic DNA Purification Kit (Promega) according to manufacturer's instructions (https://www.promega.com/-/media/files/resources/protcards/wizard-genomic-dna-purification-kit-quick-protocol.pdf?la=en).

Briefly, 900 µL of Cell Lysis Solution were added to 300 µL of whole blood and incubated for 10 min at room temperature and centrifuged at 19000 g for 20 seconds. The supernatant was discarded and the pellet vortexed before adding 300 µL of Nuclei Lysis Solution, mixing by inversion and adding 100 µL of Protein Precipitation Solution. The obtained solution was vortexed for 20 seconds and centrifuged at 19000 g for 3 min.

The supernatant was transferred to a new tube containing 300 µL of isopropanol, mixed and centrifuged at 19000 g for one minute. Discarded the supernatant, the DNA pellet was washed with 70% ethanol and centrifuged as above. After removal of the ethanol, the DNA pellet was air dryed and resuspended in 100 µL of DNAse-free water.

PCR amplification, sequencing and analysis

Primers were designed to amplify about 200 base pairs before and after all exons and UTRs of the gene ATP5G1, ATP5G2 and ATP5G3, using the Primer3Plus online software (http://www.bioinformatics.nl/cgi-bin/primer3plus/primer3plus.cgi).

PCR amplification was performed using the AmpliTaq Gold® 360 kit (Life Technologies) and 50 ng of genomic DNA per reaction. The full list of PCR primers and annealing temperatures are available in Tables S3.

After verification on agarose gel, amplicons have been purified on columns Microcon Millipore and sent for sequencing to Macrogen Europe (https://dna.macrogen.com). Chromatograms have been visualized with Chromas (version 2.33) and analyzed with Blast and Lasergene SeqMan (version 7.0.0 Build) allowing multiple alignments and direct comparison of several sequences at the same time. Identified variants have been compared with the dbSNP139 (https://www.ncbi.nlm.nih.gov/snp/) and reported in Table S3.

Predictive softwares

PolyPhen-2 (Polymorphism Phenotyping v2) was used to predict possible impact of an amino acid substitution on the structure and function of c subunit protein using straightforward physical and comparative considerations as described in (220). In the same way, RaptorX predicted secondary and tertiary protein structures, contact and distance map as described in (221).

Statistical analyses

The statistical methods included t-test (when comparing two experimental groups), one-way ANOVA with or without multiple comparisons (for three or more groups) and Spearmans's correlation coefficient r performed by GraphPad Prism. P values are reported in the figure legends and in the Results section.

References

1. Hunter DR, Haworth RA. The Ca2+-induced membrane transition in mitochondria. I. The protective mechanisms. Arch Biochem Biophys. 1979;195(2):453-9.
2. Zamzami N, Marchetti P, Castedo M, Decaudin D, Macho A, Hirsch T, et al. Sequential reduction of mitochondrial transmembrane potential and generation of reactive oxygen species in early programmed cell death. J Exp Med. 1995;182(2):367-77.
3. Zamzami N, Marchetti P, Castedo M, Zanin C, Vayssiere JL, Petit PX, et al. Reduction in mitochondrial potential constitutes an early irreversible step of programmed lymphocyte death in vivo. J Exp Med. 1995;181(5):1661-72.
4. Kroemer G, Galluzzi L, Brenner C. Mitochondrial membrane permeabilization in cell death. Physiol Rev. 2007;87(1):99-163.
5. Bonora M, Wieckowski MR, Chinopoulos C, Kepp O, Kroemer G, Galluzzi L, et al. Molecular mechanisms of cell death: central implication of ATP synthase in mitochondrial permeability transition. Oncogene. 2015;34(12):1475-86.
6. Kroemer G. The proto-oncogene Bcl-2 and its role in regulating apoptosis. Nat Med. 1997;3(6):614-20.
7. Marchetti P, Castedo M, Susin SA, Zamzami N, Hirsch T, Macho A, et al. Mitochondrial permeability transition is a central coordinating event of apoptosis. J Exp Med. 1996;184(3):1155-60.
8. Eguchi Y, Shimizu S, Tsujimoto Y. Intracellular ATP levels determine cell death fate by apoptosis or necrosis. Cancer Res. 1997;57(10):1835-40.
9. Lu X, Kwong JQ, Molkentin JD, Bers DM. Individual Cardiac Mitochondria Undergo Rare Transient Permeability Transition Pore Openings. Circ Res. 2016;118(5):834-41.
10. Szabo I, Zoratti M. The mitochondrial megachannel is the permeability transition pore. J Bioenerg Biomembr. 1992;24(1):111-7.
11. Bernardi P, Vassanelli S, Veronese P, Colonna R, Szabo I, Zoratti M. Modulation of the mitochondrial permeability transition pore. Effect of protons and divalent cations. J Biol Chem. 1992;267(5):2934-9.
12. Szabo I, Zoratti M. The mitochondrial permeability transition pore may comprise VDAC molecules. I. Binary structure and voltage dependence of the pore. FEBS Lett. 1993;330(2):201-5.
13. Szabo I, De Pinto V, Zoratti M. The mitochondrial permeability transition pore may comprise VDAC molecules. II. The electrophysiological properties of VDAC are compatible with those of the mitochondrial megachannel. FEBS Lett. 1993;330(2):206-10.
14. McEnery MW, Snowman AM, Trifiletti RR, Snyder SH. Isolation of the mitochondrial benzodiazepine receptor: association with the voltage-dependent anion channel and the adenine nucleotide carrier. Proc Natl Acad Sci U S A. 1992;89(8):3170-4.
15. Beutner G, Ruck A, Riede B, Welte W, Brdiczka D. Complexes between kinases, mitochondrial porin and adenylate translocator in rat brain resemble the permeability transition pore. FEBS Lett. 1996;396(2-3):189-95.
16. Beutner G, Ruck A, Riede B, Brdiczka D. Complexes between porin, hexokinase, mitochondrial creatine kinase and adenylate translocator display properties of the permeability transition pore. Implication for regulation of permeability transition by the kinases. Biochim Biophys Acta. 1998;1368(1):7-18.
17. Crompton M, Virji S, Ward JM. Cyclophilin-D binds strongly to complexes of the voltage-dependent anion channel and the adenine nucleotide translocase to form the permeability transition pore. Eur J Biochem. 1998;258(2):729-35.
18. Ruck A, Dolder M, Wallimann T, Brdiczka D. Reconstituted adenine nucleotide translocase forms a channel for small molecules comparable to the mitochondrial permeability transition pore. FEBS Lett. 1998;426(1):97-101.
19. Kokoszka JE, Waymire KG, Levy SE, Sligh JE, Cai J, Jones DP, et al. The ADP/ATP translocator is not essential for the mitochondrial permeability transition pore. Nature. 2004;427(6973):461-5.
20. Baines CP, Kaiser RA, Sheiko T, Craigen WJ, Molkentin JD. Voltage-dependent anion channels are dispensable for mitochondrial-dependent cell death. Nat Cell Biol. 2007;9(5):550-5.
21. Basso E, Fante L, Fowlkes J, Petronilli V, Forte MA, Bernardi P. Properties of the permeability transition pore in mitochondria devoid of Cyclophilin D. J Biol Chem. 2005;280(19):18558-61.
22. De Marchi U, Basso E, Szabo I, Zoratti M. Electrophysiological characterization of the Cyclophilin D-deleted mitochondrial permeability transition pore. Mol Membr Biol. 2006;23(6):521-30.
23. Tedeschi H, Hegarty HJ, James JM. Osmotic reversal of phosphate-induced mitochondrial swelling. Biochim Biophys Acta. 1965;104(2):612-5.
24. Palmieri F. The mitochondrial transporter family (SLC25): physiological and pathological implications. Pflugers Arch. 2004;447(5):689-709.
25. Hagen T, Lagace CJ, Modica-Napolitano JS, Aprille JR. Permeability transition in rat liver mitochondria is modulated by the ATP-Mg/Pi carrier. Am J Physiol Gastrointest Liver Physiol. 2003;285(2):G274-81.
26. Traba J, Del Arco A, Duchen MR, Szabadkai G, Satrustegui J. SCaMC-1 promotes cancer cell survival by desensitizing mitochondrial permeability transition via ATP/ADP-mediated matrix Ca(2+) buffering. Cell Death Differ. 2012;19(4):650-60.
27. Leung AW, Varanyuwatana P, Halestrap AP. The mitochondrial phosphate carrier interacts with cyclophilin D and may play a key role in the permeability transition. J Biol Chem. 2008;283(39):26312-23.

28. Alcala S, Klee M, Fernandez J, Fleischer A, Pimentel-Muinos FX. A high-throughput screening for mammalian cell death effectors identifies the mitochondrial phosphate carrier as a regulator of cytochrome c release. Oncogene. 2008;27(1):44-54.
29. Schroers A, Kramer R, Wohlrab H. The reversible antiport-uniport conversion of the phosphate carrier from yeast mitochondria depends on the presence of a single cysteine. J Biol Chem. 1997;272(16):10558-64.
30. Varanyuwatana P, Halestrap AP. The roles of phosphate and the phosphate carrier in the mitochondrial permeability transition pore. Mitochondrion. 2012;12(1):120-5.
31. Gutierrez-Aguilar M, Douglas DL, Gibson AK, Domeier TL, Molkentin JD, Baines CP. Genetic manipulation of the cardiac mitochondrial phosphate carrier does not affect permeability transition. J Mol Cell Cardiol. 2014;72:316-25.
32. Kwong JQ, Davis J, Baines CP, Sargent MA, Karch J, Wang X, et al. Genetic deletion of the mitochondrial phosphate carrier desensitizes the mitochondrial permeability transition pore and causes cardiomyopathy. Cell Death Differ. 2014;21(8):1209-17.
33. Shanmughapriya S, Rajan S, Hoffman NE, Higgins AM, Tomar D, Nemani N, et al. SPG7 Is an Essential and Conserved Component of the Mitochondrial Permeability Transition Pore. Mol Cell. 2015;60(1):47-62.
34. Bonora M, Morganti C, Morciano G, Giorgi C, Wieckowski MR, Pinton P. Comprehensive analysis of mitochondrial permeability transition pore activity in living cells using fluorescence-imaging-based techniques. Nat Protoc. 2016;11(6):1067-80.
35. Giorgio V, von Stockum S, Antoniel M, Fabbro A, Fogolari F, Forte M, et al. Dimers of mitochondrial ATP synthase form the permeability transition pore. Proc Natl Acad Sci U S A. 2013;110(15):5887-92.
36. Bonora M, Bononi A, De Marchi E, Giorgi C, Lebiedzinska M, Marchi S, et al. Role of the c subunit of the FO ATP synthase in mitochondrial permeability transition. Cell Cycle. 2013;12(4):674-83.
37. Alavian KN, Beutner G, Lazrove E, Sacchetti S, Park HA, Licznerski P, et al. An uncoupling channel within the c-subunit ring of the F1FO ATP synthase is the mitochondrial permeability transition pore. Proc Natl Acad Sci U S A. 2014;111(29):10580-5.
38. Pastorino JG, Simbula G, Gilfor E, Hoek JB, Farber JL. Protoporphyrin IX, an endogenous ligand of the peripheral benzodiazepine receptor, potentiates induction of the mitochondrial permeability transition and the killing of cultured hepatocytes by rotenone. J Biol Chem. 1994;269(49):31041-6.
39. Hirsch T, Decaudin D, Susin SA, Marchetti P, Larochette N, Resche-Rigon M, et al. PK11195, a ligand of the mitochondrial benzodiazepine receptor, facilitates the induction of apoptosis and reverses Bcl-2-mediated cytoprotection. Exp Cell Res. 1998;241(2):426-34.
40. Chelli B, Falleni A, Salvetti F, Gremigni V, Lucacchini A, Martini C. Peripheral-type benzodiazepine receptor ligands: mitochondrial permeability transition induction in rat cardiac tissue. Biochem Pharmacol. 2001;61(6):695-705.
41. Kugler W, Veenman L, Shandalov Y, Leschiner S, Spanier I, Lakomek M, et al. Ligands of the mitochondrial 18 kDa translocator protein attenuate apoptosis of human glioblastoma cells exposed to erucylphosphohomocholine. Cell Oncol. 2008;30(5):435-50.
42. Shargorodsky L, Veenman L, Caballero B, Pe'er Y, Leschiner S, Bode J, et al. The nitric oxide donor sodium nitroprusside requires the 18 kDa Translocator Protein to induce cell death. Apoptosis. 2012;17(7):647-65.
43. Campanella M, Szabadkai G, Rizzuto R. Modulation of intracellular Ca2+ signalling in HeLa cells by the apoptotic cell death enhancer PK11195. Biochem Pharmacol. 2008;76(11):1628-36.
44. Decaudin D, Castedo M, Nemati F, Beurdeley-Thomas A, De Pinieux G, Caron A, et al. Peripheral benzodiazepine receptor ligands reverse apoptosis resistance of cancer cells in vitro and in vivo. Cancer Res. 2002;62(5):1388-93.
45. Wallimann T, Dolder M, Schlattner U, Eder M, Hornemann T, O'Gorman E, et al. Some new aspects of creatine kinase (CK): compartmentation, structure, function and regulation for cellular and mitochondrial bioenergetics and physiology. Biofactors. 1998;8(3-4):229-34.
46. Dolder M, Walzel B, Speer O, Schlattner U, Wallimann T. Inhibition of the mitochondrial permeability transition by creatine kinase substrates. Requirement for microcompartmentation. J Biol Chem. 2003;278(20):17760-6.
47. Pastorino JG, Hoek JB. Regulation of hexokinase binding to VDAC. J Bioenerg Biomembr. 2008;40(3):171-82.
48. Pastorino JG, Hoek JB. Hexokinase II: the integration of energy metabolism and control of apoptosis. Curr Med Chem. 2003;10(16):1535-51.
49. Galluzzi L, Kepp O, Tajeddine N, Kroemer G. Disruption of the hexokinase-VDAC complex for tumor therapy. Oncogene. 2008;27(34):4633-5.
50. Smeele KM, Southworth R, Wu R, Xie C, Nederlof R, Warley A, et al. Disruption of hexokinase II-mitochondrial binding blocks ischemic preconditioning and causes rapid cardiac necrosis. Circ Res. 2011;108(10):1165-9.
51. Chiara F, Castellaro D, Marin O, Petronilli V, Brusilow WS, Juhaszova M, et al. Hexokinase II detachment from mitochondria triggers apoptosis through the permeability transition pore independent of voltage-dependent anion channels. PLoS One. 2008;3(3):e1852.
52. Baines CP, Song CX, Zheng YT, Wang GW, Zhang J, Wang OL, et al. Protein kinase Cepsilon interacts with and inhibits the permeability transition pore in cardiac mitochondria. Circ Res. 2003;92(8):873-80.

53. Pastorino JG, Hoek JB, Shulga N. Activation of glycogen synthase kinase 3beta disrupts the binding of hexokinase II to mitochondria by phosphorylating voltage-dependent anion channel and potentiates chemotherapy-induced cytotoxicity. Cancer Res. 2005;65(22):10545-54.
54. Nishihara M, Miura T, Miki T, Tanno M, Yano T, Naitoh K, et al. Modulation of the mitochondrial permeability transition pore complex in GSK-3beta-mediated myocardial protection. J Mol Cell Cardiol. 2007;43(5):564-70.
55. Chiara F, Gambalunga A, Sciacovelli M, Nicolli A, Ronconi L, Fregona D, et al. Chemotherapeutic induction of mitochondrial oxidative stress activates GSK-3alpha/beta and Bax, leading to permeability transition pore opening and tumor cell death. Cell Death Dis. 2012;3:e444.
56. Juhaszova M, Zorov DB, Kim SH, Pepe S, Fu Q, Fishbein KW, et al. Glycogen synthase kinase-3beta mediates convergence of protection signaling to inhibit the mitochondrial permeability transition pore. J Clin Invest. 2004;113(11):1535-49.
57. Takuma K, Phuagphong P, Lee E, Mori K, Baba A, Matsuda T. Anti-apoptotic effect of cGMP in cultured astrocytes: inhibition by cGMP-dependent protein kinase of mitochondrial permeable transition pore. J Biol Chem. 2001;276(51):48093-9.
58. Pediaditakis P, Kim JS, He L, Zhang X, Graves LM, Lemasters JJ. Inhibition of the mitochondrial permeability transition by protein kinase A in rat liver mitochondria and hepatocytes. Biochem J. 2010;431(3):411-21.
59. Shimizu S, Narita M, Tsujimoto Y. Bcl-2 family proteins regulate the release of apoptogenic cytochrome c by the mitochondrial channel VDAC. Nature. 1999;399(6735):483-7.
60. Vander Heiden MG, Chandel NS, Schumacker PT, Thompson CB. Bcl-xL prevents cell death following growth factor withdrawal by facilitating mitochondrial ATP/ADP exchange. Mol Cell. 1999;3(2):159-67.
61. Marzo I, Brenner C, Zamzami N, Jurgensmeier JM, Susin SA, Vieira HL, et al. Bax and adenine nucleotide translocator cooperate in the mitochondrial control of apoptosis. Science. 1998;281(5385):2027-31.
62. Narita M, Shimizu S, Ito T, Chittenden T, Lutz RJ, Matsuda H, et al. Bax interacts with the permeability transition pore to induce permeability transition and cytochrome c release in isolated mitochondria. Proc Natl Acad Sci U S A. 1998;95(25):14681-6.
63. Zamzami N, El Hamel C, Maisse C, Brenner C, Munoz-Pinedo C, Belzacq AS, et al. Bid acts on the permeability transition pore complex to induce apoptosis. Oncogene. 2000;19(54):6342-50.
64. Roy SS, Madesh M, Davies E, Antonsson B, Danial N, Hajnoczky G. Bad targets the permeability transition pore independent of Bax or Bak to switch between Ca2+-dependent cell survival and death. Mol Cell. 2009;33(3):377-88.
65. Vaseva AV, Marchenko ND, Ji K, Tsirka SE, Holzmann S, Moll UM. p53 opens the mitochondrial permeability transition pore to trigger necrosis. Cell. 2012;149(7):1536-48.
66. Yoshida M, Muneyuki E, Hisabori T. ATP synthase--a marvellous rotary engine of the cell. Nat Rev Mol Cell Biol. 2001;2(9):669-77.
67. Rubinstein JL, Walker JE, Henderson R. Structure of the mitochondrial ATP synthase by electron cryomicroscopy. EMBO J. 2003;22(23):6182-92.
68. Jonckheere AI, Smeitink JA, Rodenburg RJ. Mitochondrial ATP synthase: architecture, function and pathology. J Inherit Metab Dis. 2012;35(2):211-25.
69. Okuno D, Iino R, Noji H. Rotation and structure of FoF1-ATP synthase. J Biochem. 2011;149(6):655-64.
70. Lightowlers RN, Howitt SM, Hatch L, Gibson F, Cox G. The proton pore in the Escherichia coli F0F1-ATPase: substitution of glutamate by glutamine at position 219 of the alpha-subunit prevents F0-mediated proton permeability. Biochim Biophys Acta. 1988;933(2):241-8.
71. Giorgio V, Bisetto E, Soriano ME, Dabbeni-Sala F, Basso E, Petronilli V, et al. Cyclophilin D modulates mitochondrial F0F1-ATP synthase by interacting with the lateral stalk of the complex. J Biol Chem. 2009;284(49):33982-8.
72. Garcia JJ, Morales-Rios E, Cortes-Hernandez P, Rodriguez-Zavala JS. The inhibitor protein (IF1) promotes dimerization of the mitochondrial F1F0-ATP synthase. Biochemistry. 2006;45(42):12695-703.
73. Gerle C. On the structural possibility of pore-forming mitochondrial FoF1 ATP synthase. Biochim Biophys Acta. 2016;1857(8):1191-6.
74. Allegretti M, Klusch N, Mills DJ, Vonck J, Kuhlbrandt W, Davies KM. Horizontal membrane-intrinsic alpha-helices in the stator a-subunit of an F-type ATP synthase. Nature. 2015;521(7551):237-40.
75. Bonora M, Morganti C, Morciano G, Pedriali G, Lebiedzinska-Arciszewska M, Aquila G, et al. Mitochondrial permeability transition involves dissociation of F1FO ATP synthase dimers and C-ring conformation. EMBO Rep. 2017;18(7):1077-89.
76. Pogoryelov D, Klyszejko AL, Krasnoselska GO, Heller EM, Leone V, Langer JD, et al. Engineering rotor ring stoichiometries in the ATP synthase. Proc Natl Acad Sci U S A. 2012;109(25):E1599-608.
77. Pogoryelov D, Yildiz O, Faraldo-Gomez JD, Meier T. High-resolution structure of the rotor ring of a proton-dependent ATP synthase. Nat Struct Mol Biol. 2009;16(10):1068-73.
78. Symersky J, Pagadala V, Osowski D, Krah A, Meier T, Faraldo-Gomez JD, et al. Structure of the c(10) ring of the yeast mitochondrial ATP synthase in the open conformation. Nat Struct Mol Biol. 2012;19(5):485-91, S1.
79. Pandini A, Kleinjung J, Taylor WR, Junge W, Khan S. The Phylogenetic Signature Underlying ATP Synthase c-Ring Compliance. Biophys J. 2015;109(5):975-87.

80. Arselin G, Giraud MF, Dautant A, Vaillier J, Brethes D, Coulary-Salin B, et al. The GxxxG motif of the transmembrane domain of subunit e is involved in the dimerization/oligomerization of the yeast ATP synthase complex in the mitochondrial membrane. Eur J Biochem. 2003;270(8):1875-84.
81. Azarashvili T, Odinokova I, Bakunts A, Ternovsky V, Krestinina O, Tyynela J, et al. Potential role of subunit c of F0F1-ATPase and subunit c of storage body in the mitochondrial permeability transition. Effect of the phosphorylation status of subunit c on pore opening. Cell Calcium. 2014;55(2):69-77.
82. Elustondo PA, Nichols M, Negoda A, Thirumaran A, Zakharian E, Robertson GS, et al. Mitochondrial permeability transition pore induction is linked to formation of the complex of ATPase C-subunit, polyhydroxybutyrate and inorganic polyphosphate. Cell Death Discov. 2016;2:16070.
83. Morciano G, Bonora M, Giorgi C, Pinton P. Other bricks for the correct construction of the mitochondrial permeability transition pore complex. Cell Death Dis. 2017;8(3):e2698.
84. Halestrap AP. The C Ring of the F1Fo ATP Synthase Forms the Mitochondrial Permeability Transition Pore: A Critical Appraisal. Front Oncol. 2014;4:234.
85. He J, Ford HC, Carroll J, Ding S, Fearnley IM, Walker JE. Persistence of the mitochondrial permeability transition in the absence of subunit c of human ATP synthase. Proc Natl Acad Sci U S A. 2017;114(13):3409-14.
86. Oberfeld B, Brunner J, Dimroth P. Phospholipids occupy the internal lumen of the c ring of the ATP synthase of Escherichia coli. Biochemistry. 2006;45(6):1841-51.
87. Meier T, Matthey U, Henzen F, Dimroth P, Muller DJ. The central plug in the reconstituted undecameric c cylinder of a bacterial ATP synthase consists of phospholipids. FEBS Lett. 2001;505(3):353-6.
88. Stock D, Leslie AG, Walker JE. Molecular architecture of the rotary motor in ATP synthase. Science. 1999;286(5445):1700-5.
89. Zhou M, Morgner N, Barrera NP, Politis A, Isaacson SC, Matak-Vinkovic D, et al. Mass spectrometry of intact V-type ATPases reveals bound lipids and the effects of nucleotide binding. Science. 2011;334(6054):380-5.
90. Saroussi S, Schushan M, Ben-Tal N, Junge W, Nelson N. Structure and flexibility of the C-ring in the electromotor of rotary F(0)F(1)-ATPase of pea chloroplasts. PLoS One. 2012;7(9):e43045.
91. Kuhlbrandt W, Davies KM. Rotary ATPases: A New Twist to an Ancient Machine. Trends Biochem Sci. 2016;41(1):106-16.
92. Kauffman G. Aspirin-induced gastric mucosal injury: lessons learned from animal models. Gastroenterology. 1989;96(2 Pt 2 Suppl):606-14.
93. Martin LJ, Fancelli D, Wong M, Niedzwiecki M, Ballarini M, Plyte S, et al. GNX-4728, a novel small molecule drug inhibitor of mitochondrial permeability transition, is therapeutic in a mouse model of amyotrophic lateral sclerosis. Front Cell Neurosci. 2014;8:433.
94. Yin Y, Guan Y, Duan J, Wei G, Zhu Y, Quan W, et al. Cardioprotective effect of Danshensu against myocardial ischemia/reperfusion injury and inhibits apoptosis of H9c2 cardiomyocytes via Akt and ERK1/2 phosphorylation. Eur J Pharmacol. 2013;699(1-3):219-26.
95. Lardy HA, Johnson D, Mc MW. Antibiotics as tools for metabolic studies. I. A survey of toxic antibiotics in respiratory, phosphorylative and glycolytic systems. Arch Biochem Biophys. 1958;78(2):587-97.
96. Zhu Y, Xu H, Huang K. Mitochondrial permeability transition and cytochrome c release induced by selenite. J Inorg Biochem. 2002;90(1-2):43-50.
97. Chavez E, Rodriguez JS, Garcia G, Garcia N, Correa F. Oligomycin strengthens the effect of cyclosporin A on mitochondrial permeability transition by inducing phosphate uptake. Cell Biol Int. 2005;29(7):551-8.
98. Symersky J, Osowski D, Walters DE, Mueller DM. Oligomycin frames a common drug-binding site in the ATP synthase. Proc Natl Acad Sci U S A. 2012;109(35):13961-5.
99. Ylikallio E, Suomalainen A. Mechanisms of mitochondrial diseases. Ann Med. 2012;44(1):41-59.
100. Holt IJ, Harding AE, Morgan-Hughes JA. Deletions of muscle mitochondrial DNA in patients with mitochondrial myopathies. Nature. 1988;331(6158):717-9.
101. Morciano G, Preti D, Pedriali G, Aquila G, Missiroli S, Fantinati A, et al. Discovery of Novel 1,3,8-Triazaspiro[4.5]decane Derivatives That Target the c Subunit of F1/FO-Adenosine Triphosphate (ATP) Synthase for the Treatment of Reperfusion Damage in Myocardial Infarction. J Med Chem. 2018;61(16):7131-43.
102. Barth E, Stammler G, Speiser B, Schaper J. Ultrastructural quantitation of mitochondria and myofilaments in cardiac muscle from 10 different animal species including man. J Mol Cell Cardiol. 1992;24(7):669-81.
103. Hom JR, Quintanilla RA, Hoffman DL, de Mesy Bentley KL, Molkentin JD, Sheu SS, et al. The permeability transition pore controls cardiac mitochondrial maturation and myocyte differentiation. Dev Cell. 2011;21(3):469-78.
104. Brown DA, Perry JB, Allen ME, Sabbah HN, Stauffer BL, Shaikh SR, et al. Expert consensus document: Mitochondrial function as a therapeutic target in heart failure. Nat Rev Cardiol. 2017;14(4):238-50.
105. Suomalainen A, Battersby BJ. Mitochondrial diseases: the contribution of organelle stress responses to pathology. Nat Rev Mol Cell Biol. 2018;19(2):77-92.
106. Bravo-San Pedro JM, Kroemer G, Galluzzi L. Autophagy and Mitophagy in Cardiovascular Disease. Circ Res. 2017;120(11):1812-24.

107. Murray CJ, Vos T, Lozano R, Naghavi M, Flaxman AD, Michaud C, et al. Disability-adjusted life years (DALYs) for 291 diseases and injuries in 21 regions, 1990-2010: a systematic analysis for the Global Burden of Disease Study 2010. Lancet. 2012;380(9859):2197-223.
108. Roger VL. Epidemiology of myocardial infarction. Med Clin North Am. 2007;91(4):537-52; ix.
109. Murray CJ, Lopez AD. Mortality by cause for eight regions of the world: Global Burden of Disease Study. Lancet. 1997;349(9061):1269-76.
110. Abegunde DO, Mathers CD, Adam T, Ortegon M, Strong K. The burden and costs of chronic diseases in low-income and middle-income countries. Lancet. 2007;370(9603):1929-38.
111. Khera AV, Emdin CA, Drake I, Natarajan P, Bick AG, Cook NR, et al. Genetic Risk, Adherence to a Healthy Lifestyle, and Coronary Disease. N Engl J Med. 2016;375(24):2349-58.
112. Neumann FJ, Sousa-Uva M, Ahlsson A, Alfonso F, Banning AP, Benedetto U, et al. 2018 ESC/EACTS Guidelines on myocardial revascularization. Eur Heart J. 2019;40(2):87-165.
113. Hausenloy DJ, Duchen MR, Yellon DM. Inhibiting mitochondrial permeability transition pore opening at reperfusion protects against ischaemia-reperfusion injury. Cardiovasc Res. 2003;60(3):617-25.
114. Matsumoto-Ida M, Akao M, Takeda T, Kato M, Kita T. Real-time 2-photon imaging of mitochondrial function in perfused rat hearts subjected to ischemia/reperfusion. Circulation. 2006;114(14):1497-503.
115. Hausenloy DJ, Erik Botker H, Condorelli G, Ferdinandy P, Garcia-Dorado D, Heusch G, et al. Translating cardioprotection for patient benefit: position paper from the Working Group of Cellular Biology of the Heart of the European Society of Cardiology. Cardiovasc Res. 2013;98(1):7-27.
116. Ong SB, Dongworth RK, Cabrera-Fuentes HA, Hausenloy DJ. Role of the MPTP in conditioning the heart - translatability and mechanism. Br J Pharmacol. 2015;172(8):2074-84.
117. Yellon DM, Hausenloy DJ. Myocardial reperfusion injury. N Engl J Med. 2007;357(11):1121-35.
118. Campo G, Pavasini R, Morciano G, Lincoff AM, Gibson CM, Kitakaze M, et al. Clinical benefit of drugs targeting mitochondrial function as an adjunct to reperfusion in ST-segment elevation myocardial infarction: A meta-analysis of randomized clinical trials. Int J Cardiol. 2017;244:59-66.
119. Campo G, Pavasini R, Morciano G, Lincoff MA, M CG, Kitakaze M, et al. Data on administration of cyclosporine, nicorandil, metoprolol on reperfusion related outcomes in ST-segment Elevation Myocardial Infarction treated with percutaneous coronary intervention. Data Brief. 2017;14:197-205.
120. Thygesen K, Alpert JS, White HD, Joint ESCAAHAWHFTFftRoMI, Jaffe AS, Apple FS, et al. Universal definition of myocardial infarction. Circulation. 2007;116(22):2634-53.
121. Araszkiewicz A, Grygier M, Lesiak M, Grajek S. The impact of ischemia-reperfusion injury on the effectiveness of primary angioplasty in ST-segment elevation myocardial infarction. Postepy Kardiol Interwencyjnej. 2013;9(3):275-81.
122. Frank A, Bonney M, Bonney S, Weitzel L, Koeppen M, Eckle T. Myocardial ischemia reperfusion injury: from basic science to clinical bedside. Semin Cardiothorac Vasc Anesth. 2012;16(3):123-32.
123. Jennings RB, Reimer KA. The cell biology of acute myocardial ischemia. Annu Rev Med. 1991;42:225-46.
124. Hausenloy DJ, Yellon DM. Myocardial ischemia-reperfusion injury: a neglected therapeutic target. J Clin Invest. 2013;123(1):92-100.
125. Avkiran M, Marber MS. Na(+)/H(+) exchange inhibitors for cardioprotective therapy: progress, problems and prospects. J Am Coll Cardiol. 2002;39(5):747-53.
126. Piper HM, Meuter K, Schafer C. Cellular mechanisms of ischemia-reperfusion injury. Ann Thorac Surg. 2003;75(2):S644-8.
127. Contreras L, Drago I, Zampese E, Pozzan T. Mitochondria: the calcium connection. Biochim Biophys Acta. 2010;1797(6-7):607-18.
128. Talukder MA, Zweier JL, Periasamy M. Targeting calcium transport in ischaemic heart disease. Cardiovasc Res. 2009;84(3):345-52.
129. Sanada S, Komuro I, Kitakaze M. Pathophysiology of myocardial reperfusion injury: preconditioning, postconditioning, and translational aspects of protective measures. Am J Physiol Heart Circ Physiol. 2011;301(5):H1723-41.
130. Szydlowska K, Tymianski M. Calcium, ischemia and excitotoxicity. Cell Calcium. 2010;47(2):122-9.
131. Griffiths EJ, Halestrap AP. Mitochondrial non-specific pores remain closed during cardiac ischaemia, but open upon reperfusion. Biochem J. 1995;307 (Pt 1):93-8.
132. Kalogeris T, Baines CP, Krenz M, Korthuis RJ. Cell biology of ischemia/reperfusion injury. Int Rev Cell Mol Biol. 2012;298:229-317.
133. Kim JS, Jin Y, Lemasters JJ. Reactive oxygen species, but not Ca2+ overloading, trigger pH- and mitochondrial permeability transition-dependent death of adult rat myocytes after ischemia-reperfusion. Am J Physiol Heart Circ Physiol. 2006;290(5):H2024-34.
134. Halestrap AP, Clarke SJ, Javadov SA. Mitochondrial permeability transition pore opening during myocardial reperfusion--a target for cardioprotection. Cardiovasc Res. 2004;61(3):372-85.
135. Ong SB, Gustafsson AB. New roles for mitochondria in cell death in the reperfused myocardium. Cardiovasc Res. 2012;94(2):190-6.
136. Baines CP. The cardiac mitochondrion: nexus of stress. Annu Rev Physiol. 2010;72:61-80.
137. Halestrap AP. A pore way to die: the role of mitochondria in reperfusion injury and cardioprotection. Biochem Soc Trans. 2010;38(4):841-60.
138. Granger DN, Kvietys PR. Reperfusion injury and reactive oxygen species: The evolution of a concept. Redox Biol. 2015;6:524-51.

139. Morciano G, Giorgi C, Bonora M, Punzetti S, Pavasini R, Wieckowski MR, et al. Molecular identity of the mitochondrial permeability transition pore and its role in ischemia-reperfusion injury. J Mol Cell Cardiol. 2015;78:142-53.
140. Campo G, Morciano G, Pavasini R, Bonora M, Sbano L, Biscaglia S, et al. Fo ATP synthase C subunit serum levels in patients with ST-segment Elevation Myocardial Infarction: Preliminary findings. Int J Cardiol. 2016;221:993-7.
141. Murry CE, Jennings RB, Reimer KA. Preconditioning with ischemia: a delay of lethal cell injury in ischemic myocardium. Circulation. 1986;74(5):1124-36.
142. Javadov SA, Clarke S, Das M, Griffiths EJ, Lim KH, Halestrap AP. Ischaemic preconditioning inhibits opening of mitochondrial permeability transition pores in the reperfused rat heart. J Physiol. 2003;549(Pt 2):513-24.
143. Hausenloy DJ, Maddock HL, Baxter GF, Yellon DM. Inhibiting mitochondrial permeability transition pore opening: a new paradigm for myocardial preconditioning? Cardiovasc Res. 2002;55(3):534-43.
144. Argaud L, Gateau-Roesch O, Raisky O, Loufouat J, Robert D, Ovize M. Postconditioning inhibits mitochondrial permeability transition. Circulation. 2005;111(2):194-7.
145. Zhao ZQ, Corvera JS, Halkos ME, Kerendi F, Wang NP, Guyton RA, et al. Inhibition of myocardial injury by ischemic postconditioning during reperfusion: comparison with ischemic preconditioning. Am J Physiol Heart Circ Physiol. 2003;285(2):H579-88.
146. Staat P, Rioufol G, Piot C, Cottin Y, Cung TT, L'Huillier I, et al. Postconditioning the human heart. Circulation. 2005;112(14):2143-8.
147. Thuny F, Lairez O, Roubille F, Mewton N, Rioufol G, Sportouch C, et al. Post-conditioning reduces infarct size and edema in patients with ST-segment elevation myocardial infarction. J Am Coll Cardiol. 2012;59(24):2175-81.
148. Heusch G. Cardioprotection: chances and challenges of its translation to the clinic. Lancet. 2013;381(9861):166-75.
149. Hahn JY, Song YB, Kim EK, Yu CW, Bae JW, Chung WY, et al. Ischemic postconditioning during primary percutaneous coronary intervention: the effects of postconditioning on myocardial reperfusion in patients with ST-segment elevation myocardial infarction (POST) randomized trial. Circulation. 2013;128(17):1889-96.
150. Inserte J, Ruiz-Meana M, Rodriguez-Sinovas A, Barba I, Garcia-Dorado D. Contribution of delayed intracellular pH recovery to ischemic postconditioning protection. Antioxid Redox Signal. 2011;14(5):923-39.
151. Inserte J, Barba I, Poncelas-Nozal M, Hernando V, Agullo L, Ruiz-Meana M, et al. cGMP/PKG pathway mediates myocardial postconditioning protection in rat hearts by delaying normalization of intracellular acidosis during reperfusion. J Mol Cell Cardiol. 2011;50(5):903-9.
152. Andreka G, Vertesaljai M, Szantho G, Font G, Piroth Z, Fontos G, et al. Remote ischaemic postconditioning protects the heart during acute myocardial infarction in pigs. Heart. 2007;93(6):749-52.
153. Schmidt MR, Smerup M, Konstantinov IE, Shimizu M, Li J, Cheung M, et al. Intermittent peripheral tissue ischemia during coronary ischemia reduces myocardial infarction through a KATP-dependent mechanism: first demonstration of remote ischemic perconditioning. Am J Physiol Heart Circ Physiol. 2007;292(4):H1883-90.
154. Shi W, Vinten-Johansen J. Endogenous cardioprotection by ischaemic postconditioning and remote conditioning. Cardiovasc Res. 2012;94(2):206-16.
155. Hausenloy DJ, Iliodromitis EK, Andreadou I, Papalois A, Gritsopoulos G, Anastasiou-Nana M, et al. Investigating the signal transduction pathways underlying remote ischemic conditioning in the porcine heart. Cardiovasc Drugs Ther. 2012;26(2):87-93.
156. Candilio L, Malik A, Hausenloy DJ. Protection of organs other than the heart by remote ischemic conditioning. J Cardiovasc Med (Hagerstown). 2013;14(3):193-205.
157. Zhong H, Gao Z, Chen M, Zhao J, Wang F, Li L, et al. Cardioprotective effect of remote ischemic postconditioning on children undergoing cardiac surgery: a randomized controlled trial. Paediatr Anaesth. 2013;23(8):726-33.
158. Cheung MM, Kharbanda RK, Konstantinov IE, Shimizu M, Frndova H, Li J, et al. Randomized controlled trial of the effects of remote ischemic preconditioning on children undergoing cardiac surgery: first clinical application in humans. J Am Coll Cardiol. 2006;47(11):2277-82.
159. Hausenloy DJ, Mwamure PK, Venugopal V, Harris J, Barnard M, Grundy E, et al. Effect of remote ischaemic preconditioning on myocardial injury in patients undergoing coronary artery bypass graft surgery: a randomised controlled trial. Lancet. 2007;370(9587):575-9.
160. Munk K, Andersen NH, Schmidt MR, Nielsen SS, Terkelsen CJ, Sloth E, et al. Remote Ischemic Conditioning in Patients With Myocardial Infarction Treated With Primary Angioplasty: Impact on Left Ventricular Function Assessed by Comprehensive Echocardiography and Gated Single-Photon Emission CT. Circ Cardiovasc Imaging. 2010;3(6):656-62.
161. Ibanez B, Prat-Gonzalez S, Speidl WS, Vilahur G, Pinero A, Cimmino G, et al. Early metoprolol administration before coronary reperfusion results in increased myocardial salvage: analysis of ischemic myocardium at risk using cardiac magnetic resonance. Circulation. 2007;115(23):2909-16.
162. Ibanez B, Cimmino G, Prat-Gonzalez S, Vilahur G, Hutter R, Garcia MJ, et al. The cardioprotection granted by metoprolol is restricted to its administration prior to coronary reperfusion. Int J Cardiol. 2011;147(3):428-32.
163. Ibanez B, Macaya C, Sanchez-Brunete V, Pizarro G, Fernandez-Friera L, Mateos A, et al. Effect of early metoprolol on infarct size in ST-segment-elevation myocardial infarction patients undergoing

primary percutaneous coronary intervention: the Effect of Metoprolol in Cardioprotection During an Acute Myocardial Infarction (METOCARD-CNIC) trial. Circulation. 2013;128(14):1495-503.
164. Pizarro G, Fernandez-Friera L, Fuster V, Fernandez-Jimenez R, Garcia-Ruiz JM, Garcia-Alvarez A, et al. Long-term benefit of early pre-reperfusion metoprolol administration in patients with acute myocardial infarction: results from the METOCARD-CNIC trial (Effect of Metoprolol in Cardioprotection During an Acute Myocardial Infarction). J Am Coll Cardiol. 2014;63(22):2356-62.
165. Chen ZM, Pan HC, Chen YP, Peto R, Collins R, Jiang LX, et al. Early intravenous then oral metoprolol in 45,852 patients with acute myocardial infarction: randomised placebo-controlled trial. Lancet. 2005;366(9497):1622-32.
166. Roolvink V, Rasoul S, Ottervanger JP, Dambrink JH, Lipsic E, van der Horst IC, et al. Rationale and design of a double-blind, multicenter, randomized, placebo-controlled clinical trial of early administration of intravenous beta-blockers in patients with ST-elevation myocardial infarction before primary percutaneous coronary intervention: EARLY beta-blocker administration before primary PCI in patients with ST-elevation myocardial infarction trial. Am Heart J. 2014;168(5):661-6.
167. Inserte J, Garcia-Dorado D**.** The cGMP/PKG pathway as a common mediator of cardioprotection: translatability and mechanism. Br J Pharmacol. 2015;172(8):1996-2009.
168. Kitakaze M, Asakura M, Kim J, Shintani Y, Asanuma H, Hamasaki T, et al. Human atrial natriuretic peptide and nicorandil as adjuncts to reperfusion treatment for acute myocardial infarction (J-WIND): two randomised trials. Lancet. 2007;370(9597):1483-93.
169. Gao F, Gao E, Yue TL, Ohlstein EH, Lopez BL, Christopher TA, et al. Nitric oxide mediates the antiapoptotic effect of insulin in myocardial ischemia-reperfusion: the roles of PI3-kinase, Akt, and endothelial nitric oxide synthase phosphorylation. Circulation. 2002;105(12):1497-502.
170. Timmer JR, van der Horst IC, Ottervanger JP, De Luca G, van 't Hof AW, Bilo HJ, et al. Glucose-insulin-potassium infusion as adjunctive therapy in myocardial infarction: current evidence and potential mechanisms. Ital Heart J. 2004;5(10):727-31.
171. Selker HP, Beshansky JR, Sheehan PR, Massaro JM, Griffith JL, D'Agostino RB, et al. Out-of-hospital administration of intravenous glucose-insulin-potassium in patients with suspected acute coronary syndromes: the IMMEDIATE randomized controlled trial. JAMA. 2012;307(18):1925-33.
172. Lonborg J, Vejlstrup N, Kelbaek H, Botker HE, Kim WY, Mathiasen AB, et al. Exenatide reduces reperfusion injury in patients with ST-segment elevation myocardial infarction. Eur Heart J. 2012;33(12):1491-9.
173. Lonborg J, Kelbaek H, Vejlstrup N, Botker HE, Kim WY, Holmvang L, et al. Exenatide reduces final infarct size in patients with ST-segment-elevation myocardial infarction and short-duration of ischemia. Circ Cardiovasc Interv. 2012;5(2):288-95.
174. Chen WR, Hu SY, Chen YD, Zhang Y, Qian G, Wang J, et al. Effects of liraglutide on left ventricular function in patients with ST-segment elevation myocardial infarction undergoing primary percutaneous coronary intervention. Am Heart J. 2015;170(5):845-54.
175. Stone GW, Maehara A, Witzenbichler B, Godlewski J, Parise H, Dambrink JH, et al. Intracoronary abciximab and aspiration thrombectomy in patients with large anterior myocardial infarction: the INFUSE-AMI randomized trial. JAMA. 2012;307(17):1817-26.
176. Mahaffey KW, Puma JA, Barbagelata NA, DiCarli MF, Leesar MA, Browne KF, et al. Adenosine as an adjunct to thrombolytic therapy for acute myocardial infarction: results of a multicenter, randomized, placebo-controlled trial: the Acute Myocardial Infarction STudy of ADenosine (AMISTAD) trial. J Am Coll Cardiol. 1999;34(6):1711-20.
177. Ross AM, Gibbons RJ, Stone GW, Kloner RA, Alexander RW, Investigators A-I**.** A randomized, double-blinded, placebo-controlled multicenter trial of adenosine as an adjunct to reperfusion in the treatment of acute myocardial infarction (AMISTAD-II). J Am Coll Cardiol. 2005;45(11):1775-80.
178. Garcia-Dorado D, PROMISE obo, Otaegui I, PROMISE obo, Rodriguez Palomares JF, PROMISE obo, et al. Primary results of the PROMISE trial: myocardial protection with intracoronary adenosine given before reperfusion in patients with STEMI. European Heart Journal. 2013;34(suppl_1).
179. Nazareth W, Yafei N, Crompton M**.** Inhibition of anoxia-induced injury in heart myocytes by cyclosporin A. J Mol Cell Cardiol. 1991;23(12):1351-4.
180. Saxton NE, Barclay JL, Clouston AD, Fawcett J**.** Cyclosporin A pretreatment in a rat model of warm ischaemia/reperfusion injury. J Hepatol. 2002;36(2):241-7.
181. Singh D, Chander V, Chopra K**.** Cyclosporine protects against ischemia/reperfusion injury in rat kidneys. Toxicology. 2005;207(3):339-47.
182. Piot C, Croisille P, Staat P, Thibault H, Rioufol G, Mewton N, et al. Effect of cyclosporine on reperfusion injury in acute myocardial infarction. N Engl J Med. 2008;359(5):473-81.
183. Mewton N, Croisille P, Gahide G, Rioufol G, Bonnefoy E, Sanchez I, et al. Effect of cyclosporine on left ventricular remodeling after reperfused myocardial infarction. J Am Coll Cardiol. 2010;55(12):1200-5.
184. Chiari P, Angoulvant D, Mewton N, Desebbe O, Obadia JF, Robin J, et al. Cyclosporine protects the heart during aortic valve surgery. Anesthesiology. 2014;121(2):232-8.
185. Clarke SJ, McStay GP, Halestrap AP**.** Sanglifehrin A acts as a potent inhibitor of the mitochondrial permeability transition and reperfusion injury of the heart by binding to cyclophilin-D at a different site from cyclosporin A. J Biol Chem. 2002;277(38):34793-9.
186. Reutenauer J, Dorchies OM, Patthey-Vuadens O, Vuagniaux G, Ruegg UT**.** Investigation of Debio 025, a cyclophilin inhibitor, in the dystrophic mdx mouse, a model for Duchenne muscular dystrophy. Br J Pharmacol. 2008;155(4):574-84.

187. Muramatsu Y, Furuichi Y, Tojo N, Moriguchi A, Maemoto T, Nakada H, et al. Neuroprotective efficacy of FR901459, a novel derivative of cyclosporin A, in in vitro mitochondrial damage and in vivo transient cerebral ischemia models. Brain Res. 2007;1149:181-90.
188. Baines CP, Kaiser RA, Purcell NH, Blair NS, Osinska H, Hambleton MA, et al. Loss of cyclophilin D reveals a critical role for mitochondrial permeability transition in cell death. Nature. 2005;434(7033):658-62.
189. Devalaraja-Narashimha K, Diener AM, Padanilam BJ. Cyclophilin D gene ablation protects mice from ischemic renal injury. Am J Physiol Renal Physiol. 2009;297(3):F749-59.
190. Schinzel AC, Takeuchi O, Huang Z, Fisher JK, Zhou Z, Rubens J, et al. Cyclophilin D is a component of mitochondrial permeability transition and mediates neuronal cell death after focal cerebral ischemia. Proc Natl Acad Sci U S A. 2005;102(34):12005-10.
191. Kim J, Ghasemzadeh N, Eapen DJ, Chung NC, Storey JD, Quyyumi AA, et al. Gene expression profiles associated with acute myocardial infarction and risk of cardiovascular death. Genome Med. 2014;6(5):40.
192. Do R, Stitziel NO, Won HH, Jorgensen AB, Duga S, Angelica Merlini P, et al. Exome sequencing identifies rare LDLR and APOA5 alleles conferring risk for myocardial infarction. Nature. 2015;518(7537):102-6.
193. Hong S, Pedersen PL. ATP synthase and the actions of inhibitors utilized to study its roles in human health, disease, and other scientific areas. Microbiol Mol Biol Rev. 2008;72(4):590-641, Table of Contents.
194. Devenish RJ, Prescott M, Boyle GM, Nagley P. The oligomycin axis of mitochondrial ATP synthase: OSCP and the proton channel. J Bioenerg Biomembr. 2000;32(5):507-15.
195. John UP, Nagley P. Amino acid substitutions in mitochondrial ATPase subunit 6 of Saccharomyces cerevisiae leading to oligomycin resistance. FEBS Lett. 1986;207(1):79-83.
196. Nagley P, Hall RM, Ooi BG. Amino acid substitutions in mitochondrial ATPase subunit 9 of Saccharomyces cerevisiae leading to oligomycin or venturicidin resistance. FEBS Lett. 1986;195(1-2):159-63.
197. Chinopoulos C, Szabadkai G. What makes you can also break you: mitochondrial permeability transition pore formation by the c subunit of the F(1)F(0) ATP-synthase? Front Oncol. 2013;3:25.
198. Blanchet L, Grefte S, Smeitink JA, Willems PH, Koopman WJ. Photo-induction and automated quantification of reversible mitochondrial permeability transition pore opening in primary mouse myotubes. PLoS One. 2014;9(11):e114090.
199. Broekemeier KM, Dempsey ME, Pfeiffer DR. Cyclosporin A is a potent inhibitor of the inner membrane permeability transition in liver mitochondria. J Biol Chem. 1989;264(14):7826-30.
200. Suski JM, Lebiedzinska M, Wojtala A, Duszynski J, Giorgi C, Pinton P, et al. Isolation of plasma membrane-associated membranes from rat liver. Nat Protoc. 2014;9(2):312-22.
201. Jafari R, Almqvist H, Axelsson H, Ignatushchenko M, Lundback T, Nordlund P, et al. The cellular thermal shift assay for evaluating drug target interactions in cells. Nat Protoc. 2014;9(9):2100-22.
202. Martinez Molina D, Jafari R, Ignatushchenko M, Seki T, Larsson EA, Dan C, et al. Monitoring drug target engagement in cells and tissues using the cellular thermal shift assay. Science. 2013;341(6141):84-7.
203. Fedorov O, Marsden B, Pogacic V, Rellos P, Muller S, Bullock AN, et al. A systematic interaction map of validated kinase inhibitors with Ser/Thr kinases. Proc Natl Acad Sci U S A. 2007;104(51):20523-8.
204. Wahlberg E, Karlberg T, Kouznetsova E, Markova N, Macchiarulo A, Thorsell AG, et al. Family-wide chemical profiling and structural analysis of PARP and tankyrase inhibitors. Nat Biotechnol. 2012;30(3):283-8.
205. Di Lisa F, Menabo R, Canton M, Barile M, Bernardi P. Opening of the mitochondrial permeability transition pore causes depletion of mitochondrial and cytosolic NAD+ and is a causative event in the death of myocytes in postischemic reperfusion of the heart. J Biol Chem. 2001;276(4):2571-5.
206. Morciano G, Sarti AC, Marchi S, Missiroli S, Falzoni S, Raffaghello L, et al. Use of luciferase probes to measure ATP in living cells and animals. Nat Protoc. 2017;12(8):1542-62.
207. Jouaville LS, Pinton P, Bastianutto C, Rutter GA, Rizzuto R. Regulation of mitochondrial ATP synthesis by calcium: evidence for a long-term metabolic priming. Proc Natl Acad Sci U S A. 1999;96(24):13807-12.
208. Bell RM, Mocanu MM, Yellon DM. Retrograde heart perfusion: the Langendorff technique of isolated heart perfusion. J Mol Cell Cardiol. 2011;50(6):940-50.
209. Ferrari R, Balla C, Malagu M, Guardigli G, Morciano G, Bertini M, et al. Reperfusion Damage- A Story of Success, Failure, and Hope. Circ J. 2017;81(2):131-41.
210. Hausenloy DJ, Yellon DM. Combination Therapy to Target Reperfusion Injury After ST-Segment-Elevation Myocardial Infarction: A More Effective Approach to Cardioprotection. Circulation. 2017;136(10):904-6.
211. Abikhair M, Mitsui H, Yanofsky V, Roudiani N, Ovits C, Bryan T, et al. Cyclosporine A immunosuppression drives catastrophic squamous cell carcinoma through IL-22. JCI Insight. 2016;1(8):e86434.
212. Youn TJ, Piao H, Kwon JS, Choi SY, Kim HS, Park DG, et al. Effects of the calcineurin dependent signaling pathway inhibition by cyclosporin A on early and late cardiac remodeling following myocardial infarction. Eur J Heart Fail. 2002;4(6):713-8.
213. Le Hir M, Su Q, Weber L, Woerly G, Granelli-Piperno A, Ryffel B. In situ detection of cyclosporin A: evidence for nuclear localization of cyclosporine and cyclophilins. Lab Invest. 1995;73(5):727-33.

214. Matsuno-Yagi A, Hatefi Y. Kinetic modalities of ATP synthesis. Regulation by the mitochondrial respiratory chain. J Biol Chem. 1986;261(30):14031-8.
215. Beutner G, Alanzalon RE, Porter GA, Jr. Cyclophilin D regulates the dynamic assembly of mitochondrial ATP synthase into synthasomes. Sci Rep. 2017;7(1):14488.
216. Amodeo GF, Solesio ME, Pavlov EV. From ATP synthase dimers to C-ring conformational changes: unified model of the mitochondrial permeability transition pore. Cell Death Dis. 2017;8(12):1.
217. He L, Lemasters JJ. Regulated and unregulated mitochondrial permeability transition pores: a new paradigm of pore structure and function? FEBS Lett. 2002;512(1-3):1-7.
218. Jouaville LS, Pinton P, Bastianutto C, Rutter GA, Rizzuto R. Regulation of mitochondrial ATP synthesis by calcium: Evidence for a long-term metabolic priming. Proceedings of the National Academy of Sciences. 1999;96(24):13807-12.
219. Lim GB. Genetics: Mutations in APOA5 or LDLR increase risk of myocardial infarction. Nat Rev Cardiol. 2015;12(2):64.
220. Adzhubei I, Jordan DM, Sunyaev SR. Predicting functional effect of human missense mutations using PolyPhen-2. Curr Protoc Hum Genet. 2013;Chapter 7:Unit7 20.
221. Kallberg M, Wang H, Wang S, Peng J, Wang Z, Lu H, et al. Template-based protein structure modeling using the RaptorX web server. Nat Protoc. 2012;7(8):1511-22.
222. Norris U, Karp PE, Fimmel AL. Mutational analysis of the glycine-rich region of the c subunit of the Escherichia coli F0F1 ATPase. J Bacteriol. 1992;174(13):4496-9.
223. Asp J, Synnergren J, Jonsson M, Dellgren G, Jeppsson A. Comparison of human cardiac gene expression profiles in paired samples of right atrium and left ventricle collected in vivo. Physiol Genomics. 2012;44(1):89-98.
224. Milei J, Fraga CG, Grana DR, Ferreira R, Ambrosio G. Ultrastructural evidence of increased tolerance of hibernating myocardium to cardioplegic ischemia-reperfusion injury. J Am Coll Cardiol. 2004;43(12):2329-36.
225. Alluri H, Anasooya Shaji C, Davis ML, Tharakan B. Oxygen-glucose deprivation and reoxygenation as an in vitro ischemia-reperfusion injury model for studying blood-brain barrier dysfunction. J Vis Exp. 2015(99):e52699.
226. Bonora M, Giorgi C, Bononi A, Marchi S, Patergnani S, Rimessi A, et al. Subcellular calcium measurements in mammalian cells using jellyfish photoprotein aequorin-based probes. Nat Protoc. 2013;8(11):2105-18.
227. Tesco G, Vergelli M, Grassilli E, Salomoni P, Bellesia E, Sikora E, et al. Growth properties and growth factor responsiveness in skin fibroblasts from centenarians. Biochem Biophys Res Commun. 1998;244(3):912-6.
228. Eitel I, Desch S, Fuernau G, Hildebrand L, Gutberlet M, Schuler G, et al. Prognostic significance and determinants of myocardial salvage assessed by cardiovascular magnetic resonance in acute reperfused myocardial infarction. J Am Coll Cardiol. 2010;55(22):2470-9.
229. Jahandiez V, Cour M, Bochaton T, Abrial M, Loufouat J, Gharib A, et al. Fast therapeutic hypothermia prevents post-cardiac arrest syndrome through cyclophilin D-mediated mitochondrial permeability transition inhibition. Basic Res Cardiol. 2017;112(4):35.